# Control Algorithms for Bosonic Quantum Batteries: Parallel versus Collective Charging

## Sergey Borisenok<sup>1,2\*</sup>

<sup>1</sup>Abdullah Gül University, Faculty of Engineering, Department of Electrical and Electronics Engineering, 38080, Kocasinan / Kayseri, Turkey.

<sup>2</sup>Boğaziçi University, Feza Gürsey Center for Physics and Mathematics, 34684,Üsküdar/Istanbul, Turkey. \*Corresponding Author email: sergey.borisenok@agu.edu.tr

#### **Abstract**

Very recently great progress has been achieved for a new type of quantum device: quantum batteries (QBs) which are capable to be charged, to store energy and finally to transfer it to consumption centers and other quantum devices. We develop here our theoretical feedback control algorithm for charging Bosonic quantum batteries with two different topologies of interaction between the charger and the battery set: parallel versus collective transfer of energy. The model of QB is composed of non-mutually interacting elements (quantum harmonic oscillators) in a Markovian bath. The charger of such a battery is implemented via the field which is pumping the energy into the batteries. We study the control approach in the form of Kolesnikov's target attractor to track (i.e. to drive dynamically) the charging power of the batteries. We discuss the pros and cons of the control models for different charging schemes; demonstrate their efficiency, robustness and stability. The proposed algorithms can be applied to other physical types of quantum devices: Dicke QBs and spin QBs.

## **Keywords**

Feedback control, Quantum battery, Markovian environment

#### 1. INTRODUCTION

Quantum Battery (QB) represented by systems with distinct quantum states must be able to perform its three basic tasks [1]:

- It can be charged, i.e. it can be transferred from its lower energy state to more energetic states. The important fact is that charging / discharging processes are not necessarily unitary, and during this process, QB may interact with its environment.
- It can efficiently store the transferred energy at the upper energy levels.
- It can transfer the stored energy to consumption centers.

The schematic diagram of an open Quantum Battery B interacting with charger A is represented in Figure 1. Each of the sub-systems, A and B, are coupled individually into an environment. In addition, one can apply an external control field to charger A [2].

There are different types of quantum batteries that could be realized in particular systems:

2 Borisenok

• Dicke QB, where one cavity mode acting as the charger is coupled to N qubits, which play the role of the battery [3, 4];

- Spin QB composed by N qubits, acting as a charger, this charger is coupled to another set of N qubits, which play the role of the battery [5, 6];
- Bosonic harmonic oscillator QB, where the sub-system B is composed of N non-mutually interacting elements [7, 8].

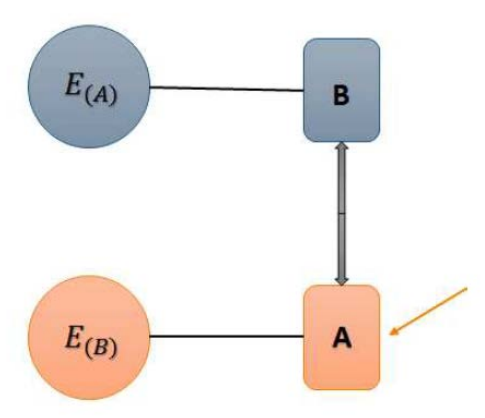


Figure 1. Diagram of an open Quantum Battery B interacting with the charger A, based on [2].

Here we discuss the last type of QB: the Bosonic quantum battery with two alternative charging schemes [9], see Figure 2.

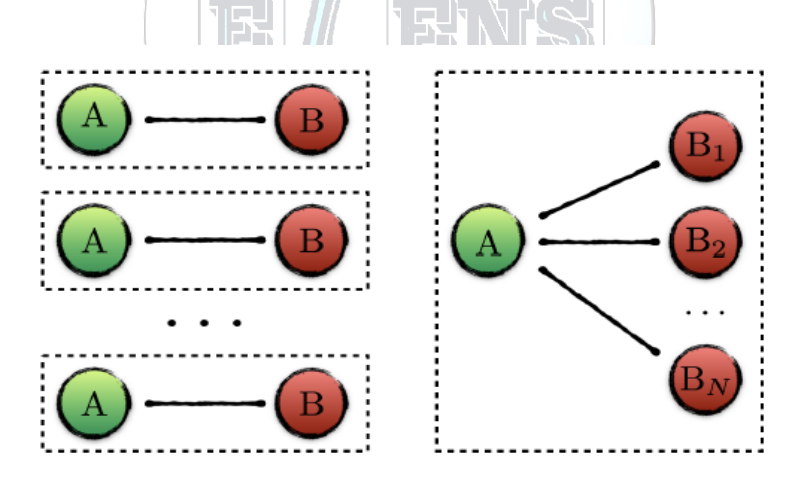


Figure 2. Two basic schemes of the parallel (left) versus collective (right) QB charging, based on [9].

The performance of QB can be enhanced by increasing the coupling strength between the nearest-neighbor environments and decreasing the size of the environments [10]. A well-engineered quantum battery is capable to store relatively more energy as compared with its non-engineered counterpart over the course of the storage phase, and the excess in such stored energy is independent of the quantum system size [11].

It has been proved also that for an array of N qubits an N-fold advantage in power per qubit can be achieved when global operations are permitted [12].

Recently, different control algorithms have been applied to quantum batteries: like the open-loop harmonic control [13] and the linear feedback [14]. Even linear feedback counteracts the randomizing influence of environmental noise and allow for stable and effective battery charging [14].

Our theoretical feedback control algorithm is applied for charging Bosonic quantum batteries with two different topologies of interaction between the charger and the battery set: parallel versus collective transfer of energy. We use Kolesnikov's target attractor algorithm to track (i.e. to drive dynamically) the charging power of the batteries.

#### 2. MATHEMATICAL MODEL FOR BOSONIC QUANTUM BATTERY

The model of QB is composed of non-mutually interacting elements (quantum harmonic oscillators) in a Markovian bath. The charger for such a battery is implemented via the field which controls pumping the energy into the batteries.

#### 2.1. Ergotropy and charging power

The energy storage of QB depends on the time-independent reference Hamiltonian H with the finite Hilbert space of the battery system. The useful energy exacted from QB in the state  $\rho$  and its energetically lowest accessible state  $\sigma_{\rho}$  is defined via its *ergotropy* [15]:

$$W = \text{Tr}(\rho H) - \text{Tr}(\sigma_{\rho} H). \tag{1}$$

The time derivative of (1) is called the *charging power* of the battery:

$$p = \frac{dW}{dt} \ . \tag{2}$$

We will use our control algorithm to drive the parameter (2) dynamically, i.e. we will discuss the tracking of charging power p as a given target function.

#### 2.2. Bosonic harmonic oscillator quantum battery

The system includes the sub-system A (charger) and the sub-system B (battery) with the corresponding Hamiltonians  $H_A$  and  $H_B$  and the Hamiltonian  $H_1$  for the coupling between A and B [1]:

 $H(t) = H_A + H_B + u(t)H_1$  , (3)

where

$$H_{A} = \omega_{0} a^{+} a ;$$

$$H_{B} = \omega_{0} \sum_{k} b_{k}^{+} b_{k} ;$$

$$H_{1} = g \sum_{k} \left( a b_{k}^{+} + a^{+} b_{k} \right) ,$$
(4)

with the corresponding creation-annihilation operators; and u(t) is a time-dependent external control parameter. The bosonic harmonic oscillator QB is composed of N non-mutually interacting elements marked with the index k.

Let's consider a single-qubit based bosonic QB in the form of a quantum oscillator with the density operator  $\rho$  in a Markovian bath. Such a system is described with the Lindblad-type operator equation [16]:

$$\frac{d\rho}{dt} = -i[H_0 + u(t)\hat{Q}, \rho] + \hat{L}[\rho], \tag{5}$$

with the terms based on the creation-annihilation operators:

$$H_0 = \left(\omega_0 + \frac{1}{2}\right)b^+b \; ; \quad \hat{Q} = \frac{b^+ + b}{\sqrt{2\omega_0}} \; ; \quad \hat{P} = i\sqrt{\frac{\omega_0}{2}}(b^+ - b) \; . \tag{6}$$

The Lindblad operator in (5) has a form:

$$\hat{L}[\rho] = \gamma \cdot (n(t) + 1)(2b\rho b^{+} - \rho b^{+}b - b^{+}b\rho) + \gamma \cdot n(t)(2b^{+}\rho b - bb^{+}\rho - \rho bb^{+}) .$$
 (7)

The positive parameter  $\gamma$  plays here a role of coupling constant between the qubit and the environment. The external fields u(t) and n(t) are our control parameters.

## 2.3 Reduced system of differential equations

The quantum model (5)-(7) can be re-written in the form of the dynamical system with real ordinary differential equations [17]:

4 Borisenok

$$\frac{dE}{dt} = 2\gamma \cdot (\omega_0 n(t) - E) - u(t)P;$$

$$\frac{dQ}{dt} = P - \gamma \cdot Q;$$

$$\frac{dP}{dt} = -\omega_0^2 Q - \gamma \cdot P - u(t) ,$$
(8)

expressed via the 'quasi-classical' variables:

$$E(t) = Tr(H_0 \rho); \ Q(t) = Tr(\hat{Q}\rho); \ P(t) = Tr(\hat{P}\rho). \tag{9}$$

The ergotropy (1) of the system (8) is defined as:

$$W(t) = E(t) - E_0, \tag{10}$$

Where  $E_0$  stands for the lowest accessible passive battery state.

#### 3. CONTROL OVER THE CHARGING POWER

To perform control over the charging power we use here Kolesnikov's Target Attractor (TA) feedback approach based on the creation in the driven dynamical system a target attractor locking the trajectories in its neighborhood [18].

#### 3.1. Kolesnikov's target attractor feedback

For the purpose of tracking the charging power (2) we define the goal function:

$$G(t) = p(t) - p_*(t)$$
, (11)

with the arbitrary differentiable target function  $p_*(t)$ . To form Kolesnikov's attractor, we demand the exponentially fast convergence towards the tracking goal:

$$\frac{dG(t)}{dt} = -\frac{1}{T_1}G(t), \qquad (12)$$

with a positive time constant  $T_1$ . Particularly, for model (8), we define the TA control equations as the following set:

$$\frac{dE}{dt} = -\frac{1}{T_1} (E - E_0); 
\frac{dP}{dt} = -\frac{1}{T_2} (P - P_*).$$
(13)

Here  $T_2$  is also a positive constant. The system (13) has the solutions:

$$E(t) = [E(0) - E_0] \cdot e^{-t/T_1} + E_0;$$

$$P(t) = P(0) \cdot e^{-t/T_2} + P_* \cdot (1 - e^{-t/T_2}).$$
(14)

The substitution of (14) into the system (8) restores the form of both control fields for a single battery element:

$$\frac{dn(t)}{dt} = \frac{p(t)}{\omega_0} + \frac{1}{2\gamma\omega_0} \left[ P \frac{du(t)}{dt} + u(t) \frac{dP}{dt} + \frac{dp_*(t)}{dt} - \frac{1}{T_1} (p(t) - p_*(t)) \right];$$

$$u(t) = \frac{P - P_*}{T_2} - \gamma \cdot P - \omega_0^2 Q \quad .$$
(14)

By Eqs (14) we can study the achievability of the control goal.

## 3.2. Achievability of the control goal as $t \gg T_1$ , $T_2$ : parallel vs collective charging

Let's check the achievability of the control goal at the limit:  $t >> T_1$ ,  $T_2$ .

For the *parallel scheme* (see Fig.2, left) we can define different target  $P_*$  for each k-th battery element:

$$P_{*,k} = -\frac{\omega_0^2}{\gamma} Q_k(0) . {15}$$

In this case, we can re-write the control fields (14) as:

$$u_{k}(t) = \omega_{0}^{2} Q_{k}(0) \cdot \left(1 - \frac{\omega_{0}^{2}}{\gamma}\right) \cdot (1 - e^{-\gamma t});$$

$$n_{k}(t) = \int_{0}^{t} \left\{ \frac{p_{*}(\tau)}{\omega_{0}} + \frac{1}{2\gamma \omega_{0}^{2}} \cdot \frac{dp_{*}(\tau)}{d\tau} - \frac{\omega_{0}^{2}}{2\gamma} \left(1 + \frac{\omega_{0}^{2}}{\gamma^{2}}\right) Q_{k}^{2}(0) e^{-\gamma \tau} \right\} d\tau .$$
(16)

For the *collective scheme* (see Fig.2, right) charger A must drive each battery for the same target state:  $P_{\iota} \to P_{*}$ ,  $\forall k$ . By that the dynamical parameter  $Q_{k}$  can be evaluated as:

$$Q_k \cong \frac{P_*}{\gamma} + \left[ Q_k(0) - \frac{P_*}{\gamma} \right] \cdot e^{-\gamma t} \quad . \tag{17}$$

By (8) that implies for the control field  $u_k$ :

$$u_k \cong -\frac{\omega_0^2 + \gamma^2}{\gamma} P_* - \omega_0^2 \left[ Q_k(0) - \frac{P_*}{\gamma} \right] \cdot e^{-\gamma t} \quad . \tag{18}$$

In the case, if we demand the target  $P_*$  to be zero:

$$P_* = 0 , \qquad (19)$$

and the pair of control fields (14) becomes:

$$u_{k} \cong -\omega_{0}^{2} Q_{k}(0) \cdot e^{-\gamma t} ;$$

$$n_{k}(t) = \int_{0}^{t} \left[ \frac{p(\tau)}{\omega_{0}} + \frac{1}{2\gamma \omega_{0}} \frac{dp_{*}(\tau)}{d\tau} \right] d\tau .$$
(20)

Now we can compare the shapes of the control fields (14) for the parallel and collective approaches. For the parallel case (16), the control fields  $u_k$  are closed to 0 for each k-th battery:  $u_k \cong 0$ , while the control fields  $n_k$  are more complex for the practical computations. For the collective case of charging (20), the fields  $u_k$  tend to 0 asymptotically:  $u_k \cong -\omega_0^2 Q_k(0) \cdot e^{-\pi}$ , while  $n_k$  are more simple for the numerical computations.

## 4. CONCLUSIONS

The algorithm of the control over the charging power proposed here has the following basic characteristics. This algorithm is *universal* and does not depend on the initial conditions of the dynamical variables. It is *robust* and stable under the perturbation of the initial conditions and a relatively small external noise.

The proposed algorithm *can be extended for different physical realizations of quantum batteries*: Dicke QB, spin QB; and for all working stages of the QB (charging, long time storage and the energy transfer to a consumption center or engine) and it can be easily extended for a multi-qubit model.

From the point of practical computation of the coherent and non-coherent fields u and n the control algorithm for Bosonic quantum batteries demonstrates different features for two alternative schemes of charging:

• For the *parallel scheme* of charging the control signal *u* (interaction between the battery and the charger) tends to 0 as the time is increasing. From another hand, the control signal *n* (interaction with the Markovian environment) is more complex for computation.

6 Borisenok

• For the *collective scheme* of charging the control signal *u* (interaction between the battery and the charger) tends exponentially to 0 as the time is increasing. At the same time, the control signal *n* (interaction with the Markovian environment) becomes simpler for the numerical computation.

#### CONFLICT OF INTEREST STATEMENT

The author declares that there is no conflict of interest.

### **REFERENCES**

- [1]. D. Ferraro, M. Campisi, G. M. Andolina, V. Pellegrini, M. Polini, "High-power collective charging of a solid-state quantum battery", *Phys. Rev. Lett.*, vol. 120(11), p. 117702, 2018.
- [2]. F. H. Kamin, F. T. Tabesh, S. Salimi, F. Kheirandish, A. C. Santos, "Non-Markovian effects on charging and self-discharging processes of quantum batteries", N. J. Phys., vol. 22, p. 083007, 2020.
- [3]. X. Zhang, M. Blaauboer, "Enhanced energy transfer in a Dicke quantum battery", arXiv:1812.10139v1, 2018.
- [4]. S. Borisenok, "Control over cavity assisted charging for Dicke quantum battery", *European Int. J. of Sci. and Technology*, vol. 9, no. 6, pp. 1-7, 2020.
- [5]. S. Ghosh, A. Sen(De), "Dimensional enhancements in a quantum battery with imperfections", *Phys. Rev. A*, vol. 105, p. 022628, 2022.
- [6]. F. Zhao, F.-Q. Dou, Q. Zhao, "Charging performance of the Su-Schrieffer-Heeger quantum battery", *Phys. Rev. Research*, vol. 4, p. 013172, 2022.
- [7]. A. I. Arbab, "The complex quantum harmonic oscillator model", *Europhysics Letters*, vol. 9843, no.3, p. 30008, 2012.
- [8]. T. K. Konar, L. G. Ch. Lakkaraju, S. Ghosh, A. Sen De, "Quantum battery with ultracold atoms: Bosons vs. Fermions", arXiv:2109.06816v1, 2021.
- [9]. G. M. Andolina, M. Keck, A. Mari, V. Giovannetti, M. Polini, "Quantum versus classical many-body batteries", *Phys. Rev. B*, vol. 99, p. 205437, 2019.
- [10]. K. Xu, H.-J. Zhu, G.-F. Zhang, W.-M. Liu, "Enhancing the performance of an open quantum battery via environment engineering", *Phys. Rev. E*, vol. 104, p. 064143, 2021.
- [11]. J. Liu, D. Segal, "Boosting quantum battery performance by structure engineering", arXiv:2104.06522v1, 2021
- [12]. F. Binder, S. Vinjanampathy, K. Modi, J. Goold, "Quantacell: Powerful charging of quantum batteries", *New Journal of Physics*, vol. 17, p. 075015, 2015.
- [13]. S. Mondal, S. Bhattacharjee, "Charging of quantum battery with periodic driving", arXiv:2112.10451v1, 2021
- [14]. M. T. Mitchison, J. Goold, J. Prior, "Charging a quantum battery with linear feedback control", *Quantum*, vol. 5, p. 500, 2021.
- [15]. G. Francica, J. Goold, F. Plastina, M. Paternostro, "Daemonic ergotropy: enhanced work extraction from quantum correlations", *npj Quantum Inf.*, vol. 3, p. 12, 2017.
- [16]. A. Pechen, "Engineering arbitrary pure and mixed quantum states", Phys. Rev. A, vol. 84,p. 042106, 2011.
- [17]. S. Borisenok, "Ergotropy of quantum battery controlled via target attractor feedback", *IOSR Journal of Applied Physics*, vol. 12(3), pp.43-47, 2020.
- [18]. A. Kolesnikov, Synergetic control methods of complex systems, Moscow: URSS Publ., 2012.

# Determination of Watershed Features Using Geographic Information System (GIS)

## Erkan Karakoyun<sup>1\*</sup>, Nihat Kaya<sup>2</sup>

<sup>1</sup>Muş Alparslan University, Faculty of Engineering and Architecture, 49250, Muşl, Turkey.

<sup>2</sup>Fırat University, Department of Civil Engineering, 23119, Elazığ, Turkey.

\*Corresponding Author email: e.karakoyun@alparslan.edu.tr

#### **Abstract**

A water basin covers the entire area giving water to the river between the source of the river and where it ends. In simple terms, it's the area that carries the water from higher altitude to lower altitude. Factors affecting the basin, such as topography, basin size, land use, and soil type affect the process of water from upstream to downstream. For this reason, it is important to know the properties of a basin for hydrological analysis. In this study, the boundaries of the Murat-1 watershed which is the subbasin of the Euphrates-Tigris basin were determined using Geographic Information System (GIS) and some hydrological features of the basin (flow direction, accumulated flow network, drainage boundaries, slope map, aspect map) is aimed to determine. Firstly, in the study, a digital elevation map (DEM) was obtained from Shuttle Radar Topography Mission (SRTM) satellite offered by USGS. The data obtained from USGS were merged using the ArcGIS 10.7 program and then the physical properties of the watershed were determined. As a result, GIS software, which gives faster and less costly results compared to traditional methods, has been accepted as a very effective tool in determining basin characteristics and boundaries.

## **Key words**

GIS, Watershed, DEM

## 1. INTRODUCTION

Water is the most important element for the continuation of life and the sustainability of the ecological balance. Nowadays, the increase in water pollution, decrease in the amount of usable water and natural disasters caused by water threaten the future of water. Because of this, water resources management is one of the problems that need to be solved. This has led to the conclusion that water should be used sparingly and that we should know the movements of water in nature [1]. For this reason, all necessary data collection, processing and analysis must be carried out reliably and quickly in order to protect water resources, which is one of the main objectives of integrated watershed management [2]. There are some basic components that become prominent for the basin characteristics. These are: basin area, slope, minimum, maximum and average elevation of basin, basin aspect etc. By revealing the characteristics of the basin, all definitions of the area can be made and these features can be used effectively in planning studies [3]. The process of

determining the boundaries of the basin and sub-basin with classical methods is done manually from printed or digital contour maps that express the surface shapes of the land. However, these classical approaches require a very long process and cost. Especially when the size of the working area is large, the operation process becomes even more difficult [4].

With the developments in Geographic Information Systems (GIS) in recent years, getting spatial data analysis become easier. In this context, digital elevation model (DEM) is created from various remote sensing data, and river drainage network and basin and sub-basin boundaries can be automatically extracted from DEM with various spatial analyzes in GIS environment, quickly, economically and with high accuracy [4,5].

In this study, the basin characteristics of the Murat-1 basin area, which was chosen as the study area, were determined with the help of GIS technologies and the effective role of this technology in hydrology studies was tried to be revealed.

#### 2. MATERIAL AND METHOD

#### 2.1. Study Area

8

Murat River, the most important branch of the Euphrates, rises from the foothills of Ağrı Mountain and joins with the Karasu River, which comes from the North, after flowing for about 500 km towards the southwest. In the region where the continental climate is effective, winters are wet and cold, summers are warm and dry. In the region where the most precipitation falls in the spring, the amount of precipitation falls below 20 mm between June and October. The Euphrates Tigris basin is the basin with the largest area in our country, Turkey. Thirty percent of the annual flow in our country flows from this basin. The important hydroelectric power plants of our country are located in this basin. The Murat-1 basin is located in the upper Euphrates basin and was selected for this study. The location of the Murat-1 basin was shown in the Fig.1.

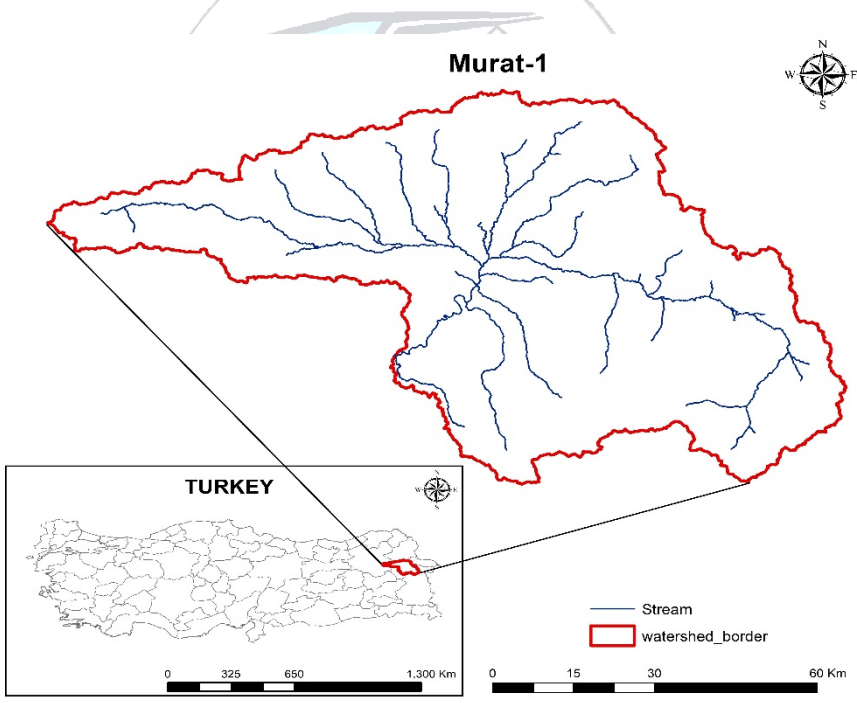


Fig.1. Study Area, Murat-1 watershed

#### 2.2. Method

Within the scope of determining the basin characteristics and boundaries, first of all, it is necessary to obtain a digital elevation map of the study area. In this context, 30m x 30m resolution data obtained from the Shuttle Radar Topography Mission (SRTM) satellite, whose DEM data are provided by the USGS, has been downloaded. When the downloaded data has more than one layer, tessellation, which is the process of merging according to the common areas of the satellite images, should be done to create a continuous data. This process is done with the help of the ArcGIS program. After mosaic, the DEM data is corrected. The accuracy of the DEM data is very important, because this step

and the next steps are performed using DEM data. In Fig. 2, mosaicked DEM data and Murat 1 watershed boundaries are seen.

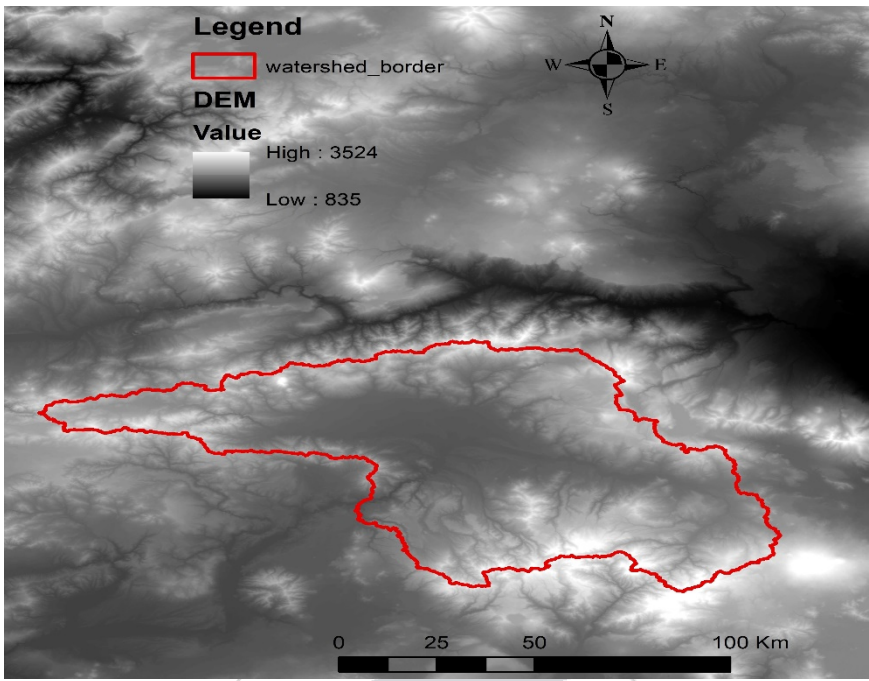


Fig.2. Mosaicked DEM and watershed border of Murat-1 watershed

After the DEM data is transferred to the ArcGIS program, the first thing to do is to remove the errors found in the DEM. When a cell is surrounded by cells with a higher elevation, the water will flow towards the area where is the lower elevation and therefore no surface flow will occur. To eliminate this error, the spaces will be filled and the height values will be rearranged by using the Fill command in the program (Fig. 3).

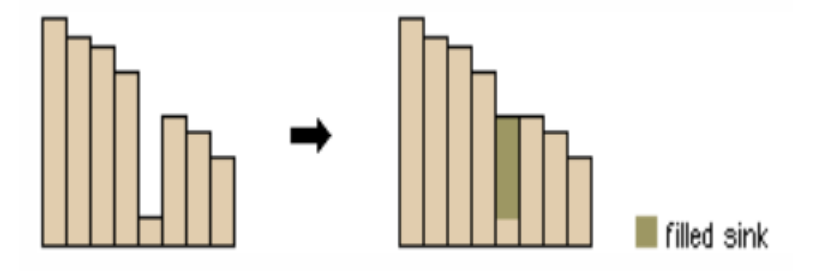


Fig.3. Correction of DEM error [6]

After the errors in the DEM are eliminated, the flow directions should be determined. Algorithms such as D8, Rho8, MFD are available for these operations. The D8 algorithm was used in the determination of the flow directions due to its ease of use and speed. D8 is a one-way algorithm that assumes that the flow in any cell is in the direction of its neighbor with the highest slope and low elevation [7]. Flow on a surface, always occurs from the highest to the lowest elevation. If the flow direction of each cell is known, the total number of cells flowing into any cell can be determined (Fig. 4). Flow direction is calculated for a given grid system with the Flow Direction command in the ArcGIS program.

10 Karakoyun and Kaya

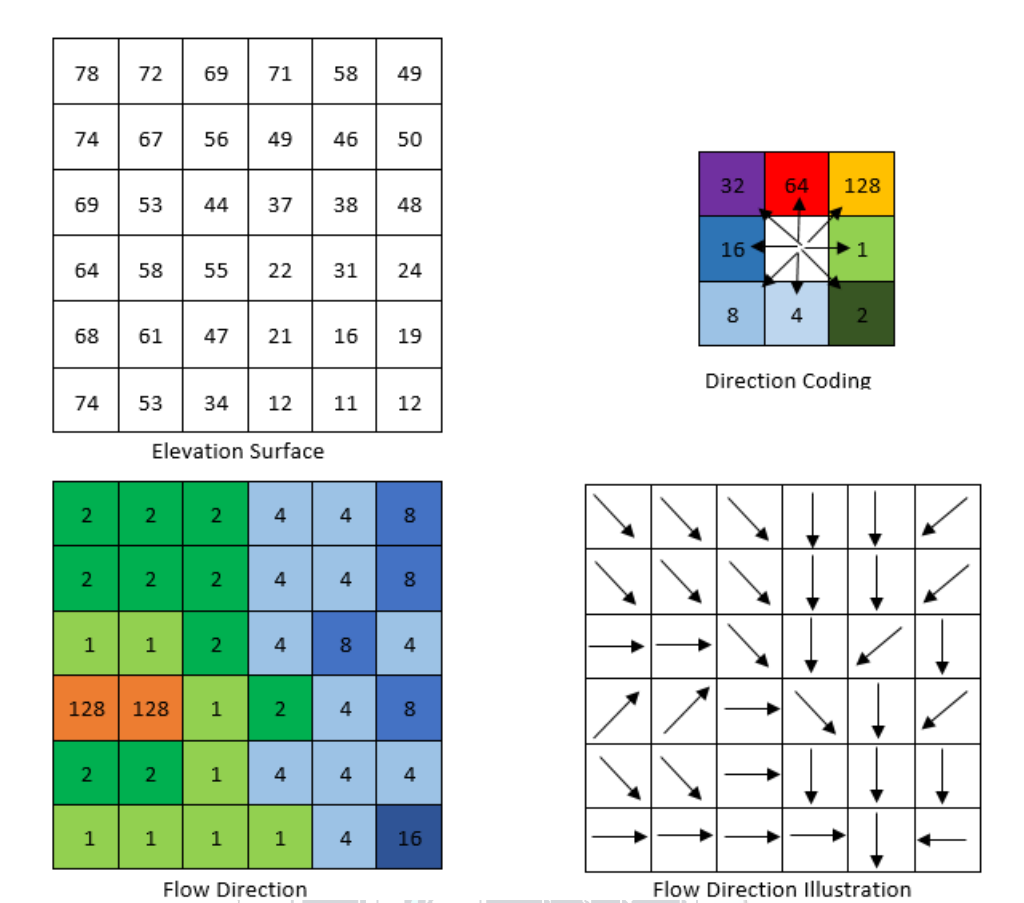


Fig.4. D8 Algorithtm [6]

After determining the flow directions, the Flow Accumulation command determines where the total flow in the cell comes from. After this process, the river branches begin to appear. The flow accumulation is illustrated in the Fig. 5 [6]. In Fig. 6, calculated flow accumulation for the Murat-1 watershed has shown.

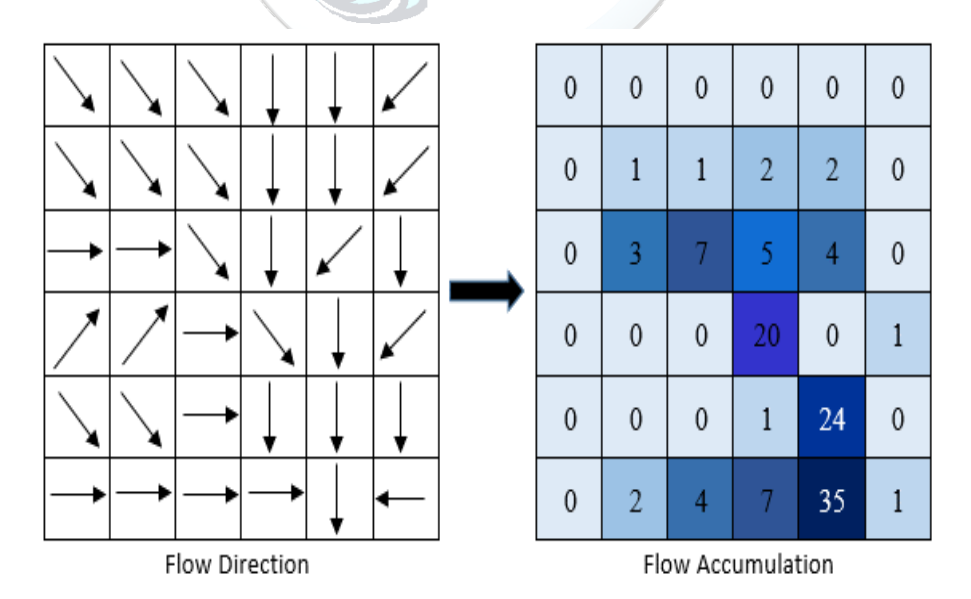


Fig.5. Flow Accumulation

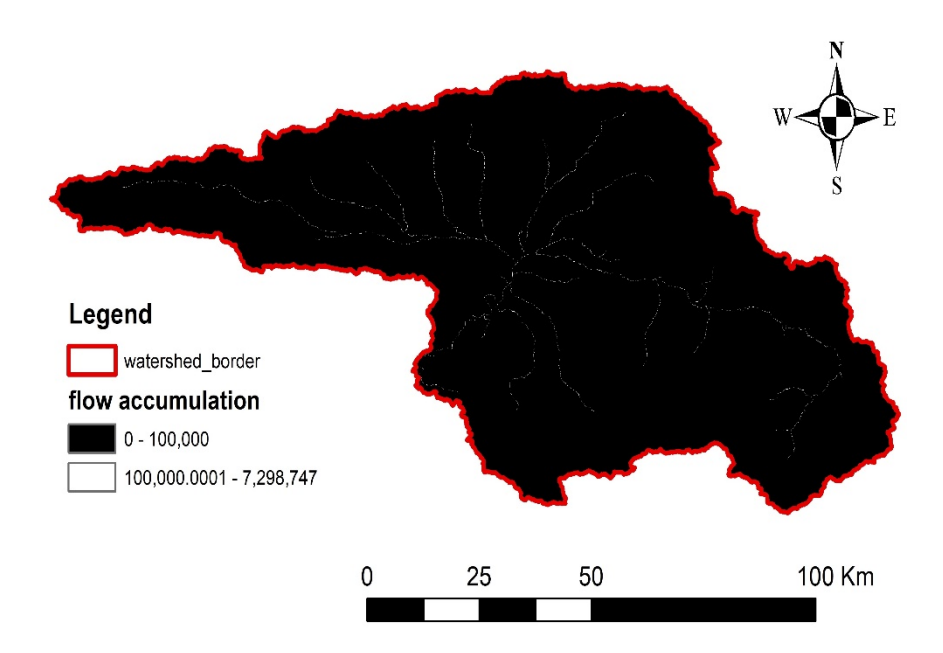


Fig.6. Murat-1 watershed flow accumulation

## 3. RESULT AND DISCUSSION

After the DEM data is transferred to the ArcGIS program, first of all, the gaps in the grid are filled with the Fill command and cut with the clip command and displayed in a way that represents only the work area. The screenshot obtained from the program is shown in Fig. 7.

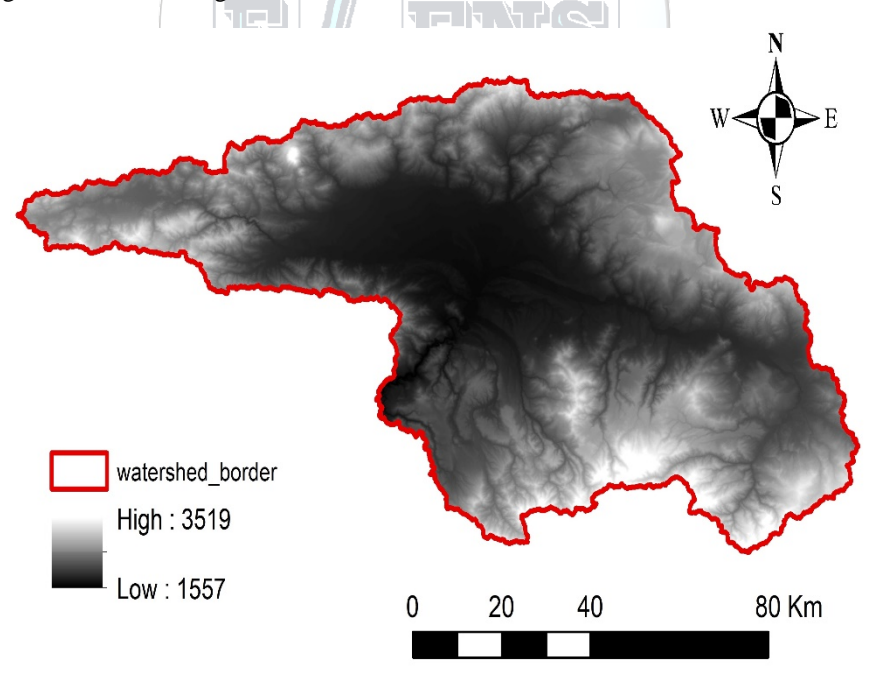


Fig.7. Correction of DEM of Murat-1 watershed

After filling the gaps in each grid, the flow direction is determined by the Flow Direction command. Flow directions map of Murat-1 basin obtained from the program and is given in Fig. 8.

12 Karakoyun and Kaya

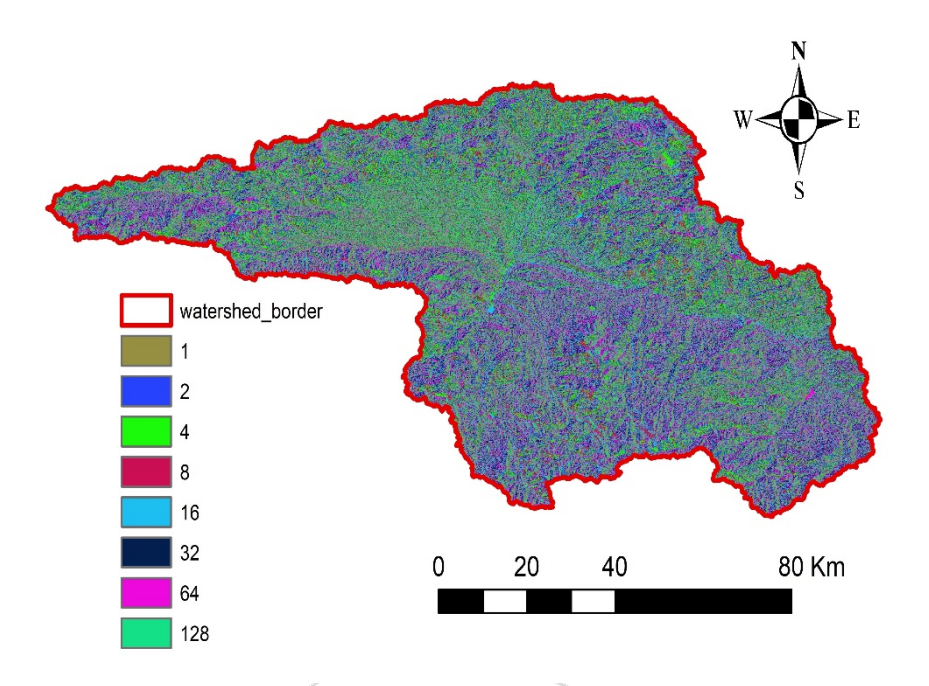


Fig.8. Flow direction of Murat-1 watershed

After the determination of the basin boundaries and the river network, the hillshade map of the region was also created and loaded on the DEM map as a basemap. The final map is shown in Fig. 9.

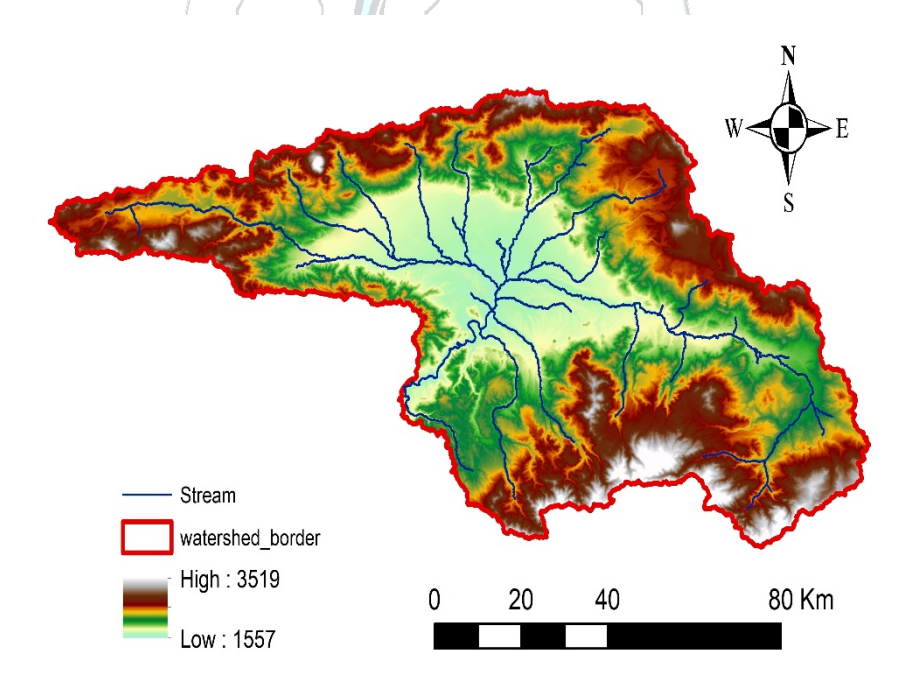


Fig. 9. Murat-1 watershed with defined DEM, watershed borders and river network

After all operations, it is aimed to create a slope and aspect map of the basin. The slope features of the basin are important in understanding the morphological features of the basin in the formation of floods and landslides. In addition, aspect can be explained as the direction in which the mountains in a region receive the Sun's rays or the part of their view towards the Sun. In Fig. 10 and Fig. 11, the slope and aspect distributions of the Murat-1 watershed are shown respectively. The average slope of the basin is found at 10.6 % and the maximum slope is 70.2 %.

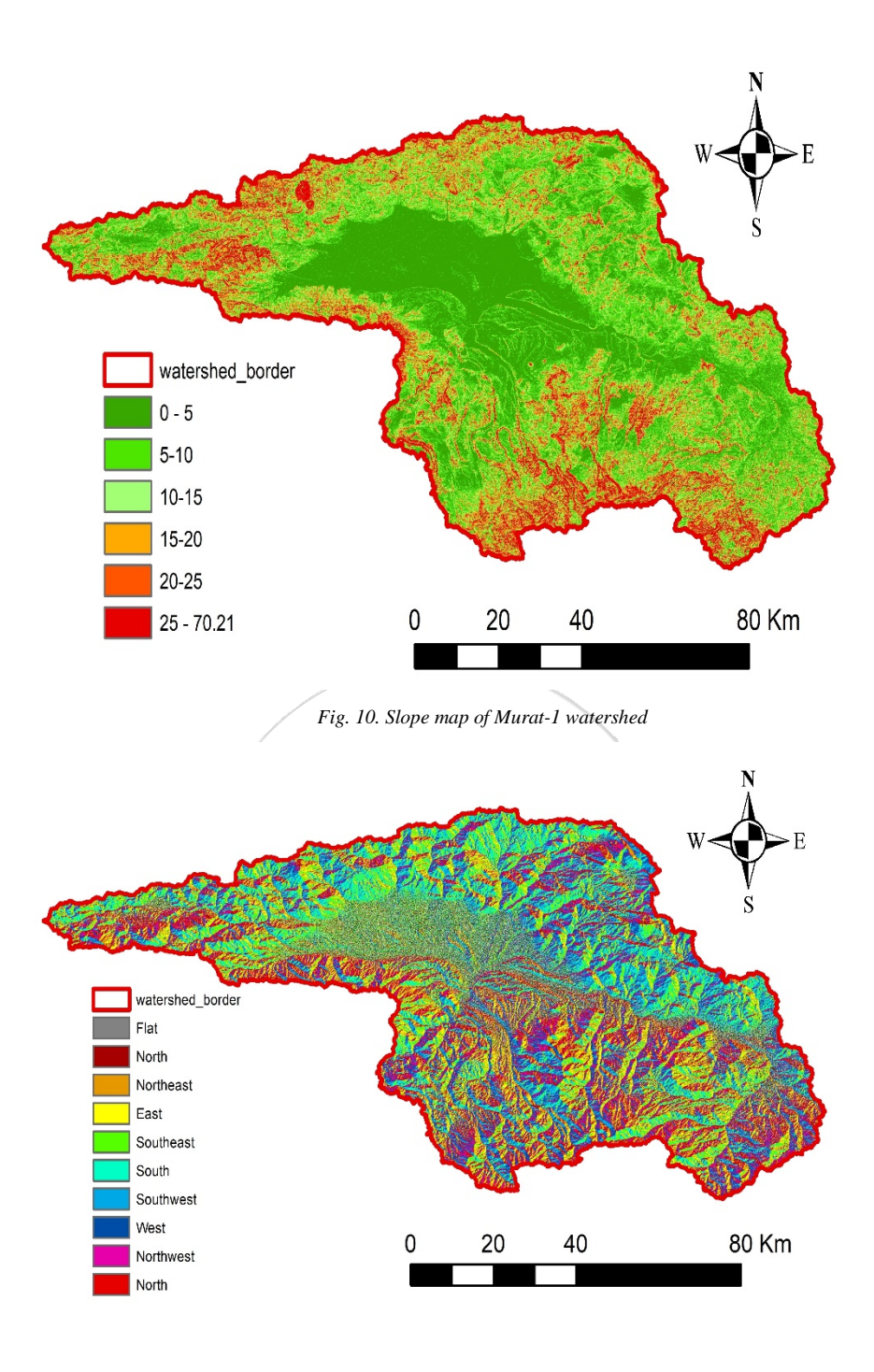


Fig. 11. Aspect map of Murat-1 watershed

## 4. CONCLUSION

Determination of basin boundaries, features and river drainage networks is a time-consuming and costly process with classical methods. These maps, which were obtained from topographic maps in the past, are obtained more quickly in the GIS environment with the rapid development of computer technology today. These analyzes, created by using the obtained DEM data, give fast and easily accessible results with the help of the programs used.

In this study, stream drainage networks of Murat-1 sub-watershed, which is a part of the Euphrates-Tigris basin, were created using DEM data, the boundaries of the basin were determined, and maps such as slope and aspect distributions of the basin were created. As a result of the study, it has been shown that GIS programs are an important

14 Karakoyun and Kaya

tool that can be used for data processing, determining watershed boundaries, creating drainage networks and visualizing the physical and morphological features of the watershed.

## CONFLICT OF INTEREST STATEMENT

The authors declare that there is no conflict of interest.

#### REFERENCES

- [1]. A.A.Karadag, "Kovada Gölü Alt Havza Sınırlarının Belirlenmesi", Düzce Üniversitesi Ormancılık Dergisi, 8(1), 58-76, 2012.
- [2]. B.T.Meric, "Su Kaynakları Yönetimi ve Türkiye", Jeoloji Mühendisliği Dergisi, 28(1), 27–38, 2004.
- [3]. M.C.Bagdatli and B.Ozturk,"Havza morfolojik özelliklerinin belirlenmesinde coğrafi bilgi sistemlerinin (CBS) etkin rolü", SAU Fen Bilimleri Enstituüsü Dergisi, 18(1), 11, 2014.
- [4]. A.Uyar, D.Ozturk, "Kızılırmak Havzası Drenaj Ağının ve Alt Havza Sınırlarının Uzaktan Algılama ve CBS İle Otomatik Çıkarımı", 3, 362–365, 2018.
- [5].T.Dindaroglu, M.Ozgul and M.Y.Canbolat, "Sayısal Yükseklik Modeli Kullanılarak Bazı Havza Karakteristiklerinin Saptanmasi ve Arazi Kullanımı", *KSU Journal of Engineering Science, Special Edition*, 197-205, 2012.
- [6]. Esri website [Online]. Available:https://pro.arcgis.com/en/pro-app/latest/tool-reference/spatial-analyst/an-overview-of-thehydrology-tools.htm.
- [7]. J.F.O'Callaghan and D.M.Mark, "The extraction of ordered vector drainage networks from elevation data", *Computer Vision, Graphics and Image Processing*, 47(1), 45–58, 1989.



## Geo-electrical characteristics of the Erecek-Çanakkale region

## Petek Sindirgi1\*

<sup>1</sup> Dokuz Eylul University, Department of Geophysics, 35390, Buca /İzmir,Turkiye \*Corresponding Author email:petek.sindirgi@deu.edu.tr

#### Abstract

Biga Peninsula is one of the tectonically active regions in Northwestern Anatolia which the middle strand of the North Anatolian Fault Zone is crossed over by it. This work is aimed to model the subsurface geological structures via vertical electrical sounding (VES) and self-potential (SP) datasets collected from the relatively less known Southern part of the Biga Peninsula. The vertical electrical sounding (VES) and self-potential (SP) datasets collected near the Erecek village of Çanakkale city were inverted by the Levenberg-Marquardt algorithm. Four profiles were generated covering some VES points to reveal the geological model. In addition, resistivity distributions at 10, 100, 200, 500, and 1000 meter depth levels were calculated. Thus, the iso-3D resistivity distribution was easily observed. Based on the VES findings, three main geological units were defined; two groups of volcanic units and a metamorphic basement. Besides, WSW-ENE and NNE-SSW trending two normal faults that have possibly water content were observed. One of them was also detected from the self-potential profile data inversion results. As a result, possible main fault locations and tectonic structures that may be associated with groundwater containment have been described using the findings of both two geoelectrical methods.

## **Key words**

Çanakkale, Erecek, Self-potential, Vertical Electrical Sounding

#### 1. INTRODUCTION

Biga Peninsula is a tectonically active region on the Alpine-Himalayan Mountain Belt that corresponds to the northward movement of the Arabian plate and the northern part of the southern segment of the NAF zone lies on it [1]. The main fault systems of this region can be listed as Balabanli, Kestanbol, Tuzla, Evciler and Edremit Faults. Accordingly (bununla iliskili olarak), this region hosts (is also hosted) also several active geothermal areas such as Tuzla, Palamutova, Kestanbol, Kucukcetmi. Many geological and geophysical studies have been done to reveal the tectonic complexity of the peninsula[1]-[11]. Most of the previous geophysical investigations were seismological studies [12], [13] related with the Northern Anatolian Fault (NAF) kinematics and structural observations. The other geophysical methods such as gravity, magnetic and electrical methods were applied in the geothermal [14], landslide [15], and archaeological [16] investigations in the region.

Geoelectrical methods supply robust information about layer rock type, thickness, and water content [17], [18]. In this study, SP and VES field datasets (Figure 1 and Figure 2) collected from near the Canakkale-Erecek village were evaluated by inverse solution techniques. This area represents the transition zone between the Beydagi Horst and Tuzla Basin. Geological units of the study area are the Balabanli volcanics, Dededag formations, and Karadag metamorphics. The Balabanli volcanics consist of pyroclastic rocks such as rhyodacitic ignimbrites and lavas. The

16 Sindirgi

Dededag formation contains andesitic and trachyandesitic lavas and flow-breccias. The Balabanli volcanics and Dededag formation lie over the metamorphic basement [3], [4], [8](Figure 2).

In this study, it is aimed to determine the electrical properties of an area located in northern part of Behram and western part of Erecek villages and combine with the possible tectonic features and accordingly possible geothermal potential. For this purpose, the VES and SP data were evaluated to distinguish main subsurface lithologies and location of the faults may associated with local groundwater movement.

#### 2. METHODS AND APPLICATIONS

VES method employs an artificial source of current which is introduced into the ground through two electrodes. The occurred potential difference is measured at other electrodes. Electrical resistivity and depth of the layers can be calculated using Ohm Law. Electrical resistivity varies with porosity, pore fluid salinity, and clay content. On the other hand, SP method based on the measurement of potential difference between the two points on the earth surface without artificial current source. Source parameters of potential anomalies occurred by the mineralization, thermoelectric or electrochemical coupling processes could be estimated by SP measurements. Both geoelectrical methods are widely used in the determination of the subsurface structures, and faults.

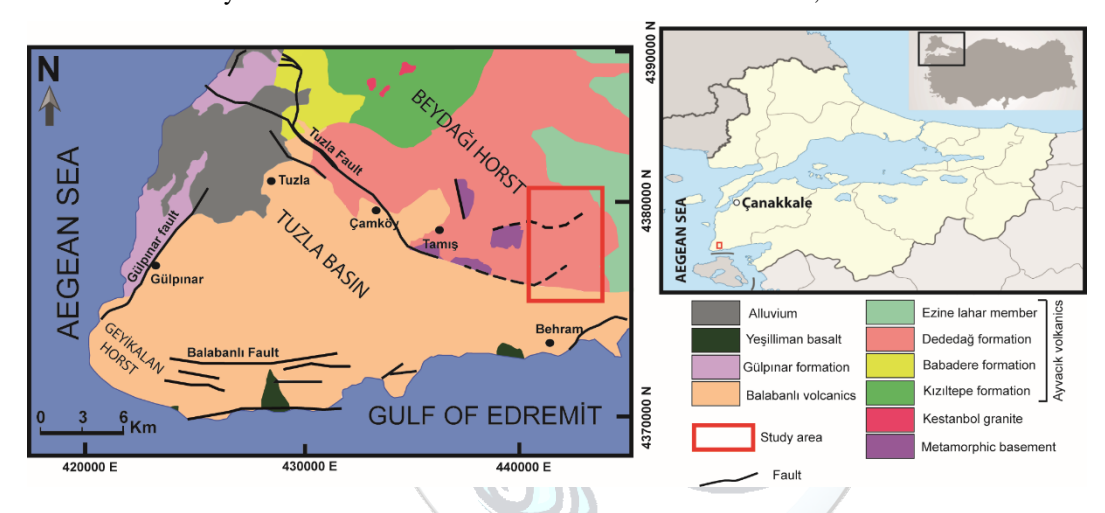


Figure 1. Geologic map of study area and surrounding (modified from [3])

In this study, investigation area is located between 26.3069N-263358N longitude and 39.5234E-39.5796E latitude and covers the area between the northern part of Behram and western part of Erecek villages of Çanakkale city (Figure 1). It is approximately spread over 30 km² area. The 43 vertical electrical soundings (Schlumberger array) and one SP profile data were evaluated by 1D inversion approach and four VES profiles (AA', BB', CC' and DD') were prepared for better interpret the geoelectrical model. AA' and BB' profiles are aligned in NNW-SSE, and CC' and DD' profiles are aligned in WSW-ENE direction. A self-potential profile (EE') data was also aligned in WNW-ESE direction (Figure 2).



Figure 2. Location of VES points, VES and SP profiles

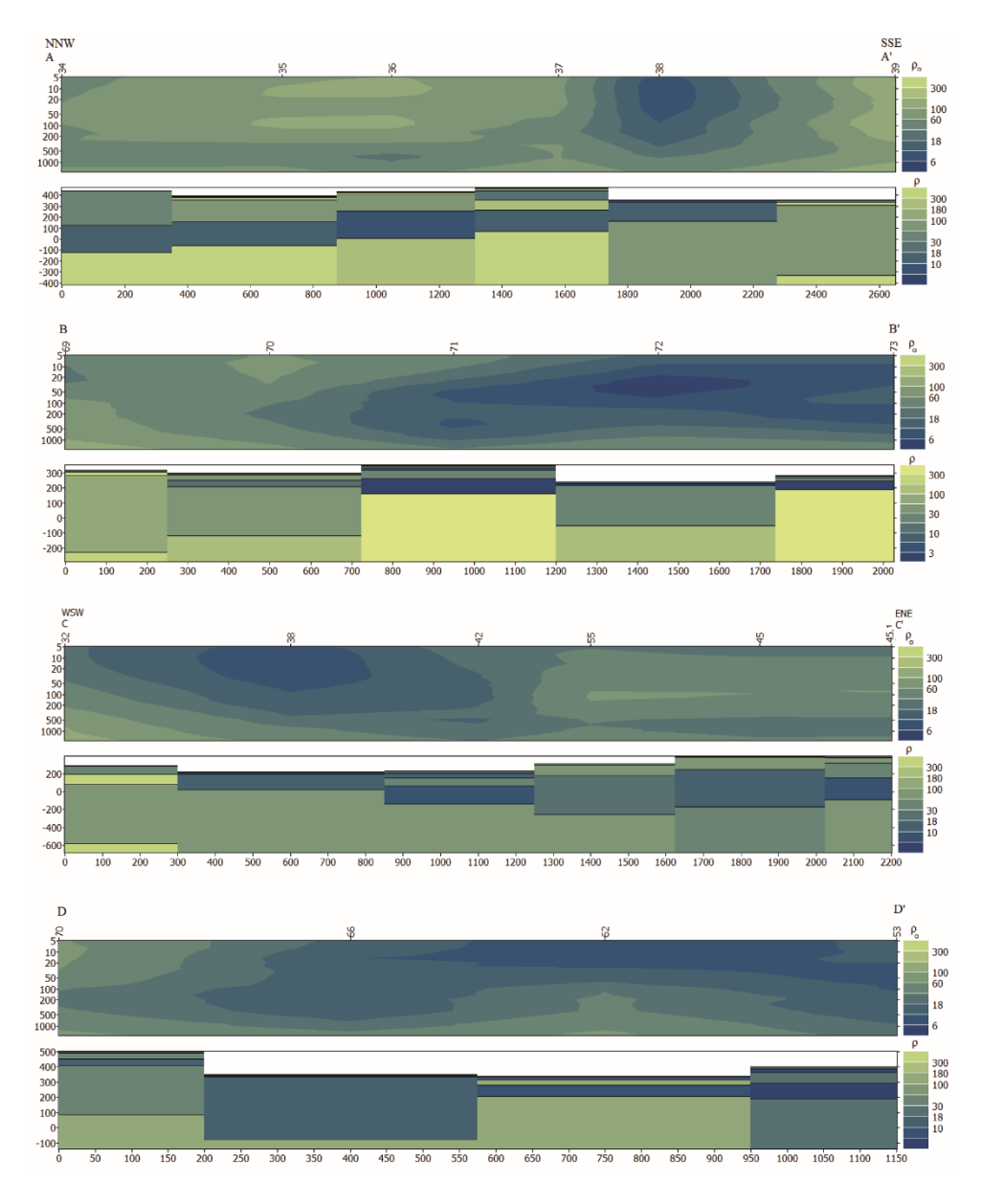


Figure 3. Pseudo and resistivity sections of AA', BB', CC', and DD' VES profiles

18 Sindirgi

The actual resistivity and thickness of the subsurface layers were obtained by inverse solution technique using the IPI2win software developed by the Geophysics Group Moscow State University [19]. (IPI2Win-1D Program, version 3.0.1a, 2003). The software realizes iterative minimization of the misfit between real and modelled data based on a least number of layers initial model using Tikhonov's approach. For all sounding curves inverted to obtain the actual resistivity and thickness of the subsurface layers. The fit between model response and the field data for the VES points were generally lower than 5%. In addition, pseudo and resistivity sections of four profiles were created by combining some selected points from them (Figure 3). According to the parameters of these sections geological models were established (Figure 4). Then, apparent resistivity distributions for many depth levels (10, 100, 200, 500, and 1000 meter) are plotted to reveal the areal resistivity distribution versus to depth (Figure 5).

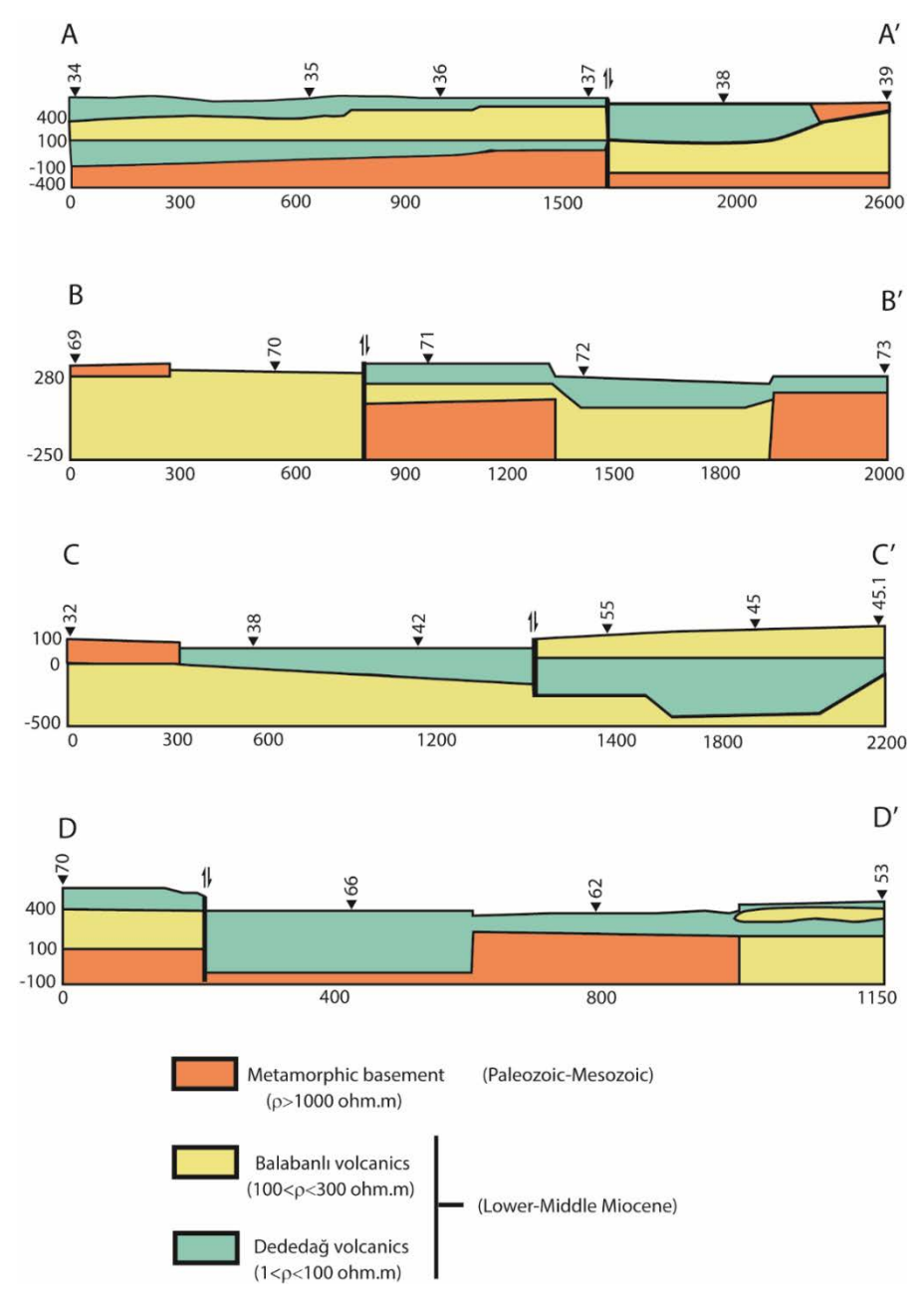


Figure 4. Geological models of VES profiles

The SP profile data (EE') were evaluated by Levenberg-Marquardt (LM) inversion algorithm [20]. Profile data were assumed produced by a simple sphere-shaped polarized causative body. Parameters of sphere model are electric dipole moment (K), horizontal distance (x), distance from the origin  $(x_0)$ , depth to the centre of the body  $(z_0)$ , and polarization angle  $(\theta)$ . The polarization angle is determined as the angle between vertical plane and polarization surface. Calculated SP parameters are shown in figure 6 and Table 1. The root mean standard error is 0.1155.

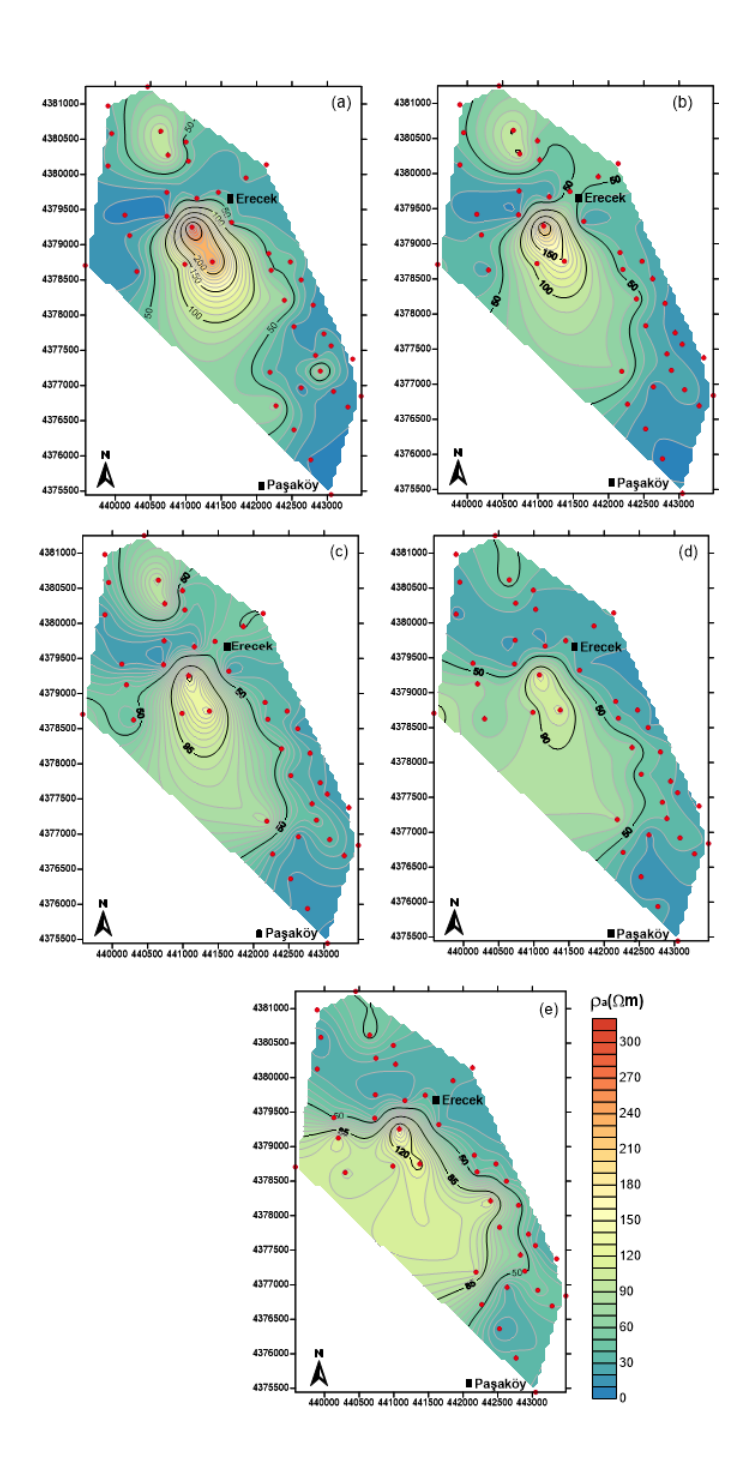


Figure 5. Contour maps of the iso-apparent resistivity values (a) AB/2=10m, (b) AB/2=100m (c) AB/2=200m, (d) AB/2=500m, (e) AB/2=1000m

20 Sindirgi

Table 1. Calculated SP model parameters

E. dipol moment (K)	Polarization angle (θ)(°)	Distance from the origin	Depth (z <sub>0</sub> ) (m)
		$(\mathbf{x_0})(\mathbf{m})$	
447432.17	1.37	216.88	145.38

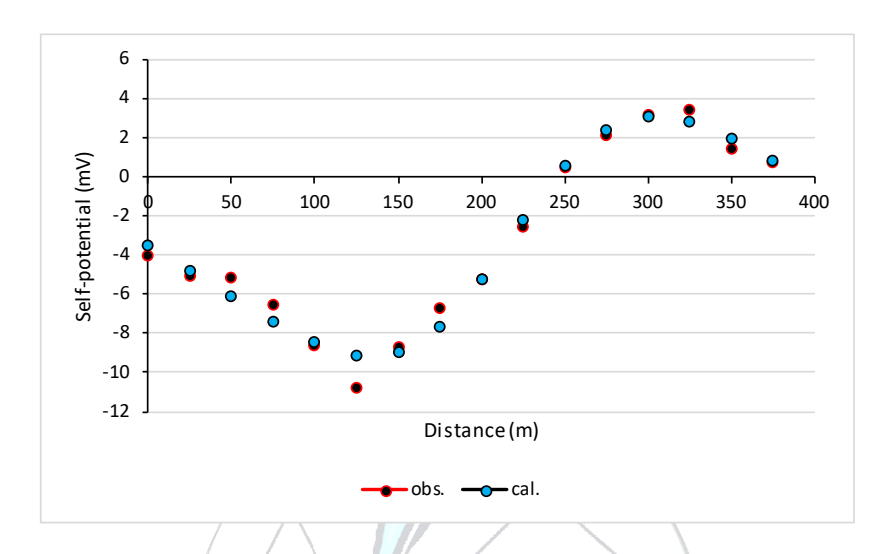


Figure 6. Observed and calculated SP values

## 3. RESULTS AND CONCLUSIONS

In this study, VES and SP methods were applied to distinguish main subsurface lithologies and locate faults that may be associated with local groundwater movement. As a result of the 1D inversion of VES, three main distinct units have been identified. The first one is the Dededag surface volcanics characterized by low and medium resistivities (1-100 ohm.m), the second one is the Balabanli volcanics having medium resistivities (100-300 ohm.m) and the third one is the metamorphic units (having resistivities higher than 1000 ohm.m) forming the basement. These geological formations were also described in the four VES profiles (AA', BB', CC' and DD'). It has been revealed that the surface volcanics become thinner and the metamorphic basement units reach to the surface near the VES 32, 38 and 69. Not only from the cross-sections but also the depth level maps it is seen that the high resistive basement spread out over the area between the southwestern part of Erecek and the northern part of Pasakov villages. WSWENE and NNE-SSW trending two normal faults that have possibly water content were observed. One of them was also detected from the self-potential profile data inversion results. The calculated polarization angle shows that the fault has a slope close to the vertical. The x0 parameter corresponds to the distance between location E and the intersection of BB' and EE' profiles in the figure 2. Since the location of fault determined as between VES 70 and 71 points at BB' profile, it well matches the x0 determined by SP inversion. Although these parameters were obtained from only one SP profile dataset, determined fault location is very similar to the results of resistivity inversion. It is observed the areas that have resistivity values below 10 ohm.m matched the alignment of the detected two faults. These areas may have contains hot or cold groundwater. Therefore, it is recommended to search geothermal potential of these areas by other hydrogeophysical and hydrogeological methods.

## ACKNOWLEDGMENT

The author thanks to Geophysical Engineer Yasin EYUP for providing the geoelectrical data used in this study.

## CONFLICT OF INTEREST STATEMENT

The author declare that there is no conflict of interest.

#### REFERENCES

- [1]. D. McKenzie, "Active tectonics of the Mediterranean region", Geophysical Journal of the Royal Astronomical Society, vol. 30, pp. 109-
- D. McKenzie, "Active tectonics of the Alpine-Himalayan belt: the Aegean Sea and surrounding regions", Geophysical Journal International, vol. 55, pp. 217-254, 1978.
- [3]. Z. Karacık and Y. Yılmaz, "Geology of the ignimbrites and the associated volcano-plutonic complex of the Ezine area, northwestern Anatolia", J. Volcan. Geother. Res., vol. 85, pp. 251-264, 1998.
- [4]. Y. Yılmaz and Z. Karacık, "Geology of the northern side of the Gulf of Edremit and its tectonic significance for the development of the Aegean grabens", Geodinamica Acta, vol. 14, pp. 31-43, 2001.
- [5]. F. Dewey and A. M. C. Şengör, "Aegean and surrounding regions: complex multiplate and continuum tectonics in a convergent zone", Geological Society of America Bulletin, vol. 90 (1), pp. 84-92, 1979.
- [6]. A. İ. Okay, M. Siyako, and K. A. Bürkan, "Geology and tectonic evolution of the Biga Peninsula", Bulletin of the Technical University of Istanbul, vol. 44, pp. 191–255, 1991.
- [7]. M. Duru, Ş. Pehlivan, İ. O. Aral, Y. Şentürk, F. Yavaş, and H. Kar, "Biga Yarımadasının Tersiyer Öncesi Jeolojisi", Maden Tetkik ve Arama Genel Müdürlüğü Yayınları, vol. 28, pp. 7-74, 2012.
- [8]. H. Sözbilir, Ö. Sümer, Ç. Özkaymak, B. Uzel, T. Güler, and S. Eski, "Kinematic analysis and palaeoseismology of the Edremit Fault Zone: evidence for past earthquakes in the southern branch of the North Anatolian Fault Zone, Biga Peninsula, NWTurkey", Geodinamica Acta, vol. 28(4), pp. 273-294, 2016.
- [9]. E. Yiğitbaş and İ. O. Tunç, "Biga Yarımadası'nda Sakarya Zonunun Prekambriyen Metamorfik Kayaları; Geç Ediyakaran Gondwanaland Aktif Kıta Kenarı", Geological Bulletin of Turkey, vol. 63, pp. 277–302, 2020.
- [10]. Y. L. Ekinci and E. Yiğitbaş, "Investigation of Plutonic Rocks in Biga Peninsula, NW Turkey, using 3D Normalized Full Gradient of Magnetic Data", in Proc. European Geosciences Union General Assembly, Austria, 2012, p. 8802.
- [11]. C. Yaltırak, E. B. İşler, A. E. Aksu, and R. N. Hiscott, "Evolution of the Bababurnu Basin and shelf of the Biga Peninsula:western extension of the middle strand of the North Anatolian Fault Zone, Northeast Aegean Sea, Turkey", Journal of Asian Earth Sciences, vol. 57, pp. 103-119, 2012.
- [12]. T. Taymaz, J. Jackson, and D. McKenzie, "Active tectonics of the north and central Aegean Sea". Geophysical Journal International, vol. 106(2), pp. 433-490, 1991.
- [13]. S. Özden, S. Över, S. A. Poyraz, Y. Güneş, and A. Pınar, "Tectonic implications of the 2017 Ayvacık (Çanakkale) earthquakes, Biga
- Peninsula, NW Turkey", *Journal of Asian Earth Sciences*, vol. 154, pp. 125–141, 2018.

  [14]. O. Tezel and F. Özçep, "Geothermal Exploration By Using Time Domain IP Method: Balikesir (Güre) and Çanakkale (Geyikli) Cases From Turkey", in AGU Fall Meeting Abstracts, 2017, p. T41A-0603.
- [15]. C. Nart, Ö. Çakır, M. Erduran, Y. A. Kutlu, and Z. S. Çetiner, "A potential landslide area investigated by 2.5D electrical resistivity tomography: case study from Çanakkale, Turkey", Arab J Geosci., vol. 9(6), 2016.
- [16]. A. Kürçer, A. Chatzipetros, S. Z. Tutkun, S. Pavlides, S. Özden, G. Syrides, K. Vouvalidis, E. Ulugergerli, Ö. Ateş, and YL. Ekinci, An assessment of the earthquakes of Ancient Troy, NW Anatolia, Turkey, in Tectonics-Recent Advances, Sharkov, E., Ed. London, UK: InTech, 2012, pp. 171-200.
- [17]. L. R. Bentley. And M. Gharibi, "Two and three dimensional electrical resistivity imaging at a heterogeneous remediation site". Geophysics, vol. 69(3), pp. 674-680, 2004.
- [18]. E. Auken and A.V. Christiansen, "Layered and laterally constrained 2D inversion of resistivity data", Geophysics, vol. 69(3), pp. 752-761, 2004.
- [19]. IPI2WIN software Moscow State University, Version 3.0; 2003
- [20]. D. Marquardt, "An Algorithm for Least-Squares Estimation of Nonlinear Parameters", SIAM Journal on Applied Mathematics, vol. 11(2), pp. 431-441, 1963.

## The Developed FEA-Based Program for Planar Dynamic Analysis with a Special 12x12 Rectangular Element

Ragib Sabah<sup>1\*</sup>, Namik Kemal Öztorun<sup>2</sup>, Baris Sayin<sup>3</sup>

<sup>1</sup>Istanbul University-Cerrahpasa, Institute of Graduate Sciences, 34320, Avcilar/ Istanbul, Turkey.

<sup>2</sup>Istanbul University-Cerrahpasa, Department of Civil Engineering 34320, Istanbul, Turkey.

<sup>3</sup>Istanbul University-Cerrahpasa, Department of Civil Engineering 34320, Istanbul, Turkey.

\*Corresponding Author email: ragib.sabah@ogr.iuc.edu.tr

#### Abstract

There are several widely used structural softwares to analyze buildings under dynamic loads, but many of these programs use arithmetic formulations to calculate the mass and stiffness matrices of shear walls with only 8x8 elements that ignore the rotational mass and stiffness values. Also, during the dynamic analysis, a system diagonal mass matrix containing only elements in the x and y directions is used. The previously mentioned calculation assumptions may lead to unrealistic structural calculations besides these assumptions should be replaced by more realistic calculation formulas and methods. In this paper, a two-part FEA computational program was developed to provide actual structural dynamic analysis. The first part of the program is called YAY2020-Static encoded by FORTRAN compiler and the second one is called YAY-Dynamic encoded by MATLAB interpreter. In YAY2020 program, a special rectangular element formula with 12x12 elements and three degrees of freedom at each element's nodes is used to calculate shear wall mass and stiffness matrices to obtain system full-size stiffness and mass matrices that contain both diagonal and non-diagonal elements. Results obtained using YAY2020 software will be compared with some structural analysis techniques such as shear building and wide column, to study the feasibility of using these techniques. All obtained results by YAY2020 will be compared with the commonly use FEA structure software SAP2000.

## **Key words**

Dynamic analysis software, FORTRAN, Finite element analysis (FEA), 12x12 Mass matrix, Shear building, Wide column

#### 1. INTRODUCTION

Turkey is one of the countries which settled in a strong seismic active location due to the presence of many seismic faults. These seismic movements cause significant physical and economic damages to building elements, which leads to catastrophic damage and loss of life. Dynamic loads are the most important factors causing structural collapse. Although many dynamic loads such as wind and blast loads may cause significant damage to buildings, earthquakes effect are the most dangerous dynamic load that structures are exposed to, because earthquakes not only affect a single building such blast loads but also affect a large scale, causing damage to entire cities and to many buildings at the same time.

Öztorun [1, 2] started his works on finite element methods in the structural engineering field, in 2006 presented the first rectangular stress elements with 12 12 matrix elements adding rotational values and the mass matrix with real and full diagonal and non-diagonal values. Wilson [3-7] introduced a set of finite element structural analysis programs which called CAL programs. In 1975 his studies were considered bases for many programs such as SAP2000, SAFE, and ETABS. In these programs, shear-wall stiffness and mass matrices contain only

8□8 elements with no stiffness and mass rotation values. So there is no rotation of the element in the vertical direction. The rotation and stress of the joints are calculated depending on the joint's movement laterally or vertically. Bathe [7, 8] presented the detailed procedure of the finite element in his book "Finite Element Procedures". This book has been a reference for many researchers in the field. Newmark [9] developed the one-step integration method to solve structural dynamics problems under blast and seismic loads. For 60 years, Newmark's method has been applied in the dynamic analysis of many applications such as structures. Chopra [10] explained the procedures of structural dynamic analysis in his book "Dynamics of Structures: Theory and Applications to Earthquake Engineering", with different methods of calculations. Öztorun and others [11, 12] made dynamic analyses of structural systems using the GP-DYNA computer program developed by Öztorun in his doctoral thesis; stated that current analysis methods may not provide sufficient assurance if vertical earthquake records are used.

During calculating the effect of earthquakes on structures general system mass and stiffness matrices must be calculated. Many literature programs considered the mass matrix as a diagonal matrix, and the mass of each floor is the same in the x and y directions with no rotational mass values. Also in calculating mass and stiffness matrices of shear wall elements, literature programs calculate it as just a matrix with 8x8 elements ignoring the rotational values. In this study, a two-part computational program based on the finite element method will be encoded using the FORTRAN compiler and MATLAB interpreter to find the response of a planar structure with a known geometry under dynamic loads. This program is called YAY2020. In principle, FORTRAN encoded YAY2020-Static software calculates the mass and stiffness matrices for each of the system elements individually and superposing them together to get system general mass and stiffness matrices. Then these matrices will be used in dynamic calculation by YAY2020-Dynamic. The system mass and stiffness matrices computed in this study contain both diagonal and non-diagonal elements as well as 12x12 elements of shear walls mass and stiffness matrices. To achieve this special formulation is used to calculate the rotational degrees of the plate elements. This formula is developed by Öztorun [1-2], and the accuracy of this formulation had been proven and demonstrated by comparing it with Timoshenko and Goodier [2, 13] analytical solution. All results obtained by YAY2020 will be compared with widely used FEA software such as SAP2000. In light of these features, this study aims to present a program that has different and more realistic calculation methods than the existing ones.

#### 2. MATERIALS AND METHODS

In this section, the YAY2020-Static and YAY2020-Dynamic mechanisms are introduced with an overview of used mathematical formulas.

#### 2.1. Frame Elements Mass Matrix

The frame element is shown in Figure 1. The element has two nodes (i and j) with three degrees of freedom at each end. The axis across from I to J is called the local x-axis and the perpendicular on the local x-axis is called the local y-axis these two axes formed the local coordinate system of the planar frame element.

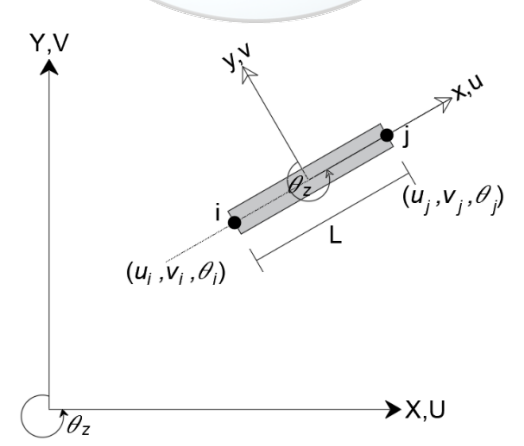


Figure 1. Planar frame element

The element length L is calculated as Eq.1.

$$L = \sqrt{(X_j - X_i)^2 + (Y_j - Y_i)^2}$$
 (1)

24 Sabah et al.

Frame element local mass matrix is written as Eq.2. [3, 8]

$$M_{e.l.}^{Frame} = WA \frac{1}{420} \begin{bmatrix} 140 & 0 & 0 & 70 & 0 & 0 \\ & 156 & 22L & 0 & 54 & -13L \\ & & 4L^2 & 0 & 13L & -3L^2 \\ & & & 140 & 0 & 0 \\ & symmetrical & & 156 & -22L \\ & & & 4L^2 \end{bmatrix}$$
 (2)

Where,

A = cross-sectional area and W = mass density

The mass matrix in Eq.2 is obtained for the local coordinates of the element. To transfer it to a global structure coordinate system a transformation matrix must be used. The planar transformation matrix is given in Eq.3. [3, 8]

$$R = \begin{bmatrix} Cos(\theta) & Sin(\theta) & 0 & 0 & 0 & 0 \\ -Sin(\theta) & Cos(\theta) & 0 & 0 & 0 & 0 \\ 0 & 0 & 1 & 0 & 0 & 0 \\ 0 & 0 & 0 & Cos(\theta) & Sin(\theta) & 0 \\ 0 & 0 & 0 & -Sin(\theta) & Cos(\theta) & 0 \\ 0 & 0 & 0 & 0 & 0 & 1 \end{bmatrix}$$
(3)

Here;

$$Cos(\theta) = \frac{x_{j} - x_{i}}{L} \tag{4}$$

$$Sin(\theta) = \frac{Y_j - Y_i}{L} \tag{5}$$

The global frame element mass matrix is obtained by multiplying the transpose of the transformation matrix by the local mass matrix and then multiplies the result by the transformation matrix itself, as given in Eq.6.

$$M_{e.g.}^{frame} = [R^T].[M_{e.l.}^{frame}].[R]$$
(6)

Here,

 $M_{e.g.}^{\text{frame}}$ : Frame element global mass matrix.

 $R^T$ : Transposition of the transformation matrix.

 $M_{e.l.}^{\text{frame}}$ : Frame element local mass matrix.

#### 2.2. Shear Wall Elements Mass Matrix

The shear wall element is analyzed as a rectangular stress element. A special formulation presented by Öztorun is used to analyze rectangular stress elements in YAY2020 program. Figure 2 shows the plane stress rectangular element with four nodes and three degrees of freedom at each node (1 rotation and 2 displacements). The plane stress element mass matrix is given in Table 1.

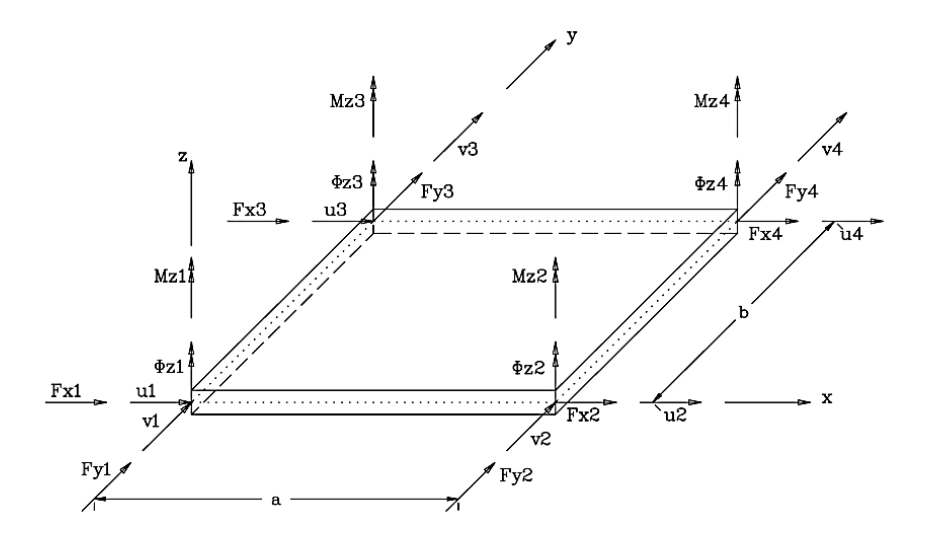


Figure 2. Generalized forces and displacements for finite plate elements for plane stress problems [1]

Table 1. Stiffness matrix of plane stress element [1]

$\Delta^{\mathrm{T}}$	$\Delta_{X1}$	$\Delta_{Y1}$	$\theta_{Z1}$	$\Delta_{X2}$	$\Delta_{Y2}$	$\theta_{Z2}$	$\Delta_{X3}$	$\Delta_{Y3}$	$\theta_{Z3}$	$\Delta_{X4}$	$\Delta_{Y4}$	$\theta_{Z4}$
I/J	1	2	3	4	5	6	7	8	9	10	11	12
1	$M_{S_{1,1}}$	0	$M_{S_{1,3}}$	$M_{S_{1,4}}$	0	$M_{S_{1,6}}$	$M_{S_{1,7}}$	0	$M_{S_{1,9}}$	$M_{S_{1,10}}$	0	$M_{S_{1,12}}$
2		$M_{S_{1,1}}$	$M_{S_{2,3}}$	0	$M_{S_{1,7}}$	$M_{S_{2.6}}$	0	$M_{S_{1,4}}$	$M_{S_{2,9}}$	0	$M_{S_{1,10}}$	$M_{S_{2,12}}$
3			$M_{S_{3,3}}$	$M_{S_{1,6}}$	$-M_{S_{2,6}}$	$M_{S_{3,6}}$	$-M_{S_{1,9}}$	$M_{S_{2,9}}$	$M_{S_{3,9}}$	$-M_{S_{1,12}}$	$-M_{S_{2,12}}$	$M_{S_{3,12}}$
4			2,2	$M_{S_{1,1}}$	0	$M_{S_{1/3}}$	$M_{S_{1,10}}$	0	$M_{S_{1,12}}$	$MS_{1.7}$	0	$MS_{1.9}$
5				-,-	$M_{S_{1,1}}$	$-M_{S_{2,3}}$	0	$M_{S_{1,10}}$	$-M_{S_{2,12}}$	0	$M_{S_{1,4}}$	$-M_{S_2}$
6					-,-	$M_{S_{3,3}}$	$-M_{S_{1,12}}$	$M_{S_{2,12}}$	$M_{S_{3-12}}$	$-M_{S_{1,9}}$	$-M_{S_{2,9}}$	$M_{S_{3,0}}$
7						-,-	$M_{S_{1,1}}$	0	$-M_{S_{1,3}}$	$M_{S_{1,4}}$	0	$-M_{S_1}$
8							-,-	$M_{S_{1,1}}$	$M_{S_{2,3}}$	0	$P_{1,7}$	$M_{S_{2,6}}$
9								-,-	$M_{S_{3,3}}$	$-M_{S_{1,6}}$	$-M_{S_{2,6}}$	$M_{S_{3,6}}$
10		SYMMI	ETRIC						2,2	$M_{S_{1,1}}$	0	$-M_{S_1}$
11										-,-	$M_{S_{1,12}}$	$-M_{S_2}$
12											-,	$M_{S_{3,3}}$

Plane stress element mass matrix parameters are given as follows: [1]

$$\begin{split} K_S &= \frac{\rho_S.\,a.\,b.\,t_S}{176400} \\ M_{S_{1,1}} &= K_S\,.\,21840 \\ M_{S_{1,6}} &= -K_S\,.\,1540.\,b \\ M_{S_{1,10}} &= K_S\,.\,3780 \\ M_{S_{2,6}} &= -K_S\,.\,1820.\,a \\ M_{S_{3,3}} &= K_S\,.\,560.\,(a^2 + b^2) \\ M_{S_{3,12}} &= -K_S\,.\,210.\,(a^2 + b^2) \\ M_{S_{1,3}} &= -K_S\,.\,3080.\,b \\ M_{S_{1,7}} &= K_S\,.\,7560 \end{split}$$

$$\begin{split} &M_{S_{1,12}} = K_S .910.\, b \\ &M_{S_{2,9}} = K_S .1540.\, a \\ &M_{S_{3,6}} = K_S .140.\, (-3a^2 + 2b^2) \\ &M_{S_{1,4}} = K_S .10920 \\ &M_{S_{1,9}} = K_S .1820.\, b \\ &M_{S_{2,3}} = K_S .3080 \\ &M_{S_{2,12}} = -K_S .910.\, a \\ &M_{S_{3,9}} = K_S .140.\, (2a^2 - 3b^2) \end{split}$$

Sabah et al.

## 2.3. Equation of Motion of the Dynamical System

The system has mass, stiffness, and damping and has movement in just u direction is called a single degree of freedom (Figure 3). According to Newton's second law of motion, the equation of motion of this system is written as Eq.7 [10].

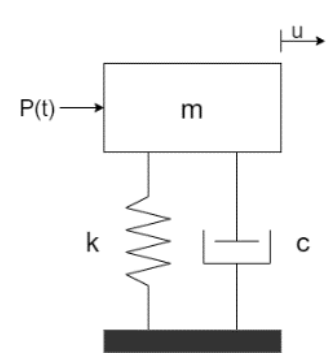


Figure 3. Single degree of freedom system

$$m\ddot{u} + c\dot{u} + ku = -m\ddot{u}_q \text{ or } p(t) \tag{7}$$

Where;

*u* : Displacement vector

 $\dot{u}$ : Velocity vector

 $\ddot{u}$ : Acceleration vector

 $\ddot{u}_q$ : Ground motion acceleration vector (Earthquake data)

m: System mass

*k* : System stiffness

c: System damping

p(t): Dynamic load



Time history analysis was performed in YAY2020 software using the Newmark method. Newmark method depends on numerical integration methods to solve Eq.7. In systems of multi-degree freedom, there is a mode that corresponds to each degree of freedom. To consider these modes and study structure as a single part, the equation of motion should be written as Eq.8 [3-8, 10].

$$\Phi^{T} m \Phi \ddot{q} + \Phi^{T} c \Phi \dot{q} + \Phi^{T} k \Phi q = -\Phi^{T} m [\ddot{u}_{q}(t) \quad or \quad \Phi^{T} p(t)$$
(8)

Eq.8 can be written also as Eq.9.

$$M\ddot{q} + C\dot{q} + Kq = F(t) \tag{9}$$

Here.

M: Modal mass matrix

**K:** Modal stiffness matrix

**C:** Modal damping matrix

q: Modal displacement vector

**I:** The identity matrix equal in size with the system degree of freedom

The modal matrices M, K, and C here are diagonal matrices. Meanwhile, m, k, and c system matrices have both diagonal and non-diagonal elements

In the Newmark numerical calculation method, the displacement and velocity changes by the time  $\Delta t$  according to Taylor's series are given in Eqs. 10 and 11.

$$u_t = u_{t-\Delta t} + \Delta t \dot{u}_{t-\Delta t} + \frac{\Delta t^2}{2} \ddot{u}_{t-\Delta t} + \frac{\Delta t^3}{6} \ddot{u}_{t-\Delta t} + \cdots$$

$$\tag{10}$$

$$\dot{u}_t = \dot{u}_{t-\Delta t} + \Delta t \ddot{u}_{t-\Delta t} + \frac{\Delta t^2}{2} \ddot{u}_{t-\Delta t} + \cdots$$
(11)

Newmark abbreviated Eq.10 and Eq.10 by using  $\beta$  and  $\gamma$  Newmark constants as Eqs.12 and 13.

$$u_t = u_{t-\Delta t} + \Delta t \dot{u}_{t-\Delta t} + \frac{\Delta t^2}{2} \ddot{u}_{t-\Delta t} + \beta \Delta t^3 \ddot{u}_{t-\Delta t}$$
(12)

$$\dot{u}_t = \dot{u}_{t-\Delta t} + \Delta t \ddot{u}_{t-\Delta t} + \gamma \Delta t^2 \ddot{u}_{t-\Delta t} \tag{13}$$

The acceleration equation can be written in Eq.14 assuming that the acceleration is linear in the time step.

$$\ddot{u}_t = \frac{(\ddot{u}_t - \ddot{u}_{t - \Delta t})}{\Delta t} \tag{14}$$

If Eq.14 is written in Eq.12 and Eq.13 the standard form of Newmark equations is obtained as Eqs.15 and 16.

$$u_t = u_{t-\Delta t} + \Delta t \dot{u}_{t-\Delta t} + (\frac{1}{2} - \beta) \Delta t^2 \ddot{u}_{t-\Delta t} + \beta \Delta t^2 \ddot{u}_t$$
(15)

$$\dot{u}_t = \dot{u}_{t-\Delta t} + (1 - \gamma)\Delta t \ddot{u}_{t-\Delta t} + \gamma \Delta t \ddot{u}_{t-\Delta t} \tag{16}$$

Displacements, velocities, and accelerations of each node of the system are obtained by iteration of the last two equations by the time.

## 2.5. Shear Building Analysis

The type of structure that is expected to move only horizontally under various static or dynamic loads without rotation of a horizontal section on the floor level is called Shear Building. It's also a type of idealization of a building to resist only shear forces without any bending as shown in Figure 4.

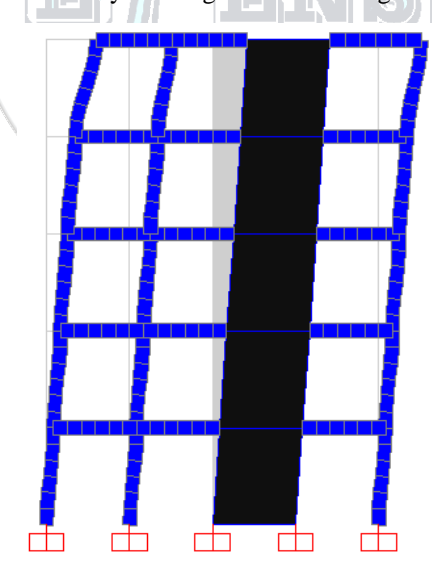


Figure 4. Shear building system example

This method is a quick method for determining the dominant period of structures. It is based on calculating the mass and stiffness of each floor separately and obtaining the general mass and stiffness matrices of the structure. The mass and stiffness matrices of a 5-storey shear structure like shown in Figure 4 are written as Eqs.17 and 18, respectively [14].

28 Sabah et al.

$$M_{sis} = \begin{bmatrix} m_1 & 0 & 0 & 0 & 0 \\ 0 & m_2 & 0 & 0 & 0 \\ 0 & 0 & m_3 & 0 & 0 \\ 0 & 0 & 0 & m_4 & 0 \\ 0 & 0 & 0 & 0 & m_5 \end{bmatrix}$$

$$(17)$$

$$M_{sis} = \begin{bmatrix} m_1 & 0 & 0 & 0 & 0 \\ 0 & m_2 & 0 & 0 & 0 \\ 0 & 0 & m_3 & 0 & 0 \\ 0 & 0 & 0 & m_4 & 0 \\ 0 & 0 & 0 & 0 & m_5 \end{bmatrix}$$

$$K_{sis} = \begin{bmatrix} k_1 + k_2 & -k_2 & 0 & 0 & 0 \\ -k_2 & k_2 + k_3 & -k_3 & 0 & 0 \\ 0 & -k_3 & k_3 + k_4 & -k_4 & 0 \\ 0 & 0 & -k_4 & k_4 + k_5 & -k_5 \\ 0 & 0 & 0 & -k_5 & k_5 \end{bmatrix}$$

$$(17)$$

Here,

 $M_{sis}$ : System mass matrix

 $K_{sis}$ : System stiffness matrix

 $m_i$ : Total mass of i floor

 $k_i$ : Total stiffness of i floor

#### 2.6. Wide Column Analysis

A wide column is an easy method to analyze structure without using shear wall formulations. It depends on replacing the shear wall with a wide column that has the same rigidity and mass as the shear wall and places rigid beams at each floor level as shown in Figure 5.

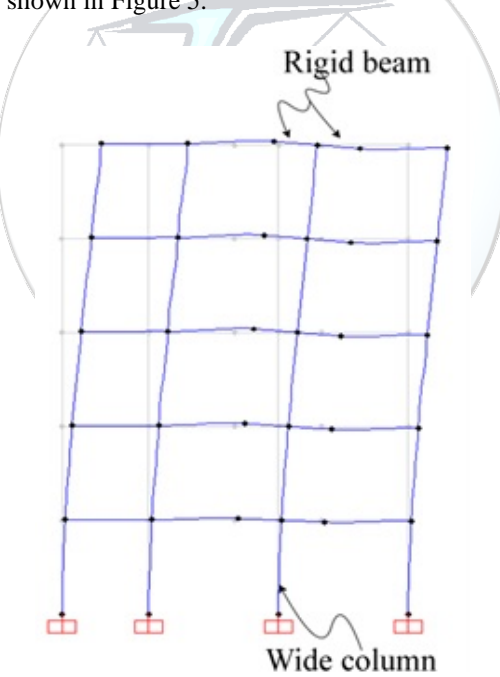


Figure 5. Wide column system example

## 3. RESULTS AND DISCUSSION

In this section, some examples will be solved dynamically using YAY2020 and compared with SAP2000.

#### 3.1. Shear Wall-Frame Structure

A 3-storey 4-span shear wall-frame structure is analyzed by YAY2020 (Figure 6). All storey heights are h = $350 \ cm$  and span distance  $L = 300 \ cm$ . Shear walls are located between the 3rd and 4th axes. The properties of all frame elements are the same and they are square in shape. Frame elements cross sectional-area A = $2500 \text{ cm}^2$ , Modulus of elasticity  $E = 13025000 \text{ N/cm}^2$ , a moment of inertia  $I = 520833.33 \text{ cm}^4$  and mass

per unit volume  $\rho = 0.00025 \, kg/cm^3$ . Shear wall elements have the same modulus of elasticity and mass per unit volume of frame elements. Shear wall elements thickness  $t = 50 \, cm$  and Poisson ratio v = 0.2. A  $1000 \, N$  single loads applied on the top-left and top-right points of the structure. Figure 7 shows the results of the time history analysis of the shear wall-frame structure as a displacement-time graph of joint 20 in x-direction under the Chūetsu 6.6 magnitude earthquake which happened in Japan in 2007. The obtained modal analysis result by YAY2020 and Sap2000 are given in Table 2. The table shows that YAY2020 can find 45 modes meanwhile; the SAP2000 can just find 30 modes.

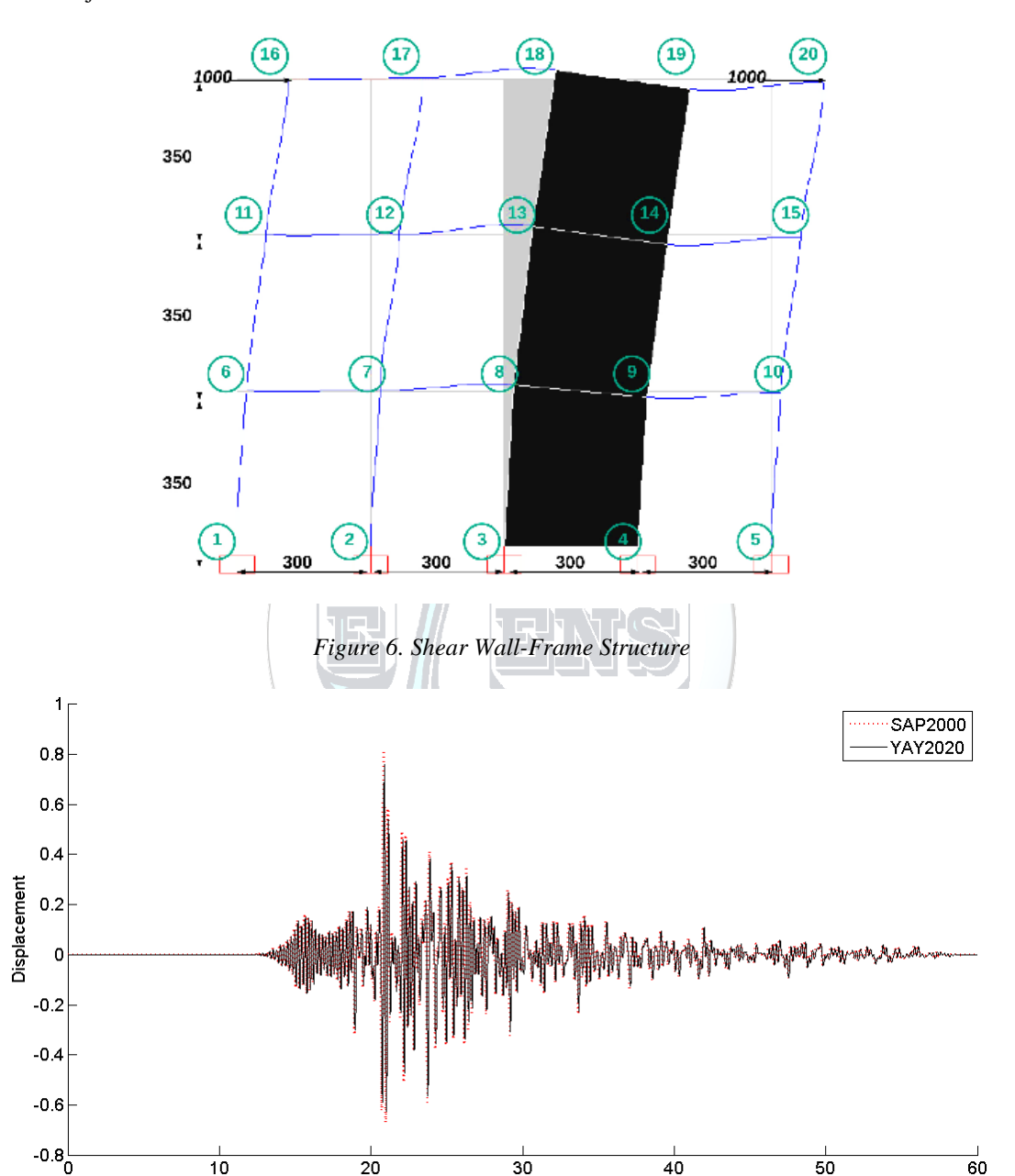


Figure 7. Shear wall-frame structure displacement-time graph

Time

30 Sabah et al.

Table 2. Modal analysis of the shear wall-frame structure

SAP2000 – Modal analysis						YAY	2020 - Mod	lal analysi	S
Mode	Period	Frequenc	Angular <sup>y</sup> frequency	Eigenvalues	Mode	Period	Frequency	Angular	Eigenvalues
			frequency				/	frequency	
No	sec	cyc/sec	rad/sec	rad2/sec2	No	sec	cyc/sec	rad/sec	rad2/sec2
1 2	0.23965 0.06172	4.17 16.20	26.22 101.80	687.40 10363.00	1 2	0.2365 0.0798	4.23 12.52	26.56 78.69	705.65 6191.98
3	0.05064	19.75	124.09	15397.00	3	0.0798	18.06	113.45	12871.27
4	0.03004	22.19	139.45	19446.00	4	0.0334	20.50	128.78	16583.93
5	0.04300	22.19	139.43	19884.00	5	0.0488	24.11	151.47	22943.98
6	0.04430	24.93	156.66	24543.00	6	0.0413	24.11	154.25	23794.06
7	0.04011	26.26	164.97	27214.00	7	0.0407	25.54	160.45	25745.63
8	0.03180	31.45	197.59	39040.00	8	0.0332	29.47	185.19	34296.32
9	0.03180	35.75	224.64	50464.00	9	0.0339	30.63	192.44	37032.71
10	0.02797	38.63	242.71	58910.00	10	0.0327	32.00	201.09	40436.20
11	0.02389	49.06	308.24	95012.00	11	0.0312	32.65	201.09	40430.20
12	0.02038	50.49	317.24	100640.00	12	0.0300	34.14	203.13	46007.44
13	0.01981	51.99	326.64	106690.00	13	0.0293	39.32	247.06	61039.49
13	0.01924	58.12	365.16	133340.00	13	0.0234	39.32 41.77	262.47	68888.93
15	0.01721	58.12	365.16	133950.00	15	0.0239	44.82	281.64	79322.14
16	0.01717	58.23	366.35	134220.00	16	0.0223	48.59	305.32	93219.59
17	0.01713	62.30	391.42	153210.00	17	0.0200	52.08	303.32	107082.83
18	0.01603	66.09	415.27	172450.00	18	0.0192	57.20	359.39	129157.94
19	0.01313	68.01	427.32	182600.00	19	0.0173	58.82	369.58	136591.09
20	0.01470	69.68	427.32	191680.00	20	0.0170		383.95	130391.09
20	0.01433	69.85	437.82	191680.00	21	0.0164	68.61	431.06	185811.85
22	0.01432	76.04	477.78	228270.00	22	0.0140	70.38	442.20	195536.48
23	0.01313	76.04	488.82	238950.00	23	0.0142	70.38	458.03	209794.57
23 24	0.01283	80.15	503.61	253630.00	23 24	0.0137	74.33	458.03	218111.60
25	0.01248	80.13	503.79	253810.00	25	0.0133	78.71	494.52	244554.70
25 26	0.01247	83.54	524.89	275510.00	$\frac{23}{26}$	0.0127	79.05	494.32	244534.70
27	0.01197	89.26	560.86	314560.00	27	0.0127	83.72	526.05	276732.32
28	0.01120	90.50	568.64	323360.00	28	0.0119	89.25	560.75	314445.91
28 29	0.01103	101.96	640.62	410400.00	29	0.0112	91.19	572.95	328270.69
30	0.00981	116.48	731.88	535640.00	30	0.0110	96.59	606.92	368355.92
30	0.00839	110.40	/31.00	333040.00	31	0.0104	96.39	608.31	370036.87
					32	0.0103	102.68	645.13	416195.93
					33	0.0097	102.08	697.06	485895.27
					34	0.0090	117.96	741.16	549313.12
					35		120.35		
					36	0.0083 0.0075	134.11	756.16 842.62	571784.18 710005.68
					37	0.0073	134.11	867.40	752382.60
					38	0.0072	158.03	956.93	915721.14
					38 39	0.0059	168.39	1058.01	1119385.88
					40	0.0039	196.84	1236.81	1529695.64
					40	0.0051	200.00		1579119.41
					42	0.0030	206.24		1679246.66
					42	0.0048	208.24		1716941.94
					43 44	0.0048	208.54		2105302.50
					45	0.0043	300.63		3567881.43
					+3	0.0055	500.03	1000.00	3307001.43

#### 3.2. Period-Based Comparison of Shear Building and Wide Column

A 5-story planar shear wall-frame system which is shown in Figure 4 adopted to study.

Table 3. Period analysis-based comparison of the normal FEM, shear building, and wide column methods

Mode	Normal FEM		Wide C	Column	Shear building		
number	YAY2020	SAP2000	YAY2020	SAP2000	YAY2020	SAP2000	
1	0.48545	0.49573	0.47530	0.50270	0.50559	0.51791	
2	0.13537	0.12554	0.11294	0.12730	0.17419	0.17843	
3	0.10084	0.07821	0.07723	0.07825	0.11179	0.11452	
4	0.07569	0.07005	0.06807	0.07022	0.08861	0.09077	
5	0.06379	0.06517	0.06001	0.06517	0.07951	0.08145	
6	0.06220	0.06092	0.05429	0.06076			
7	0.05564	0.05791	0.04881	0.06001			
8	0.04458	0.04064	0.03564	0.04266			
9	0.03848	0.03692	0.03460	0.03779			
10	0.03543	0.03243	0.03135	0.03150			
Max. mode No.	75	50	60	40	5	5	

All floors' height is 350 cm. All elements Modulus of elasticity =  $3180098.312\ N/cm^2$ , Poisson ratio v=0.2 and unit volume mass of concrete  $\rho=0.00025\ kg/cm^3$ . All frame elements cross sectional-area  $A=2500\ cm^2$  and moment of inertia =  $520833.33\ cm^4$ . Table 3 comparing the first system 10 periods calculated with normal FEM, wide column, and shear building analyzing methods.

#### 4. CONCLUSIONS

In the modal analysis, YAY2020 can find more modes than SAP2000. Since SAP2000 isn't added the angular rotation perpendicular to the plate into the calculation of shear wall stiffness and mass matrices and the system mass matrix has just diagonal elements. These reasons decreased the degree of freedom of the system causing decreased mode's number.

The displacement values calculated by YAY2020 are lower than those calculated by SAP2000 because YAY2020 uses a full stiffness matrix, which a little bit increased the rigidity of the structure.

The modal analysis values obtained using a wide column are close to the values obtained using a regular shear wall. Because the wide column and shear building have the same mass and stiffness values. So, building mass and stiffness matrices are preserved as a whole.

Shear building analysis quickly gives the dominant period of the structure and this value is close to the real one.

## **ACKNOWLEDGMENTS**

This paper is prepared using the data of the master thesis titled "Behavior of High-Rise Planar Shear-Wall-Frame Structures under Dynamic Loads" by Ragib Sabah. The thesis is supervised by Prof. Namik Kemal Öztorun. The other author, Baris Sayin, put a lot of effort into organizing data, conceptualizing, methodology, writing-reviewing, and editing.

#### **BIOGRAPHY**

Ragib Sabah was born in 1993. He is also known as Ragheb Alsabbagh. In 2014 Mr. Sabah started his undergraduate degree in the Civil Engineering Department at Pamukkale University in Turkey and graduated in 2018 with high honor degree. In 2021, Mr. Sabah completed his master's degree at Istanbul University-Cerrahpasa. He is interested in computational sciences, applicable technology, and management areas.

32 Sabah et al.

#### REFERENCES

[1]. Öztorun N.K., (2006) "A rectangular finite element formulation", Finite Elem. Anal. Des. 42 (12), 1031–1052.

- [2]. Öztorun N.K., (2007) *Reply to "discussion on: 'Rectangular finite element formulation"*, Finite Elements in Analysis and Design 43, 733 736.
- [3]. Ed. Wilson, (2002) "Three-Dimensional Static and Dynamic Analysis of Structures", Computers and Structures Inc. University of California, Berkeley, USA.
- [4]. Computers and Structures, Inc. (2016) "SAP2000 CSI Analysis Reference Manual, Structural Analysis Program", California, Berkeley, USA.
- [5]. Ed. Wilson, (1991) "Computer Assisted Learning of Static and Dynamic Analysis of Structural Systems user's manual", University of California, Berkeley, USA.
- [6]. Ed. Wilson, E. Ray, W. Clough, (1952) "Dynamic response by step-by-step matrix analysis", Computers in Civil Engineering Symposium.
- [7]. Ed. Wilson, Bathe K.J., L. Farhoomand, (1973) "Nonlinear dynamic analysis of complex structures", earthquake engineering and structural dynamics, 1, 241-252
- [8]. Bathe K.J., (2014) "Finite Element Procedures Second edition", Prentice-Hall, Pearson Education, Inc. 978-0-9790049-5-7.
- [9]. Newmark, (1959) "A method of computation for structural dynamics", Engineering Mechanics Division. 2094.
- [10]. Chopra, A.K, (1995) "Dynamics of Structures: Theory and Applications to Earthquake Engineering", Prentice-Hall, Englewood Cliffs, New Jersey, ISBN: 0-13-855214-2.
- [11]. E., Öztorun, 2020, "Köprülerin Deprem Etkileri Altındaki Davranışları", Thesis (PhD), Istanbul University.
- [12]. E., Öztorun, N.K., Öztorun ve C., Alhan 2019, "Yapıların Düşey Deprem Etkisi Altındaki Davranışları: Bir Köprü Örneği", 21. Ulusal Mekanik Kongresi, 02-06 Eylül. 2019, Niğde Ömer Halisdemir Üniversitesi, Niğde, 57-65.
- [13]. Timoshenko S., Goodier J.N., (1951) "Theory of Elasticity", McGraw-Hill, New York.
- [14]. Paz M., Leigh W., (1991) "Structural Dynamics", Kluwer Academic Publishers Springer Science Business Media Dordrecht.
- [15]. Adams J. C., Brainerd W.S., Martin J.T., Smith B.T., Wagener J.L., (1992) "Fortran 90 Handbook", Library of Congress Catalog Card Number 91-77211.

# Taxidermy effluent characterisation: A case study in the City of Tshwane

Anoesjka Masilela 1\*, Martie A.A Coetzee 2, Lizzy Mpenyana-Monyatsi3

<sup>1,2,3</sup> Department of Environmental, Water and Earth Sciences, Faculty of Sciences, Tshwane University of Technology, P/B X 680, Pretoria, 0001, South Africa

\*Corresponding Author email: anoesjkam@gmail.com

Publication Info Abstract

South Africa is a well-known destination for both domestic and international trophy hunters. Taxidermies, which are mainly located near hunting farms, process the carcasses of hunted animals to produce game trophies. Processing of skins and skulls produce effluents containing chemicals which could pose environmental risks. Furthermore, data about the quantity and quality of taxidermy effluents are scarce. This study focused on a taxidermy workshop on the outskirts of Tshwane, South Africa, that discharged its effluent into an evaporation pond known to emit bad smell. Over a two-year period, COD, chrome, chloride, fats and oils, sulfates, salt, pH and electrical conductivity were measured in the effluents from the various processes. During the same time period, the volumes of water used in each of the treatment processes were calculated. The concentrations of pollutants in the final effluent were determined using a mass balance approach. The concentration of major pollutions in the effluent were as follows: 11 035.60 mg O<sub>2</sub>/L (COD), 469.78 mg Cr/L, 1 635.79 mg fats and oils /L. The pH and electrical conductivity ranged between pH 3.2 - 7.9 and 120 - 9 741 mS/m, respectively. The volume of the effluent produced was ca 34 m3/a, which resulted in mass loads of 372.34 kg COD/a, 15.85 kg Cr/a, and 55.19 kg fats and oils/a. If these pollutants were discharged into a large waterbody, they would be diluted, however the high concentrations of COD, fats and oils, and Cr pose serious environmental risks. The high COD, fat, and oil concentrations below the effluent outfall would result in anaerobic conditions which might harm the aquatic environment. Chromium (III) could accumulate to toxic levels in the environment. As a result, it is recommended that the effluent be treated to remove fats and oils and to reduce COD and chromium levels.

## **Key words**

Taxidermy effluent, Production of animal trophies, Water pollution

#### 1. INTRODUCTION

South Africa has a significant number of different wild animal species which can be hunted, making it a popular destination for foreign trophy hunters. According to the Professional Hunters Association of South Africa (PHASA) about 7 500 foreign hunters visited South Africa in 2005 [4]. Moreover, based on the results of a survey conducted by PHASA in 2017, 86% of trophy hunters were from the United States of America [11].

The number of hunters was expressed as a percentage and their contribution to the South African economy through trophy hunting had increased to approximately R1,98 billion from R410 million in 2005 ([11],[4]). The trophies are produced from hunted animal carcasses, which are then processed into game trophies at a taxidermy workshop. For display, game trophies are usually fully tanned skins and/or mounts such as full, half, and shoulder in a lifelike manner. This includes the treatment of skulls (bones), horns/antlers, hooves, claws, teeth [12]. Furthermore, the

34 Masilela et al.

taxidermy industry is estimated to contribute approximately R1,5 billion towards the South African wildlife economy, as wildlife hunted elsewhere in Africa is also processed in South Africa [22].

As of 2017, there were 150 registered taxidermies in South Africa, with 80 000 trophies exported [22]. There are 17 registered and active taxidermies in Gauteng [13]. Taxidermies that do not engage in import and export are not required to register with the National Department of Agriculture and Forestry, hence, the total number of taxidermies in South Africa is unknown [15]. Effluents from taxidermies could be high in organic biodegradable matter, dissolved salts, oils and fat and chromium considering the treatment processes and chemicals commonly used to produce these trophies. These taxidermies are usually situated close to game farms, in rural areas or on the outskirts of cities and towns, and are not always connected to wastewater treatment plants. Considering the treatment processes involved in the production of game trophies, effluents from taxidermies pose serious environmental and health risks. The monitoring of effluent being discharged from such facilities is rarely done. Therefore, there is a need to establish the possible impact of taxidermy effluent on the environment and evaluation management options to mitigate risk.

The taxidermy that was investigated is situated in the periphery of the City of Tshwane, in an area where there is no sewer reticulation system. They draw water from a borehole on their premises, which is used at their factory to process game trophies (skulls and skins) as well as for sanitation purposes such flushing toilets and cleaning. The effluent produced from the processing of skins and skulls is currently discharged into an evaporation pond. There is a rotten egg smell emitted from the pond, which may be the source of complaints by neighboring industries. This undesirable condition of the evaporation pond led to a need to investigate and evaluate other management options for the disposal and treatment of the effluent.

The aim of this study was to identify the different processes used in order to characterize the quality of the effluent and determine the mass loads that are discharged by the taxidermy. Knowing the quality and quantity of effluent would assist in evaluating the associated environmental risks and suitability for discharge into the municipal sewer system.

#### 2. MATERIALS AND METHODS

## 2.1. Taxidermy Treatment Processes

Processing of raw game trophies, according to Figure 1, involves different treatment processes. The treatment of game trophies involves washing, curing, and soaking, pre-pickling, shaving and fleshing, post-pickling for all skins. The treatment process following pre-pickling may differ depending on the skin type to be processed either mount or flat skin. For flat skins, post-pickling is followed by degreasing and chrome tanning. With mounts, post-pickling is followed by tanning without the use of chrome salts. Horns, bones and heads undergo a different form of treatment which is boiling in water at 30 °C to remove the remaining skin and fats after shaving, followed by bleaching in a bleach solution. After bleaching, the skulls are scrubbed in a solution of soap and water. This process is known as washing [12].

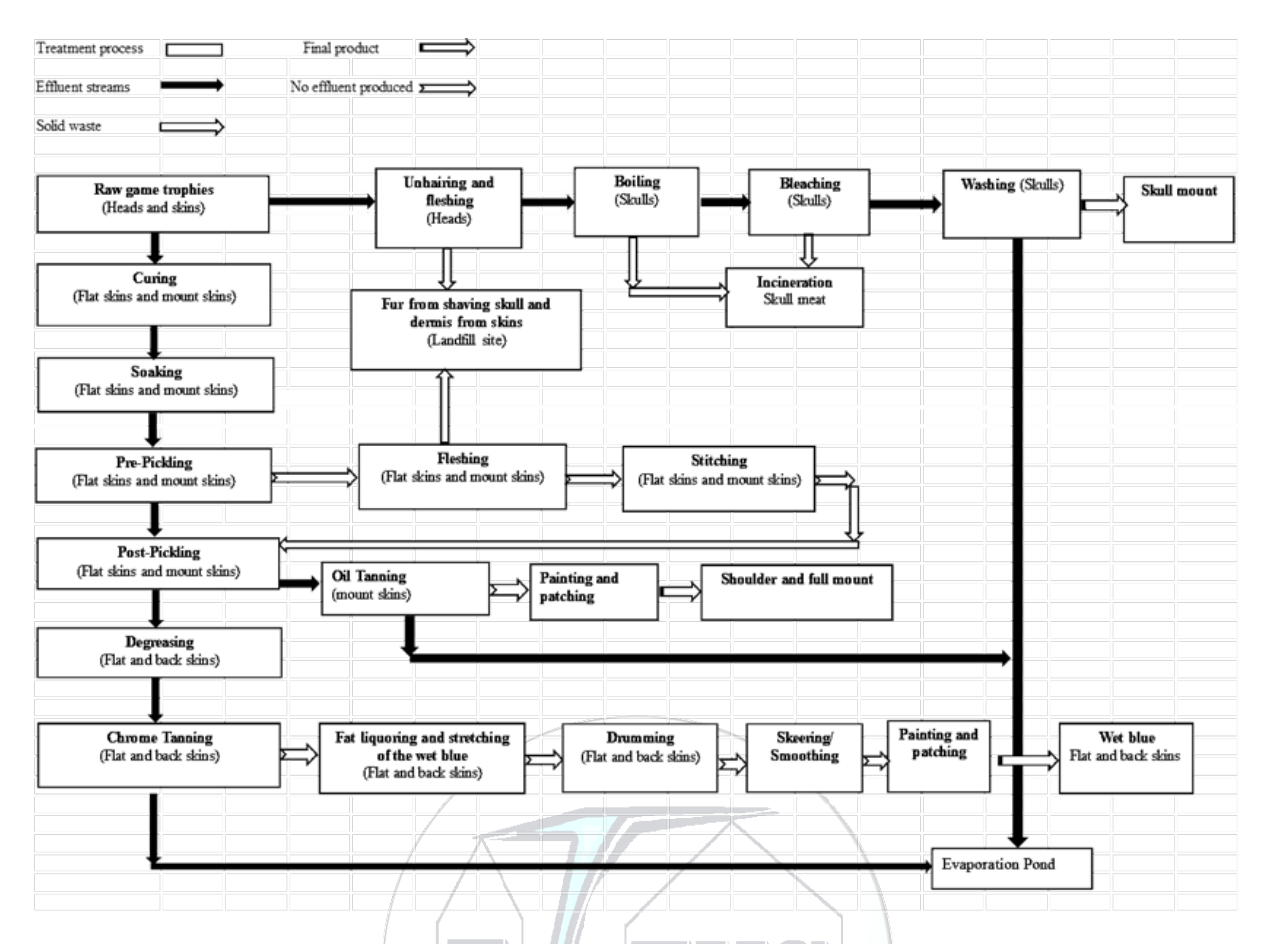


Figure 1: Flow diagram of effluent generation during treatment of game trophies (heads and skins) at a taxidermy

|--|

Process	Chemicals					
	Skins					
Curing	Sodium Chloride					
Soaking	Sodium Chloride washed out of cured hides and skins					
	Detergent which was discontinued					
Pre-pickling	Sodium Chloride					
	Formic Acid					
Post-pickling	Sodium Chloride					
	Formic Acid					
Oil Tanning	Sodium Chloride					
	Eskatan GLH Liquid (synthetic fatliquor)					
Degreasing	Bicarbonate of soda					
	Gelcon PK Degreaser Conc					
	Sodium chloride					
Chrome Tanning	Aluminum Sulfate					
	Chromosol B (chrome (III) sulfate)					
	Eskatan GLH Liquid					
	Lutan FN (aluminum complex salt)					
	Sodium Chloride					
	Skulls					
Boiling	Sodium Chloride					
Bleaching	Hydrogen peroxide (Bleach)					
Washing	Detergent					

36 Masilela et al.

#### 2.2 Assessing the water quality of the effluent produced by the taxidermy

Effluent samples from soaking, pre-pickling, post-pickling oil tanning, degreasing, chrome tanning, boiling, bleaching and washing processes were collected weekly, bi-weekly and monthly for a period of two years

The final concentration of each parameter from the total discharge of all the processes was calculated (Equation 1) based on the mass loads discharged (Equation 2) by the different processes and the total volume.

$$Effluent\ concentration\left(\frac{mg}{L}\right) = \frac{Average\ mass\ discarged\ per\ annum, mg}{Average\ total\ volume\ discharge\ per\ annum, L}\ .....(1)$$

The mass load was calculated as follows:

Average mass of parameter discharged, 
$$\frac{mg}{annum} = C_P x V_P$$
 .....(2)

 $C_P$  = average concentration of a parameter, mg/L, discharged from a process

V<sub>P</sub> = average volume discharged from a process, L/annum

or expressed in kg/annum:

$$Mass in \frac{kg}{annum} = \frac{mass in mg}{10^6}$$
 (3)

## 2.3 Calculation for the volume of effluent produced by the taxidermy

Processing of the skins and skulls were done in batches. The volume of effluent discharged per cycle of taxidermy treatment process was done by measuring the dimensions of each container (or bath) used in a unit process. The height of liquid that would be remaining within the bath after the treatment was then used to determine the volume to be discharged. The frequency of discharging the liquors into the evaporation dams varies from process to process. Soaking liquors are discharged after 24 hours, pre-pickling and post pickling could be discharged once in 6 months and sometimes once a year, oil tanning liquor is discharged at a similar frequency as the pickling process liquors, degreasing liquor is discharged after 24 hours and chrome tanning once in two weeks to a month.

The following calculations was used to determine the effluent discharged  $\pi x r^2 x h$  and (L x W) x h.

## 2.4 Sample analysis

## Methods used to analyse the parameters of concern

#### **Determination of Ammonia, Chlorides Orthophosphates and Sulphates**

Standard Methods for the Examination of Water and Wastewater (APHA., 2012: 2-34, 4-110, 4-76, 4-153, 4-191) Thermo Scientific Aquakem 250 Instrument

#### **Determination of Chromium and Sodium**

Optical Emission Spectrometer 5300 DV Instrument, Standard Methods for the Examination of Water and Wastewater (APHA., 2012: 3-69,97)

**Determination of Chemical oxygen demand** 

Open Reflux Method (APHA., 2012: 5-20)

**Determination of Electrical Conductivity and Ph** 

Measured onsite with a multi meter Hatch HQ40d

**Determination of Fats and Oils** 

Partition-Gravimetric Method (APHA., 2012:5-45)

## 3. RESULTS AND DISCUSSIONS

#### 3.1 Volume of water used by the taxidermy

The volume of water used annually was calculated based on the dimensions and frequency of effluent discharge from each batch (Table 4). For the period (May 2016 - April 2018) the taxidermy processed 2 248 skins and 1 125 skulls as shown in Figure 2.

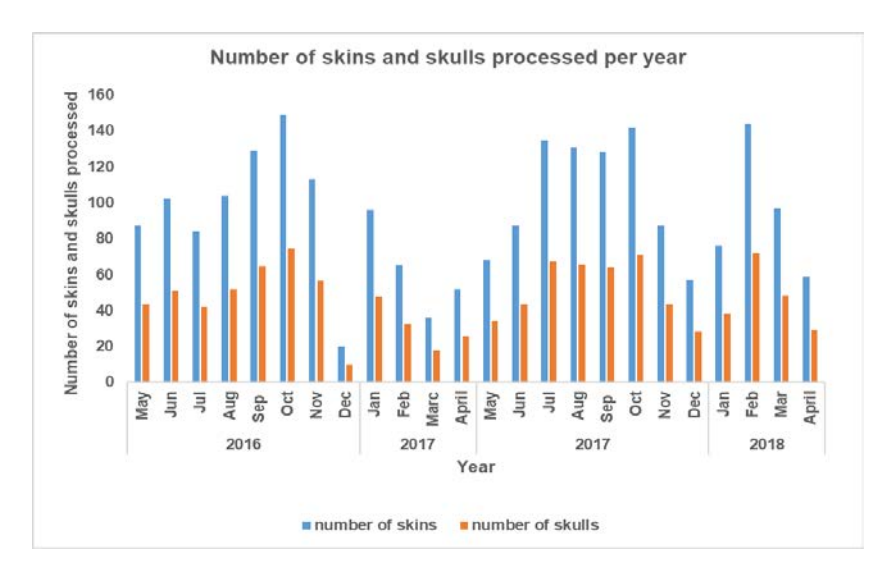


Figure 2: Number of skins and skulls processed between May 2016 and April 2018

\_\_\_\_\_

The volume of effluent discharged into the evaporation pond was determined by the number of skins and skulls produced during the effluent monitoring period. Each process generated the following volume of effluent annually: soaking 1.  $75\pm0.27$  m³, pre-pickling  $1.16\pm0.001$  m³, post-pickling  $1.02\pm0.001$  m³, oil tanning  $1.12\pm0.001$  m³, degreasing  $1.10\pm0.12$  m³, chrome tanning  $4.72\pm0.37$  m³, boiling  $16.86\pm1.85$  m³, bleaching  $3.15\pm1.06$  m³ and washing  $2.86\pm0.31$  m³ (Table 2).

Table 2: Volume of effluent produced per annum at the taxidermy

Process	Number of skins produced per annum	Effluent produced per annum (m³)	
	Skins		
Soaking	1 124±123	1. 75±0.27	
Pre-pickling	1 124±123	1.16±0.001	
Post-pickling	1 124±123	1.02±0.001	
Oil Tanning	337±37	1.12±0.001	
Degreasing	787±86	$1.10\pm0.12$	
<b>Chrome Tanning</b>	787±86	$4.72\pm0.37$	
Total for skins	1124±123 10.87±0.76		
	Skulls		
Boiling	562±62	16.86±1.85	
Bleaching	562±62 3.15±1.06		
Washing	562±62 2.86±0.31		
Total for skulls	562±62 22.87±3.22		
<b>Total for Taxidermy</b>	1989±183	33.74±3.98	

# 3.2 Assessing the water quality in each production process

Figures 3-8 shows the average mass load of the parameters assessed in the effluents from the various skin/skull treatment processes during the sampling period. While Figure 9-10 show the average concentration of the pH and electrical conductivity measured during the sampling period.

# Chemical oxygen demand (COD)

Chemical oxygen demand is defined as the oxygen required to breakdown complex organic compounds into simple intermediate compounds [1]. The average chemical oxygen demand concentration of the taxidermy treatment processes which were above 5 000 mg  $O_2/L$  were as follows, pre-pickling 15 028±3 742.12 mg  $O_2/L$ , post pickling

38 Masilela et al.

 $16\,720.91\pm4\,072.83$  mg  $O_2/L$ , oil tanning 23  $863.21\pm10\,610.51$  mg  $O_2/L$ , degreasing 23  $272.38\pm7\,937.81$  mg  $O_2/L$ , chrome tanning 21  $799.40\pm10\,071.66$  mg  $O_2/L$ , boiling 8  $479.16\pm3\,432.09$  mg  $O_2/L$ , bleaching 6  $307.42\pm5\,707.74$  mg  $O_2/L$  and washing 5  $974\pm3\,124.07$  mg  $O_2/L$ . The calculated COD concentration in the effluent would be 11 035.60 mg  $O_2/L$  with a mass load of 372.34 kg  $O_2/a$ . The highest COD mass loads in Figure 3 were from, the Boiling  $(142.96\pm57.87\text{kg}\,O_2/a)$ , Chrome Tanning  $(102.91\pm47.55\text{ kg}\,O_2/a)$ , and processes.

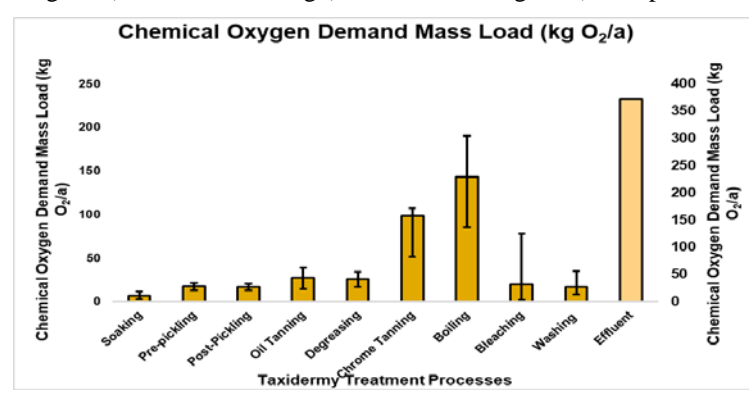


Figure 3: Chemical oxygen demand mass load, kg O2/a, for the skin/skull treatment process

The high concentrations were due to the chemicals added as well as the physical properties of the skins and skulls. The high COD was mainly due to the skulls as they were boiled with some fat attached to them. The oils and fats originated from processing of skulls and skins.

The skins were soaked in Eskatan GLH solution during chrome and oil tanning processes. Eskatan GLH is known as a synthetic fatliquor or tanning oil ([20],[7]). The COD in the pre and post pickling process was mostly caused by the use of formic acid, which is used to preserve the skins and to prepare them for the tanning processes [3]. The degreasing solution contains organic solvents or surfactants (Gelcon PK Degreaser) which composed of nonionic tensides and hexylene glycol. The function of a degreaser is to remove fats and oils from the skins. Because of the degreasing of the skins, the liquors from this process will contain a high chemical oxygen demand concentration [5].

# Nitrogen compounds (Ammonia and Nitrate/Nitrite)

Nitrogen within tanning effluents exists as ammonia and nitrate/nitrite emanating from protein material found in hides [18].

#### Ammonia

The soaking process had the highest ammonia concentration and mass load, at  $74.73 \pm 28.29$  mg N/L and  $0.13 \pm 0.05$  kg N/a, respectively, whereas the other treatment processes had concentrations of less than 1 mg N/L. The calculated final ammonia concentration was 3.95 mg N/L with a total mass load of 0.13 kg N/a.

The high ammonia concentrations in the soaking process (74.73±28.29 mg N/L) could be due to traces of urine, dung and soluble proteins on the game trophy skins. Reference [8] revealed in their study that ammonia is caused by urine on the hides/skins in the effluent of soaking process

#### Nitrate/Nitrite

The nitrate/nitrite concentration during soaking, pre-pickling, post-pickling, oil tanning, degreasing, chrome tanning, boiling, bleaching and washing was found to be less than 1 mg N/L. The calculated final nitrate/nitrite concentration was 0.15 mg N/L with a mass load of 0.01 kg N/a.

#### Ortho-phosphate

Ortho-phosphate is most commonly found in detergents, which are widely used in taxidermy effluent treatment processes. As shown in Figure 4, orthophosphate mass loads were all less than 1 kg P/a while the ortho-phosphate concentration for the skin treatment processes which was above 8 mg P/L were: soaking  $18.64\pm5.63$  mg P/L, prepickling  $17.61\pm1.28$  mg P/L, post-pickling  $29.23\pm25.87$  mg P/L, for skins, while for skulls it was from the boiling  $15.18\pm5.82$  mg P/L. With a mass load of 0.35 kg P/a, the calculated orthophosphate concentration in the effluent was found to be 10.28 mg P/L.

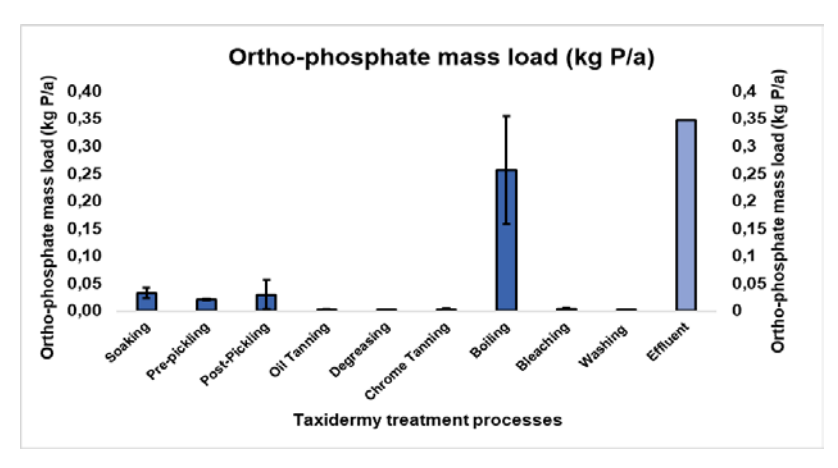


Figure 4: Ortho-phosphate mass load in (kg P/a) for the skins/skull's treatment processes

Soaking and the two pickling processes were the major contributors of ortho-phosphate (from the detergents) to the taxidermy effluent. When the remaining flesh, fats, and oil from the skulls were removed by boiling them in water, a broth was formed. Because bones contain high concentrations of phosphate, this broth contained high phosphate. This was showed in an experiment conducted by Dalby to determine the mineral content of two bones, which yielded the following phosphorus results: 8.9 mg / 240 mL and 12.5 mg / 240 mL [14].

#### Chloride

The chloride in the tanning process liquors yielded the following results for skin treatment: soaking  $16\,799.33\pm1\,971.62\,$  mg Cl<sup>-</sup>/L, pre-pickling  $20\,694.31\pm2\,282.51\,$  mg Cl<sup>-</sup>/L, post pickling  $20\,733.91\pm2\,409.61\,$  mg Cl<sup>-</sup>/L, degreasing  $16\,171.03\pm1\,595.79\,$  mg Cl<sup>-</sup>/L, oil tanning  $18\,938.72\pm2\,181.49$ mg Cl<sup>-</sup>/L, chrome tanning  $16\,073.00\pm5\,342.62\,$  mg Cl<sup>-</sup>/L, while the concentrations for boiling in skull treatment was  $1\,313.87\pm566.43\,$  mg Cl<sup>-</sup>/L, bleaching  $295.39\pm488.90\,$  mg Cl<sup>-</sup>/L and washing  $76\pm27.61\,$  mg Cl<sup>-</sup>/L which were all above the discharge limit of  $69\,$  mg Cl<sup>-</sup>/L for chloride. With a mass load of  $209.92\,$  kg Cl<sup>-</sup>/a, the calculated chloride concentration in the effluent was  $6\,222.46\,$  mg Cl<sup>-</sup>/L. Figure  $5\,$  shows that the highest chloride mass load was  $73.14\,$  kg Cl<sup>-</sup>/a, which was achieved through Chrome tanning.

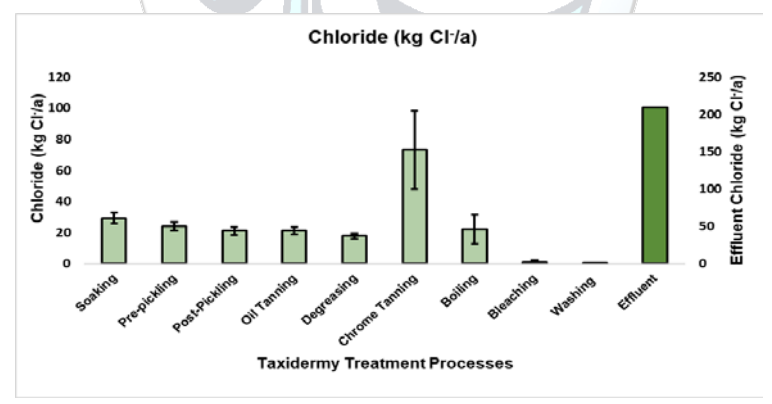


Figure 5: Chloride mass load in, kg Cl/a, for the skins/skull's treatment processes

The use of sodium chloride throughout the taxidermy treatment processes has resulted in the high chloride concentration in the final effluent. The high chloride in effluent is of concern because it is not removed during biological wastewater treatment processes, resulting in high chloride concentration in the effluent discharged into the receiving water bodies [1]. High chloride has a negative impact on the receiving water bodies as it inhibits the growth of plants, bacteria and fish due to cell structure breakdown. Water containing high chloride concentrations cannot be used for irrigation since surface salinity will increase due to evaporation, resulting in a decrease in crop yields [19].

# Sodium

The sodium analysis results for the treatment processes which were above the limit of 300 mg Na<sup>+</sup>/L were: soaking 15 125.97±3 442 mg Na<sup>+</sup>/L, pre-pickling 27 279.79±4 774.97 mg Na<sup>+</sup>/L, post-prickling 28 737.55±4 462.02 mg

40 Masilela et al.

 $Na^+/L$ , oil tanning 21 916±2 737.75 mg  $Na^+/L$ , degreasing 24 492.65±4 186.35 mg  $Na^+/L$ , chrome tanning 22 711.49±4 466.81 mg  $Na^+/L$  and boiling 1 043.25±592.57 mg  $Na^+/L$ . The calculated sodium concentration in the effluent was 7 834.91 mg  $Na^+/L$  with a mass load of 264.35 kg  $Na^+$ /a. Figure 6 shows the highest sodium mass load of 107.22 kg  $Na^+$ /a, which was achieved through Chrome tanning.

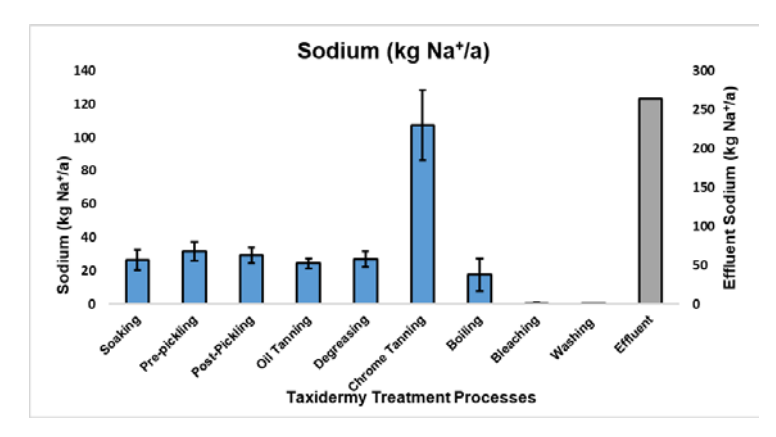


Figure 6 Sodium mass loads, kg Na<sup>+</sup>/a, for the skins/skulls treatment processes

Sodium chloride is widely used in the taxidermy treatment processes, resulting in an increase in the total sodium concentration in the final taxidermy effluent.

#### **Sulfates**

The sulfate analysis results obtained above 1 800 mg  $SO_4^2$ /L for treatment processes were as follows: pre-pickling 2 370.23±780.76 mg  $SO_4^2$ /L, post pickling 2 179.45±1 529.06 mg  $SO_4^2$ /L, oil tanning 3 812.67±292.58 mg  $SO_4^2$ /L, degreasing 1 978.37±1 587.01 mg  $SO_4^2$ /L chrome tanning 7 592.52±2 060.39 mg  $SO_4^2$ /L. The sulfates concentration in the effluent was calculated to be 1 580 mg  $SO_4^2$ /L. From Figure 7, the highest sulfates mass load was 35.84±9.72 kg  $SO_4^2$ -/a achieved from chrome tanning. The calculated sulfates mass load was 53.44 kg  $SO_4^2$ -/a.

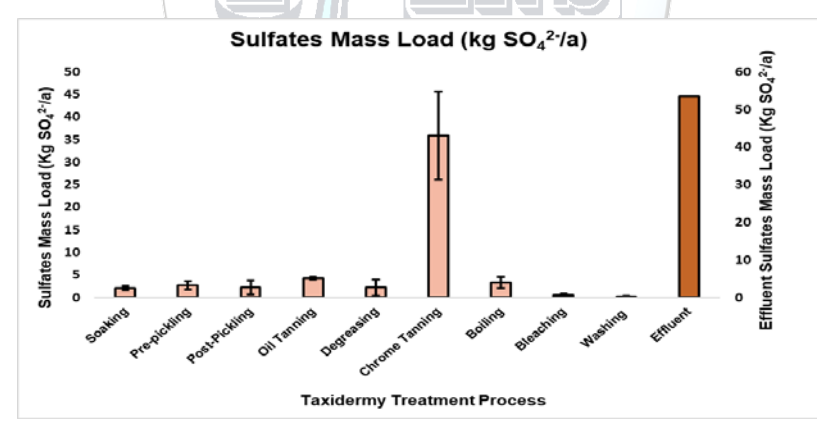


Figure 7: Sulfates mass loads, kg SO<sub>4</sub><sup>2</sup>/a, for the skins/skull's treatment processes

The presence of sulfates in tanning effluents is due to the use of chrome (III) sulfate as a tanning agent during chrome tanning [18]. Both these ion salts are problematic for treatment of effluents which contain them. The conversion of sulfates to hydrogen sulfide can result in the corrosion of metal components of the sewer line conveying the effluent containing hydrogen sulfide, as well as erosion of the sulfate resistant concrete sewer system

## **Total Chromium**

Pre-pickling ( $18.5\pm2.08$  mg Cr/L), degreasing ( $2.63\pm1.26$  mg Cr/L) and chrome tanning ( $3.352.55\pm750.22$  mg Cr/L) were the only treatment processes that contained chromium. With a mass load of 15.85 kg Cr/a, the calculated concentration was 469.78 mg Cr/L.

The use of chrome (III) sulfate has contributed to the presence of the high concentration of chrome (III) in the final effluent. Chrome (III) is highly stable and easily adsorbed onto soil particles when the pH is less than 4, whereas

chrome (VI) is simply mobilized in acidic and alkaline soils [17]. In soils that are alkaline, chrome (III) will not be absorbed and can pollute groundwater. Chlorination of water containing chrome (III) can cause the oxidation of chrome (III) to results into the more toxic chrome (VI) in areas where groundwater is the primary water source [10].

#### **Total Fats and Oils**

Fats and oils were detected in the following processes: oil tanning  $10\,528\pm4\,434.51$  mg/L, chrome  $3\,962\pm1\,576.89$  mg/L, boiling  $1\,788.13\pm570.11$  mg/L and bleaching  $1\,157.53\pm1\,170$  mg/L. Mass load and effluent concentration were 55.19 kg/a and  $1\,635.79$  mg/L, respectively. The highest mass load in Figure 3.8b was from the boiling ca 18.70 kg/a.

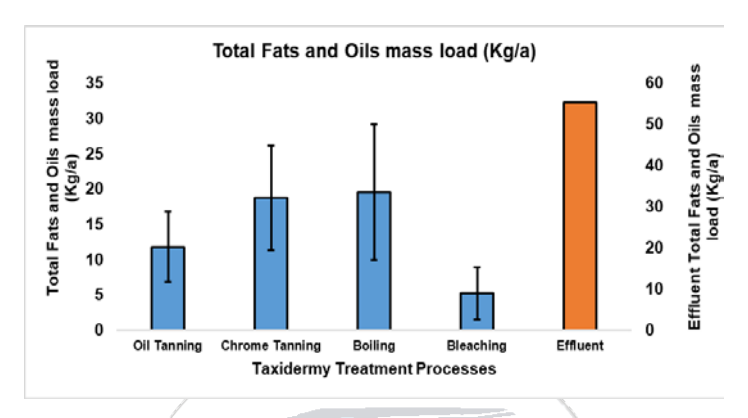


Figure 8: Total Fats and Oils in kg/a, for the skins/skull's treatment processes

During the tanning process, natural oils and grease are released from within the skin structure [8]. Some fatty substances maybe produced through inter-reaction when effluents are mixed. While some processes such as oil tanning and chrome tanning make use of synthetic fatliquours these also contribute towards the fats and oils in the final effluent.

# pН

The pH values ranged between pH 3.2 and 7.9 (Figure 3.9). The pH values for each process were as follows: soaking  $7.12\pm0.36$ , degreasing  $7.17\pm0.43$ , pre pickling  $3.18\pm0.12$ , post pickling  $3.14\pm0.31$ , oil tanning  $3.4\pm0.18$ , chrome tanning  $3.19\pm0.28$ , boiling  $7.00\pm0.51$ , bleaching  $7.59\pm0.5$  and washing  $7.92\pm0.43$ .

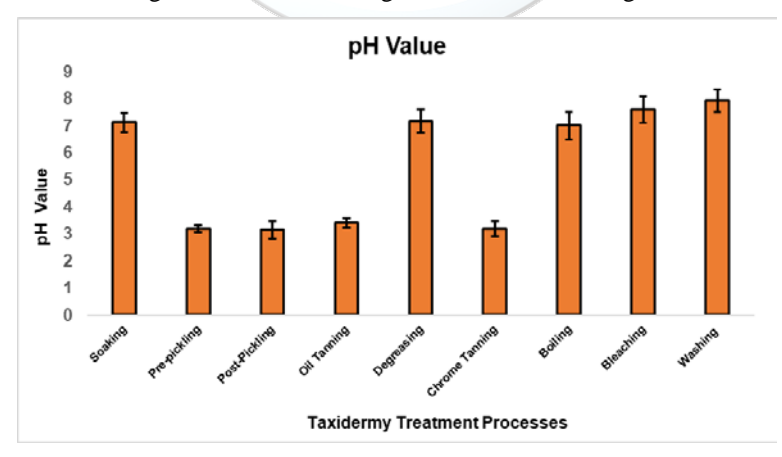


Figure 9: pH for the skins/skull's treatment processes

The pH values for each process differed due to the use of acids, bases and other chemicals, which impacted the pH values of the treatment processes. Soaking is used to rehydrate the skin to prepare for tanning, while formic acid is used to preserve the skins and prevent degradation. Chrome salts, such as chromium (III) sulfate, are best absorbed into the skins in acidic conditions. To achieve neutral pH values, chemicals which may affect the pH of the skin are not added during soaking [8]. Acidic liquors were present in the following processes: pre-pickling pH  $3.18\pm0.12$ , post-pickling pH  $3.14\pm0.31$ , oil tanning pH  $3.4\pm0.18$ , and chrome tanning pH  $3.19\pm0.28$ , while the other processes had near neutral pH values.

42 Masilela et al.

#### **Electrical conductivity**

The electrical conductivity measured for the soaking process was 5 631.16 $\pm$ 1 243.93 mS/m, pre-pickling 9 678 $\pm$ 1 602.48 mS/m, post pickling 9 741.55 $\pm$ 1 478.01 mS/m, oil tanning 7 320 $\pm$ 1 035.06 mS/m, degreasing 7 667.59 $\pm$ 1 177.73 mS/m, chrome tanning 7 240.50 $\pm$ 891.72 mS/m, boiling 835.72 $\pm$ 343.12 mS/m, bleaching 154.17 $\pm$ 45.98 mS/m and washing 120 $\pm$ 27.11 mS/m.

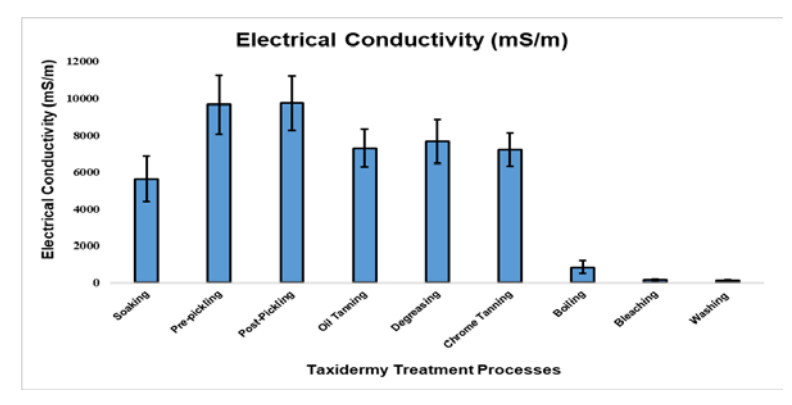


Figure 10: Electrical conductivity in mS/m for the skins/skull's treatment processes

Borehole water is used to make solutions which are used in taxidermy treatment processes. The electrical conductivity in the treatment process was increased due to the use of sodium chloride and other salts when preparing the treatment solutions [8].

Table 3: Calculated final effluent concentrations discharged from the taxidermy

Parameter	Calculated effluent concentrations discharged by the taxidermy (mg/L)	Limits set by City of Tshwane (mg/L)	Mass load discharged by the taxidermy (kg/a)
Ammonia (mg N/L)	4	25	0.13
Chemical Oxygen Demand (mg O <sub>2</sub> /L)	11 035.6	600 – 5 000	372.34
Chloride (mg Cl <sup>-</sup> /L)	6 221.62	69*	209.92
Chrome (Total), Cr <sup>3+</sup> ) (mg Cr/L)	469.86	20	15.85
Ortho-phosphate (mg P/L)	10.28	10	0.35
Fats and Oils (mg/L)	1 635.79	500 – 2 000	55.19
Sulfates (mg SO <sub>4</sub> <sup>2</sup> -/L)	1 580	1 800	53.44
Sodium (mg Na <sup>+</sup> /L)	7 835.95	300	264.35

<sup>\*</sup> Chloride limit determined by designated wastewater treatment works inflow chloride concentration.

All parameters have relatively low mass loads (Table 3) and will be diluted if treated in a large wastewater treatment plant, which treats 85 ML/d. However, permission to discharge the effluent into the municipal sewer line still remains the prerogative of the municipality while taking into consideration the long-term impact of such effluents.

The concentration of ammonia was within the City of Tshwane's permissible limits of 25 mg N/L [9] for effluent discharge from the taxidermy, whereas the other parameters such chemical oxygen demand with a concentration of 11 035.60 mg  $O_2/L$ , Chrome ( $Cr^{3+}$ ) with 469.86 mg Cr/L, Chloride with 6 221.62 mg  $Cl^{-}/L$  and Sodium with 7 834.91 mg  $Na^{+}/L$  were not within the permissible limits for discharge into the sewer line as shown in Table 3.

The COD in the taxidermy effluent was found to be quite high (approximately 11 000 mg O<sub>2</sub>/L), some of the chemical compounds used in taxidermy are known to be unbiodegradable. Particularly synthetic fat liquoring compounds, such as Eskatan GLH, are known to have low biodegradability [16], reducing the efficiency of biological treatment processes.

Because of the high COD concentration in the effluent, it may be possible to treat it using a biological process. However, due to the relatively small volumes of wastewater generated in taxidermy, treatment in an on-site system would be possible. On-site treatment systems have low capital expenditures for new infrastructure and low operational costs for maintenance [21]. Consequently, septic tanks with French drains and fenced-off treatment ponds are the most often used on-site treatment systems in South Africa currently.

# 4. CONCLUSIONS

The taxidermy investigated was a medium sized facility which produced less than 2 000 trophies per annum, and discharged an estimated effluent of  $33.7~\text{m}^3/\text{a}$ . Several of the treatment processes in the taxidermy produced highly polluted effluents, which could pose serious risks for groundwater pollution. The effluent contained high concentrations of COD with a concentration of 11~035.60~mg O<sub>2</sub>/L, Chrome (Total), (in the form of Cr<sup>3+</sup>) at 469.86~mg Cr/L, Chloride at 6~222~mg CL/L, Ortho-phosphates at 10.28~mg P/L, Fats and oils at 1~635.79~mg/L and Sodium at 7~835~mg Na<sup>+</sup>/L.

It is recommended that these pollutants are removed before discharge into the environment or an alternative would be applying for permission to discharge into a municipal sewer and complying with municipal discharge regulations.

Further studies should be done to determine the most efficient and cost-effective method for discharge.

# 5. ACKNOWLEDGMENT

The authors would like to thank;

- City of Tshwane for their collaboration and access to laboratory for sample analysis
- The Taxidermy providing access to sampling and trade methods
- Tshwane University of Technology for support in conducting this research

# 6. CONFLICT OF INTEREST STATEMENT

The author(s) declare(s) that there is no conflict of interest.

# 7. REFERENCES

- [1].P. Pybus. (ed.). Handbook For The Operation Of Wastewater Treatment Works. 3rd ed. Pretoria: Water Institute Of Southern Africa, 2002.
- [2].APHA, AWWA and WEF. Standard Methods for the Examination of Water and Wastewater, 22nd ed. Washington, DC,2012.
- [3].M. Eiroa, A. Vilar, C. Kennes, and M.C. Veiga. Biological treatment of industrial wastewater containing formaldehyde and formic acid. Water SA, 32 (1), Jan: 116 118. 2006.
- [4].A. Kitshoff. Economic Contribution: Hunting Indaba. The Ranch, Polokwane: 11 12 November 2013. [Online]. Available: <a href="https://www.dffe.gov.za/sites/default/files/docs/economic\_contribution\_ofhunting.pdf">https://www.dffe.gov.za/sites/default/files/docs/economic\_contribution\_ofhunting.pdf</a>
- [5].Naturgerechte Technologien, Bau-und Wirtschaftsberatung (TBW) GMBH. Treatment of Tannery Wastewater. Frankfurt, Germany. 2002.
- [6].(2020) Karoo Taxidermy Field Preparation. website. [Online] Available: <a href="https://www.karootaxidermy.com/page/trophy-preparation">https://www.karootaxidermy.com/page/trophy-preparation</a>
- [7].Glass Eyes South Africa. 2021.Chemical product list. [Online]. Available: <a href="https://www.glasseyessa.co.za/page">https://www.glasseyessa.co.za/page</a> chem product list.html.
- [8].C.D. Swartz, C. Jackson-Moss, R.A. Roswell, A.B. Mpofu, and P.J. Welz. Water and Wastewater management in the tanning and leather finishing industry. WRC Report no TT 713/17. Water Research Commission, Pretoria, South Africa Pretoria.2017.
- [9]. City Of Tshwane Metropolitan Municipality: Sanitation By-Laws. Provincial Gazette extraordinary Gauteng (South Africa). 647:19-36, Sep.10.2014.
- [10]. N.D. Rogers. "Chromium Oxidation by Disinfectants and Oxidants Used in Drinking Water Treatment," MSC. thesis, Utah State University, USA, 2016.

44 Masilela et al.

[11]. D. Van Coller. Trophy hunting's contribution towards South Africa's GDP. AgriSA /WRSA Action Shop 27 October 2017.

- [12]. Department of Agriculture, Forestry and Fisheries. Standards for the registration of a veterinary approved taxidermy or dip and pack facility. Pretoria: National Directorate Animal Health, South Africa. 2009.
- [13]. T.R. Motsi, (TatendaM@daff.gov.za). Request For Information Pertaining To Taxidermies in Gauteng. [E-mail to:] A. Masilela, (anoesjkam@gmail.com) 20 Jun.2019.
- [14]. M. Dalby 2014. Bone Broth Mineral Content. [Online] Available: <a href="https://honey-guide.com/2014/01/21/bone-broth-mineral-content">https://honey-guide.com/2014/01/21/bone-broth-mineral-content</a>
- [15]. M. Bronkhorst, (MariettaB@daff.gov.za). Paraphrasing of Taxidermy PowerPoint Slide. [E-mail to:] Masilela, A (anoesjkam@gmail.com) 10 May 2019.
- [16]. R. Saranya, A.Tamil Selvi, J. Jayapriya and R Aravindhan. Synthesis of Fat Liquor Through Fish Waste Valorization, Characterization and Applications in Tannery Industry. Waste and Biomass Valorization, 11, 6637–6647.2020.
- [17]. A.Ertani, A. Mietto, M. Borin and S. Nardi .Chromium in Agricultural Soils and Crops A Review. Water, Air, & Soil Pollution, 228: 190 DOI 10.1007/s11270-017-3356-y.2017.
- [18]. J. Buljan, I. Kral, M. Bosnic, and R.P. Daniels. Pollutants in Tannery Wastewater 2nd ed. United Nations Industrial Development Organization (UNIDO).2016.
- [19]. M. Bosnic, J Buljan, and S.R.P. Daniels. Pollutants in Tannery Wastewater, United Nations Industrial Development Organization (UNIDO), Regional Programme for Pollution Control in the Tanning Industry in South-East Asia, Report US/RAS/92/120.2000.
- [20]. D.R. Bohme.Pickling and Lubricating group Eskatan GLH & GLS. Birikim Kimya Deri San.ve Tic.Ltd. Sti. [Online] Available <a href="http://www.birikimkimya.com/Boehme.html">http://www.birikimkimya.com/Boehme.html</a>. 2011.
- [21]. Paladino and Company Incorporated. Onsite Wastewater Treatment Systems: A Technical Review. [Online] Available: <a href="http://www.paladinoandco.com/wpcontent/uploads/2012/11/OnsiteWastewaterTreatmentSystems">http://www.paladinoandco.com/wpcontent/uploads/2012/11/OnsiteWastewaterTreatmentSystems</a> TechnicalReview.pdf. 2008.
- [22]. M. Rantlha. South African Taxidermy Industry Development Plan. Industrial Development Division Department OF Trade AND Industry East London International Convention Centre, Eastern Cape. 2018.

# Groundwater Vulnerability Mapping Using DRASTIC Model: A Case Study at the Palas Basin in Turkey

Ugur Bozdoganlio<sup>1</sup>, Mehmet Soylu<sup>2</sup>, Filiz Dadaser-Celik<sup>3\*</sup>

<sup>1</sup>Erciyes University, Department of Geomatics Engineering. 38039, Talas/Kayseri, Turkey.

<sup>2</sup> Cappadocia University, Department Of Medical Services And Techniques, 50400, Ürgüp/Nevsehir, Turkey.

<sup>3</sup>erciyes University, Department Of Environmental Engineering, 38039, Talas/Kayseri, Turkey.

\*Corresponding Author email: fdadaser@erciyes.edu.tr

# **Abstract**

The study aims to estimate groundwater vulnerability against pollution at the Palas Basin (Turkey) by using geographical information system based DRASTIC model. A DRASTIC model integrates information for seven hydrogeological parameters: depth to water (D), net recharge (R), aquifer media (A), soil media (S), topography (T), impact of vadose zone (I), and hydraulic conductivity (C), and identifies spatial vulnerability. The study area, Palas Basin, is a hydrologically closed, agricultural basin, where groundwater is used for meeting irrigation and municipal water requirements. Seven hydrogeological parameters were combined to classify the basin into three vulnerable zones (as low, moderate, and high). The central part of the basin was identified to be highly vulnerable, while the eastern and southern parts were characterized by moderate to low vulnerable areas. Intensive agricultural activities, widespread in the central basin, create high pollution potential. This study showed that the DRASTIC approach provided a simple and efficient tool for evaluating groundwater vulnerability. The results can be used by water managers in groundwater management in the Palas Basin.

# **Key words**

Aquifer Vulnerability, DRASTIC, GIS, Palas Basin

#### 1. INTRODUCTION

Freshwater resources are limited and not equally distributed throughout the world. Human activities and climate change pose direct or indirect impacts on scarce freshwater resources [1;2]. The number of countries experiencing water scarcity and the population that can reach sufficient amount of water decrease [3;4;5], while water stress increases [6;7]. It is, therefore, crucial to use existing water resources efficiently.

Vulnerability modeling approaches can help determine how vulnerable groundwater is to various stresses. DRASTIC is a geographic information system (GIS) based model that can be applied to shallow groundwater systems [8]. In this method, it is assumed that all pollutants in the basin can infiltrate, be transported, and dissolved in groundwater [8]. Thus, by determining the potential effects of pollutants in the basin, regions susceptible to pollution can be determined. DRASTIC based vulnerability maps can be used in groundwater planning, especially in agricultural basins. The information obtained plays a role in planning activities such as water use, agricultural land use planning, animal husbandry, and fertilization.

46 Bozdoganlio et al.

In this study, we estimated groundwater vulnerability against pollution at the Palas Basin in Turkey. This basin is a hydrologically closed basin where intensive irrigated agriculture takes place. Irrigation and drinking water requirements in the basin are almost entirely met from groundwater. Agricultural activities can pose threats for groundwater quality. In this study, we aim to show how vulnerable is the groundwater system to pollution.

#### 2. METHODS

# 2.1. Study Area

This study was carried out at the Palas Basin (Figure 1). Palas Basin is an agricultural basin, located in Kayseri, in the Central Anatolia Region of Turkey. The basin is a hydrologically closed basin. The altitude of the region range from 1131 to 2119 meters, and its area is approximately 100 km² [9]. Tuzla Lake is located to the west of the basin. Tuzla Lake is an ecologically important area as it is located in the junction point of routes of birds migrating from Asia, Europe and Africa and hosts endemic plant species [10]. A small stream, named Değirmen Stream, flows towards Tuzla Lake by joining two branches from Koyunabdal and Kahveci locations. The flow in the stream is very low and it is mostly dry during summer months. Therefore, the major water source in the basin is groundwater. Groundwater is used for meeting irrigation and drinking water requirements.

Economic activities in the region are agriculture, animal husbandry, and salt extraction. Average annual air temperature of the Palas Basin is 11°C. The hottest month is July, where the average temperature is 20°C. In January, the coldest month, the average air temperature is -2.5°C. Average annual precipitation is 402 mm. [9].

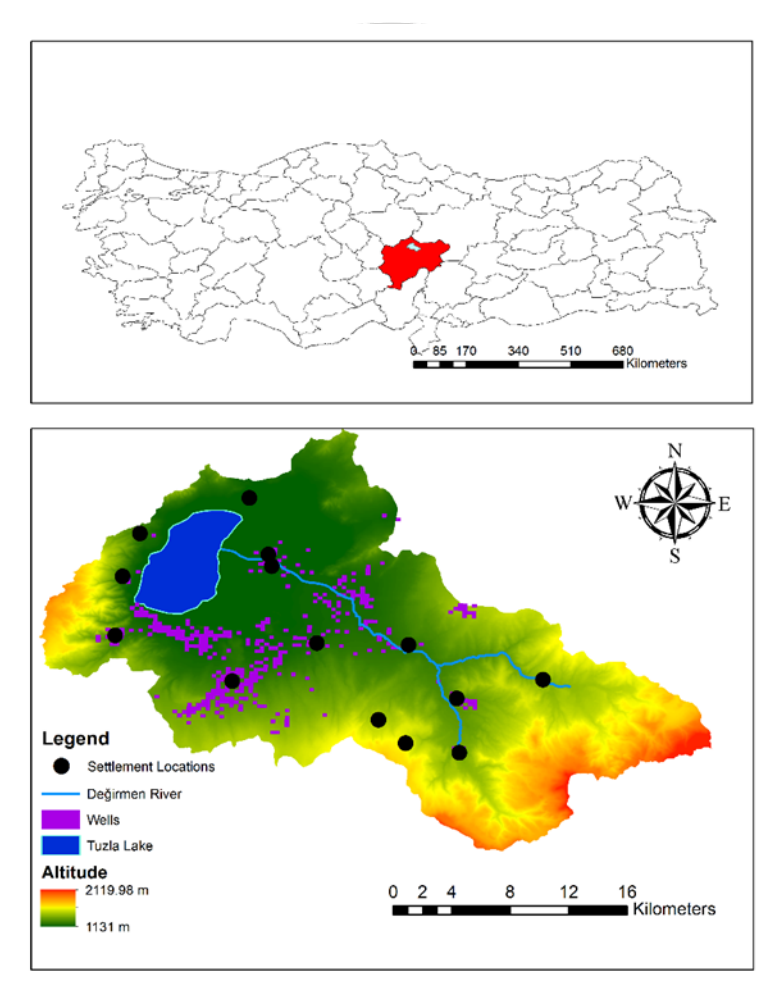


Figure 1: Study area representation

Groundwater in the Palas Basin can be vulnerable to pollution due to intensive agricultural activities taking place in the basin. Nitrate concentrations in groundwater are already high in some parts of the basin. Groundwater

levels are also decreasing as a result of intensive use of groundwater. The change in groundwater salinity can be a problem due to the interaction of the saline Tuzla Lake with groundwater in the region [10].

The DRASTIC method basically uses seven hydrogeological factors to assess the susceptibility of groundwater to contamination. The DRASTIC parameters' weights, defined according to Aller et al. [8], range from 1 to 5 (Table 2). The most important parameter is given weight 5 and the least important parameter is given weight 1. The weights are chosen depending on the parameters affecting the spread of the pollutants. In addition, each parameter is divided into degrees according to its pollution potential. The degrees are determined according to rating classes in layers and the impact rating values of that layer are determined. Later, these layers were combined according to their weight values and the DRASTIC index layer is created. Mathematical equation for the DRASTIC index is given in Eq. 1.

$$DI = \sum_{i=1}^{7} (W_i * R_i)$$
 (1)

In Equation 1, the variable "i" denote the layers such as Depth to Water (D), Net Recharge (R), Aquifer Media (A), Soil Media (S), Topography (T), Impact of Vadose Zone (I), Hydraulic Conductivity (C). "W" variable is weighted number for each layer, "R" variable is rating number for each by "i" layer class. Finally, "DI" is the DRASTIC Index. The summary of the raw data sources and the operations applied for the "i" layers obtained are given in Table 1. Also, the weighted values and rating values selected according to the literature are given in Table 2.

Table 1: Summary of the raw data sources and the operations applied for the DRASTIC layers

Layers	Raw Data Source	Data Adjustments	
Depth to Water	Log Data for Different Location at Basin	* Coordinate transformation * GRID installation (100mx100m) *Classification	
Net Recharge	SWAT Model	* Coordinate transformation * GRID installation (100mx100m) *Classification	
Aquifer Media	* Coordinate transformatic GRID installation (100mx *Classification		
Soil Media	FAO World Soil Map	* Image Clip Process * Coordinate transformation * GRID installation (100mx100m) *Classification	
Topography	Using DEM image by SRTM Satellite	* Image Clip Process * Coordinate transformation * GRID installation (100mx100m) *Slope Analysis *Classification	
Impact of Vadose Zone	FAO World Soil Map	* Image Clip Process * Coordinate transformation * GRID installation (100mx100m) *Classification	
Hyraulic Conductivity SPAW Hydrology Programme		*Hydraulic Conductivity Values Search and Input for Soil Types * Coordinate transformation * GRID installation (100mx100m) *Classification	

48 Bozdoganlio et al.

Table 2: Weights and ratings assigned to seven parameters used in the DRASTIC vulnerability index modelling

Parameter	Classes	Rating	Weig	
_	0-1.5	10		
Ξ	1.5-4.6	9		
Depth to Water (m)	4.6-9.1	7		
×	9.1-15.2	5	5	
£	15.2-22.9	3		
de	22.9-30.5	2		
_	>30.5	1		
61	0-0.141	1		
Net Recharge (m/year)	0.141-0.282	3		
t Rechar (m/year)	0.282-0.494	6	4	
E E	0.494-0.705	8		
z	>0.705	9		
	Silty Clay, Sand, Gravel	4		
ë	Sandstone	6		
Aquifer Media	Siltstone, sandstone, clay limestone	6		
fer	Silty clay	7	3	
ła de i	Broken cracked rock	3		
•	Impervious tuffs	9		
	Sandy clay Ioam	2	2	
_	Clay silty	3		
Soil Media	Silty clay loam, sandy clay loam, clay loam	4		
Σ	Sandy clayey gravelly	6		
So	Fine sandy loam - sandy loam	8		
	Clay - silty clay - sandy clay	2		
	0-2	10		
<u> </u>	2-6	9		
cent	6-12	5	1	
Topography (percent)	12-18	3		
<u> </u>	>18	1		
Se	Sandy clay loam	2		
Impact of Vadose Zone	Clay silty	3	5	
t of V. Zone	Silty clay loam, sandy clay loam, clay loam	4		
act Z	Sandy clayey gravelly	6		
<u>Ĕ</u>	Fine sandy loam - sandy loam	8		
	Clay - silty clay - sandy clay	2		
Hyraulic Conductivity (m/day)	0.19	1		
	0.21	1		
ic Condu (m/day)	0.18	1	3	
يَّا قَ	0.23	1		
yrau	0.24	1		
£	0.27	1		

# 3. RESULTS

Seven hydrogeological parameters were combined to create the drastic index map for the Palas Basin. Figure 2 presents each layer and their categories. Here, the depth to water layer is the distance of the groundwater aquifer from the surface. As this distance decreases, groundwater becomes more vulnerable to pollutants. Depth to water layer values were divided into seven categories according to Aller et. al. [8]. Another layer is the net recharge layer. The increase in the net recharge value in this layer means that the groundwater is more vulnerable for potential contamination. Net recharge values were obtained from a previously developed SWAT model and classified into three [11]. In this study, aquifer media is divided into 6 classes. In the aquifer media variable, contamination potentials may increase or decrease depending on the permeability of aquifer materials. A similar situation is valid for the soil media and impact of vadose zone. In the topography layer, the contamination potential changes depending on the slope. As the slope value increases, the leakage into the groundwater will decrease, so a low pollution rating value is stated. As the slope value decreases, the contamination potential degree increases as the water flow will go towards leakage. Finally, in the hydraulic conductivity layer, the increase in conductivity value is the effect that increases the potential for groundwater contamination. When the hydraulic conductivity value increases, the rating value of the variable class also increases.

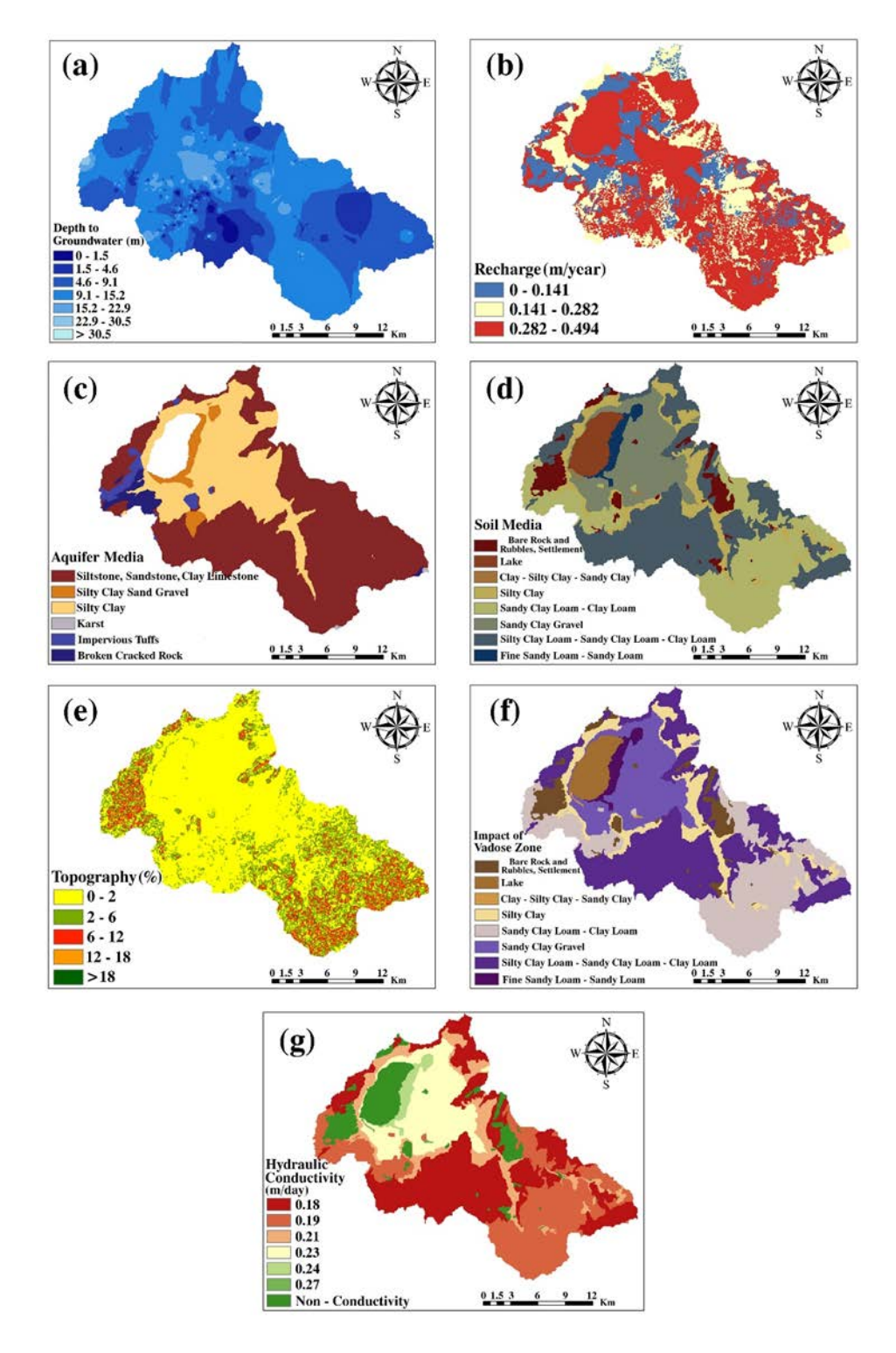


Figure 2: DRASTIC layers and classes of each layer

DRASTIC Index map was created by combining seven separate layers (Figure 3). In this map, a numerical output value was created for each grid value and these values were divided into three classes as low, moderate, and high vulnerability zones.

50 Bozdoganlio et al.

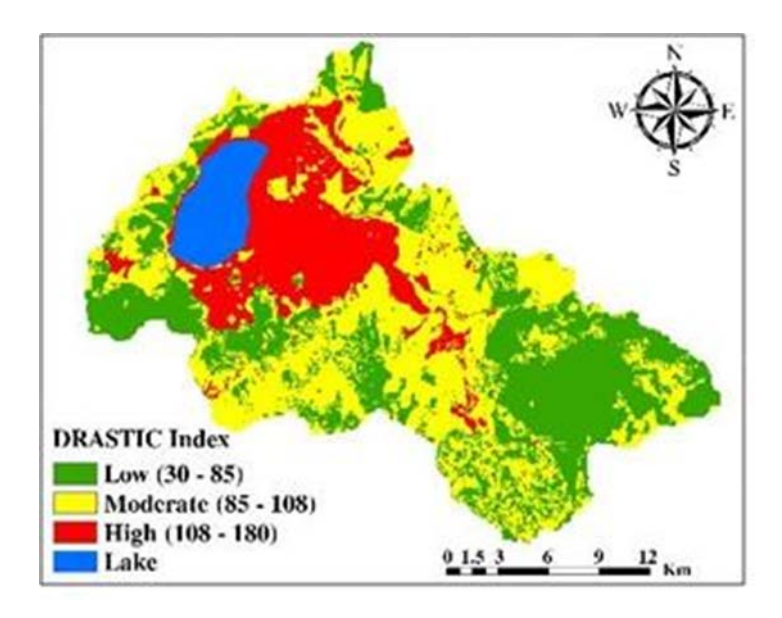


Figure 3: Drastic index map for Palas Basin

According to Figure 3, majority of the basin is covered by moderate vulnerability class (66%). Low vulnerability zone covers 17% and high vulnerability zone covers 23%. However, the areas with high vulnerability are located in the region where agricultural activities are intense and settlements are located. This situation creates a potential risk for groundwater quality. Therefore, the use of chemicals such as fertilizers and pesticides in the region should be strictly controlled.

#### 4. CONCLUSION

This study was conducted for groundwater vulnerable assessment in the Palas Basin. DRASTIC model with inputs for depth to water (D), net recharge (R), aquifer media (A), soil media (S), topography (T), impact of vadose zone (I), and hydraulic conductivity (C) were used to estimate spatial vulnerability of Palas Basin. Vulnerability studies reflect the potential for contamination of the region's groundwater. As a result of the study, approximately 23% of the groundwater in the basin was determined to be highly vulnerable to pollution. The data obtained in this study can be used for comparison with actual pollution values or to determine the effects of land use changes on the basin.

#### **ACKNOWLEDGMENT**

This study was supported by the Scientific and Technological Research Council of Turkey (TUBITAK) (Project No: 118Y178). The first author received funding from the 2247-C STAR-Intern Researcher Scholarship Programme provided by TUBITAK.

# REFERENCES

- [1]. Howe, C., Jones, R., Maheepala, S., Rhodes, B., "Implications of potential climate change for Melbourne's water resources. A collaborative project between Melbourne Water CSIRO Urban Water Climate Impact Groups", Australia, p. 26., 2005.
- [2]. Matonse, A.H., Pierson, D.C., Frei, A., Zion, M.S., Anandhi, A., Schneiderman, E., Wright, B., "Investigating the impact of climate change on New York City's primary water supply." *Climatic Change*, vol. 116, pp. 437-456., 2013.
- [3]. Iglesias, A., Garrote, L., Flores, F., Moneo, M., "Challenges to manage the risk of water scarcity and climate change in the Mediterranean." *Water Resources Management* vol. 21, pp. 775-788., 2007
- [4]. Schewe, J., Heinke, J., Gerten, D., Haddeland, I., Arnell, N.W., Clark, D.B., Dankers, R., Eisner, S., Fekete, B.M., Colón-González, F.J., "Multimodel assessment of water scarcity under climate change." *Proceedings of the National Academy of Sciences*, vol. 111, pp. 3245-3250., 2014.
- [5]. Gosling, S.N., Arnell, N.W., "A global assessment of the impact of climate change on water scarcity." *Climatic Change* vol. 134, pp. 371-385., 2016.

- [6]. Eitzinger, J., Štastná, M., Žalud, Z., Dubrovský, M., 2003. "A simulation study of the effect of soil water balance and water stress on winter wheat production under different climate change scenarios." *Agricultural Water Management* vol. 61, pp. 195-217., 2003.
- [7]. Siegfried, T., Bernauer, T., Guiennet, R., Sellars, S., Robertson, A.W., Mankin, J., Bauer-Gottwein, P., Yakovlev, A., "Will climate change exacerbate water stress in Central Asia?" *Climatic Change*, vol. 112, pp. 881-899, 2012.
- [8]. Aller L., Benett T., Lehr J.H. and Petty R.J., "DRASTIC: a standardized system for evaluating ground water pollution potential using hydrogeologic settings." Office of Research and Development, Environmental Protection Agency USA, 1987.
- [9]. Cengiz, E., Dadaser-Celik, F., "Hydrological Changes at Tuzla (Palas) Lake in Turkey." BALWOIS, Republic of Macedonia, 2012
- [10]. Dadaser-Celik, F., Celik, M., "Modelling surface water-groundwater interactions at the Palas Basin (Turkey) using FREEWAT." *Acque Sotterranee-Italian Journal of Groundwater*, 2017.
- [11]. Amiri A.M., Azgın, S.T., Dadaser-Celik, F. "Calibration and Validation of a SWAT model for Palas Basin (Kayseri) using SUFI2 Algorithm." International Conference on Civil and Environmental Engineering (ICOCEE), Nevsehir, Turkey, pp.1, 2017.



# Climate Change Impacts on Potential Groundwater Recharge in the Palas Basin, Turkey

# Mehmet SOYLU1, Filiz DADASER-CELIK2\*

<sup>1</sup> Cappadocia University, Department of Medical Services and Techniques, 50400, Ürgüp/Nevsehır, Turkey.

<sup>2</sup>erciyes University, Department Of Environmental Engineering, 38280, Talas/Kayseri, Turkey.

\*Corresponding Author email: fdadaser@erciyes.edu.tr

#### **Abstract**

Climate change poses a major threat for sustainability of groundwater resources. In this study, we aimed to determine how climate change can affect groundwater recharge potential in the Palas Basin. Palas Basin is a semi-arid closed basin located in Kayseri, in the central Anatolia region of Turkey. Agriculture is the major economic activity in the region and groundwater is used extensively for irrigation purposes. In this study, we estimated potential groundwater recharge for the Palas Basin under two representative concentration pathway (RCP) scenarios (RCP4.5 and RCP8.5) projected by the HadGEM2-ES, MPI-ESM-MR, GFDL-ESM2M global climate models. All models projected a decrease in mean annual potential groundwater recharge under the RCP8.5 scenario. Under the RCP4.5 scenario, the trends in annual potential groundwater recharge were downward according to the HadGEM2-ES and MPI-ESM-MR models but slightly positive according to the GFDL-ESM2M model. For the sustainability of groundwater system and agricultural activities in the basin, climate change adaptation strategies should be developed for the agricultural sector.

# **Key words**

Climate Change, Groundwater Recharge Potential, Palas Basin

# 1. INTRODUCTION

Water resources sector is among the major sectors to be affected by climate change. Changes in climatic conditions can affect hydrologic characteristics of both surface waters and groundwater [1;2]. These changes, in turn, cause other effects such as the reduction of biological diversity, water quality changes, etc.

The effects of climate change on groundwater recharge have been investigated in a number of studies [3]. Net recharge and potential recharge were estimated based on climate projections. These studies showed that precipitation changes were mostly responsible for decreases or increases in groundwater recharge. Majority of the studies predicted a decrease in groundwater recharge [4;5;6;7]. Some other studies examined the effects of changes in evapotranspiration and land cover [7]. Increases in evapotranspiration and land cover changes, which increased impervious areas, also projected to cause decreases in groundwater recharge.

Turkey is among the countries, expected to be adversely affected by climatic changes. Turkey has diverse climatic conditions, changing from Mediterranean along the coasts to continental in central regions. Regions with different climatic characteristics can respond differently to climatic changes [8]. In coastal areas, changes in precipitation patterns can cause changes in frequency flood events [9;10]. In central regions, where continental

climate prevails, decreases in precipitation can increase the frequency of droughts [10;11;12]. Previous studies showed that downward trends in precipitation have already been detected in central regions and these trends are expected to continue in the future [13]. The decreases in precipitation can affect the groundwater recharge [14]. The reductions in groundwater recharge, in turn, can have negative impacts on the agricultural sector and on groundwater-dependent ecosystems [9;10].

In this study, we examined the changes in potential groundwater recharge due to climate change in the Palas Basin, Kayseri, Turkey. We estimated potential groundwater recharge by considering hydrogeological characteristics of the Palas Basin and precipitation projections for the future. Precipitation projections developed with three global circulation models (HadGEM2-ES, MPI-ESM-MR, GFDL-ESM2M) under RCP4.5 and RCP8.5 scenarios were used in the analyses. This study can show the sensitivity of groundwater to climate change in the Palas Basin and in other semi-arid regions.

#### **2. 2. METHODS**

# 2.1. Study Area

This study was conducted in the Palas Basin, located in Kayseri, Turkey (Figure 1). The basin is a closed basin where the elevation changes between 1131 and 2120 m above sea level [15]. The average altitude of the basin is 1336 meters and it covers an area of approximately 100 km<sup>2</sup> [15].

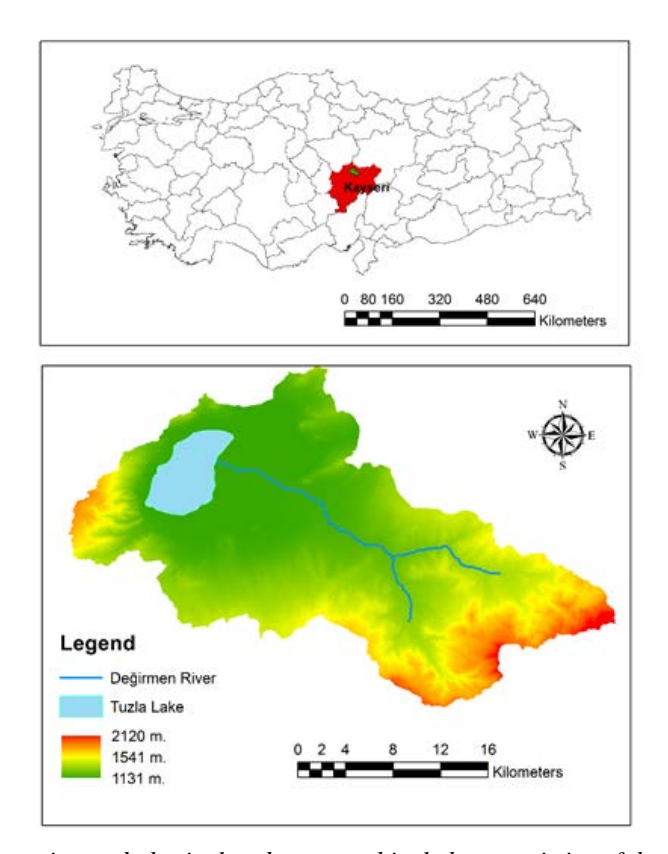


Figure 1: Location and physical and topographical characteristics of the Palas Basin

Figure 2 shows the geological characteristics of the Palas Basin. Mesozoic ophiolitic complex, sedimentary rocks, Mesozoic aged magmatic rocks, Eocene and Neogene aged sediments, Plio Quaternary clayey silty fine-grained sediments, Quaternary slope accumulation and alluviums can be identified in the basin. In general, geological formations in the Palas Basin can be divided into three main groups. These are Quaternary alluviums in the lake and its immediate surroundings, Tertiary aged formations spread over a wide area in the east of the basin and Mesozoic formations located in a narrow area in the southwest of the basin.

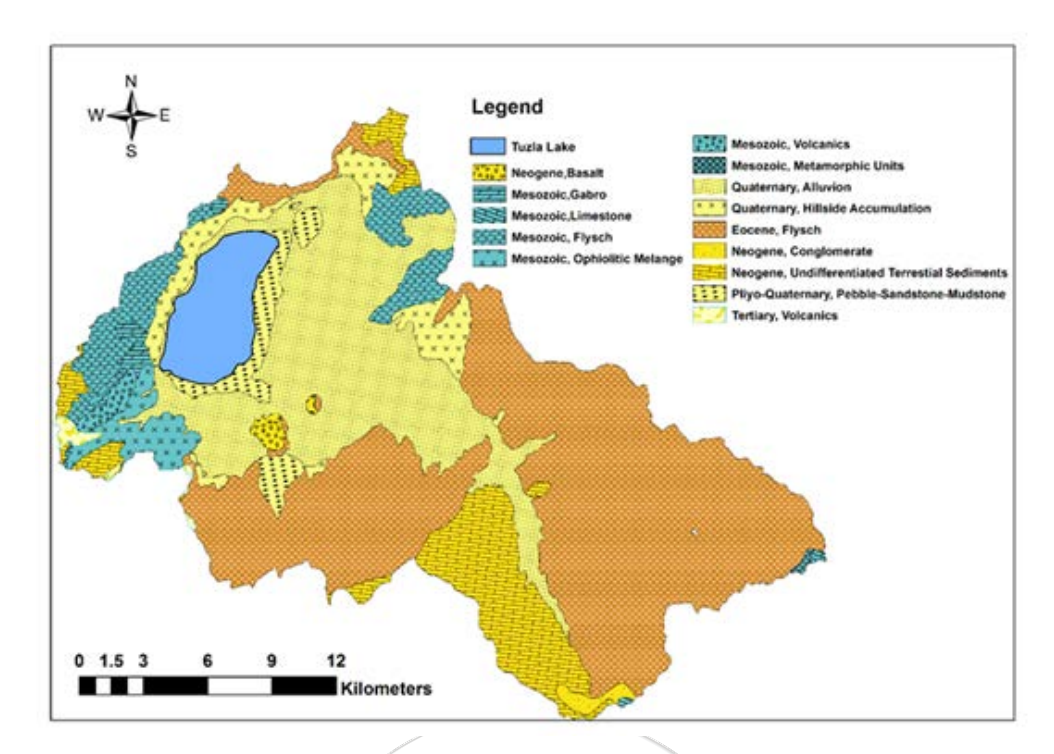


Figure 2: Geological characteristics of the Palas Basin [16]

The climate is semi-arid with an annual average temperature of about 11°C and the annual precipitation of 400 mm. Surface water resources are scarce in the basin. There is a small stream, Değirmen River, flows from southeast to northwest and discharges into Tuzla (Palas) Lake, located to the west of the basin. In summer months, the stream becomes completely dry and is lost before reaching the lake. Tuzla Lake is a saline playa lake, fed by rainfall and surface and groundwater flows. It is the second largest saline lake in Turkey and is a nature conservation area due to its ecological characteristics.

Agriculture is the major economic activity in the region and other economic activities are animal husbandry and salt extraction. Groundwater is the major water source used for irrigation activities. In irrigated areas, maize, sugar beets and vegetables are cultivated. Cereals are common in unirrigated areas.

# 2.2. Estimating Potential Groundwater Recharge

Potential groundwater recharge was estimated according to Equation 1, based on lithological classes and precipitation.

$$R = \sum_{i=1}^{n} P A_i I_i \tag{1}$$

In Equation 1, R is expressed as the potential recharge (m³/year), A is the area of each lithological unit (I) (m²), P is the annual precipitation (m/year), n is the total number of lithological units. I represents the percolation coefficient for each lithological unit. The area of each lithological unit was estimated from the geological map given in Figure 1. The percolation coefficients for each lithological unit was estimated as given in Table 1 [16].

Lithological **Lithological Class** Area (km<sup>2</sup>) Percolation 105.18 0.15 Quaternary, Alluvium Quaternary, Hillside Accumulation 9.15 0.05 Pliyo-Quaternary, Pebble, Sandstone, Mudstone 5.62 0.10 Neogene, Basalt 2.27 0.10 Neogene, Unconsolidated Terrestrial Sediments 15.99 0.05 0 Eocene, Flysch 59.64 0 Mesozoic, Flysch 5.80 Mesozoic, Ophiolitic Melange 0.13

Table 1: Lithological units, their areal coverages and percolation coefficients [16]

# 2.3. Climate Projections

We obtained precipitation projections in daily timescale from the Turkish State Meteorological Service (MGM). MGM produced downscaled precipitation data by using input from three Global Circulation Models, GFDL-ESM2M, HadGEM2-ES and MPI-ESM-MR, for two representative concentration pathways (RCPs): RCP 4.5 and RCP 8.5. The data were downscaled with the RegCM4.3.4 Regional Model by MGM based on the 1971-2000 reference period [17]. GFDL-ESM2M model is produced by Geophysical Fluid Dynamics Laboratory (United States) with a resolution of  $2.5^{\circ} \times 2.0^{\circ}$ . HadGEM2-ES model is produced by Met Office Hadley Centre (United Kingdom). It has resolution of  $1.875^{\circ} \times 1.250^{\circ}$ . MPI-ESM-MR is run by Max Plank Institute (Germany) with  $1.865^{\circ} \times 1.875^{\circ}$  resolution. The RCP 4.5 assumes that greenhouse gas concentration will peak around 2040, then decline from the mid-century, while the RCP8.5 assumes that greenhouse gas concentration increasing until the 21st century. The projections for the 2021-2098 period were used in the analyses.

# 3. RESULTS

In this study, potential groundwater recharge was calculated for the 2021-2098 period based on RCP4.5 and RCP8.5 scenarios from the HadGEM2-ES, MPI-ESM-MR, GFDL-ESM2M models. RCP4.5 was the scenario with lower carbon emissions on a global scale and it is the scenario, targeted globally. RCP8.5, on the other hand, is the scenario with higher carbon emissions and is farther from the target point.

Below, we first present projected precipitation changes under RCP4.5 and RCP8.5 scenarios with HadGEM2-ES, MPI-ESM-MR, GFDL-ESM2M models. Then, we discuss projected changes in potential groundwater recharge.

# 3.1. Changes in Precipitation from 2021 to 2098

Annual precipitation data estimated based on RCP4.5 and RCP8.5 scenarios from 2021 to 2098 with HadGEM2-ES, MPI-ESM-MR, GFDL-ESM2M models were shown in Figure 3.

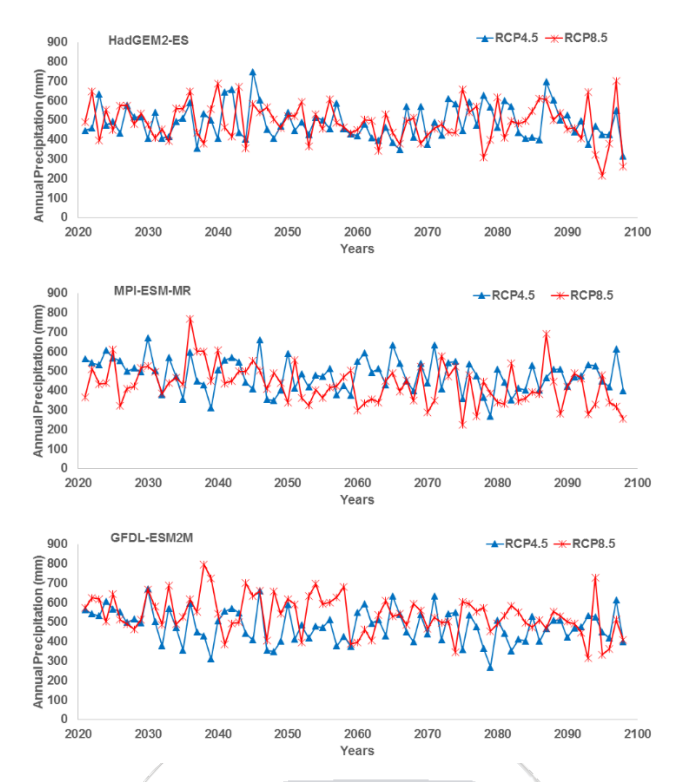


Figure 3: Projected annual precipitation from 2021 to 2098

We estimated the trends in precipitation series using the linear regression method. According to the HadGEM2-ES and MPI-ESM-ER models, downward trends were detected under both RCP4.5 and RCP8.5 scenarios. GFDL-ESM2M model estimated a slightly positive trend under the RCP4.5 scenario but downward trend under the RCP8.5 scenario. The trends detected for RCP8.5 scenarios with GFDL-ESM2M and MPI-ESM-ER models were statistically significant at the 0.01 level.

Table 2: Trends in precipitation series and their statistical significance

<b>D</b> 1 1 1 1	RCF	24.5	RCP	8.5
Precipitation	Trend (mm/year)	P Value	Trend (mm/year)	P Value
HadGEM2-ES	-0.26	0.558	-0.75	0.126
MPI-ESM-ER	-0.80	0.062	-1.55	0.002
GFDL-ESM2M	0.11	0.851	-1.51	0.002

We also analyzed precipitation data for the 2021-2040 (near future), 2041-2070 (medium future) and 2071-2098 (distant future) periods. Compared to the 2021-2040 period, mean annual precipitation is predicted to decrease by 46.9 mm (%8.67) (GFDL-ESM2M), 1.7 mm (%0.35) (HadGEM2-ES), and 25.3 mm (%5.01) (MPI-ESM-ER) during the 2041-2070 period according to the RCP4.5 scenario. The decrease would be 0.1 mm (%0.02) (GFDL-ESM2M) and 42.3 mm (%9.11) (MPI-ESM-ER) from the 2021-2040 to the 2071-2098 period. HadGEM2-ES estimated a slight increase of 12.3 mm (%2.54) in the 2071-2098 period compared to the 2021-2040 period.

According to the RCP8.5 scenario, mean annual precipitation during the 2041-2070 period would decrease by 33.8 mm (%5.80) (GFDL-ESM2M), 29.6 mm (%5.80) (HadGEM2-ES), and 66.1 mm (%13.50) (MPI-ESM-ER) compared to the 2021-2040 period. GFDL-ESM2M, HadGEM2-ES and MPI-ESM-ER models predicted that the annual precipitation would be 82.17 mm (%14.20), 32.86 mm (%6.4), 89.9 mm (%18.40) lower from 2021-2040 to the 2071-2098 period. As can be seen from these results, precipitation predicted with RCP8.5 scenarios are lower than those predicted by RCP 4.5 scenarios.

# 3.2. Changes in Potential Groundwater Recharge from 2021 to 2098

Precipitation values produced by three models, GFDL-ESM2M, HadGEM2-ES and MPI-ESM-ER, were used as input for estimating potential groundwater recharge under the RCP4.5 and RCP8.5 scenarios. Changes in potential groundwater recharge from 2021 to 2098 are shown in Figure 4.

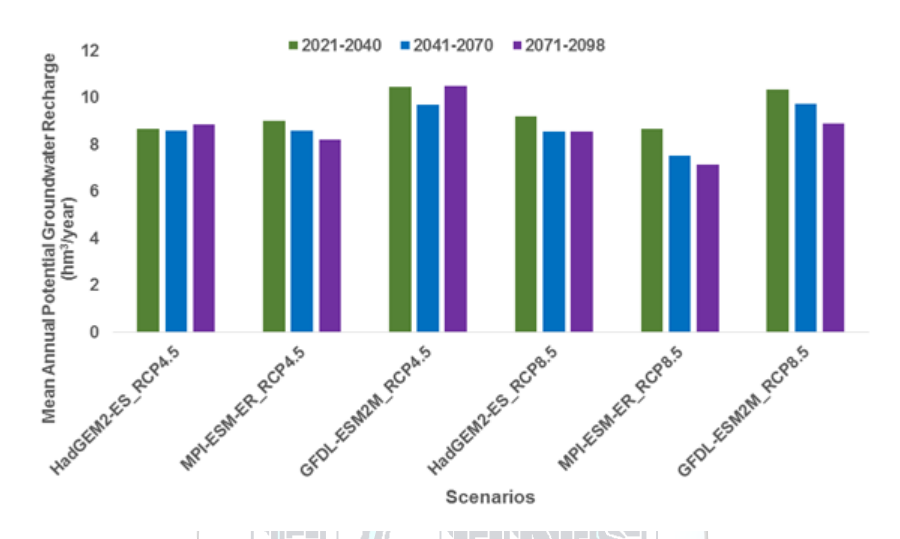


Figure 4: Potential groundwater recharge under the RCP4.5 and RCP8.5 scenarios

Compared to the 2021-2040 period, mean annual potential groundwater recharge is predicted to decrease by 0.78 hm<sup>3</sup> (%7.42) (GFDL-ESM2M), 0.09 hm<sup>3</sup> (%1.02) (HadGEM2-ES), and 0.44 hm<sup>3</sup> (%4.87) (MPI-ESM-ER) during the 2041-2070 period according to the RCP4.5 scenario. The increase would be 0.02 hm<sup>3</sup> (%0.23) (GFDL-ESM2M), 0.18 hm<sup>3</sup> (%2.13) (HadGEM2-ES) while we expect a decrease of 0.80 hm<sup>3</sup> (decrease %8.87) with MPI-ESM-ER from the 2021-2040 to the 2071-2098 period.

According to the RCP8.5 scenario, from the 2021-2040 to the 2041-2070 period, the average annual potential groundwater recharge decrease would be 0.61 hm³ (5.90%) (GFDL-ESM2M), 0.62 hm³ (6.70%) (HadGEM2-ES), and 1.11 hm³ (12.80%) (MPI-ESM-ER). In the RCP 8.5 scenario, the decrease from 2021-2040 to 2071-2098 is 1.47 hm³ (14.20%) (GFDL-ESM2M), 0.65 hm³ (7.10%) (HadGEM2-ES), 1.50 hm³ (17.40%) (MPI-ESM-ER). Figure 4 shows that potential groundwater recharge values in the RCP4.5 scenario in GFDL-ESM2M and MPI-ESM-ER projections are higher than those in the RCP8.5 scenario.

We estimated the trends in annual potential groundwater recharge using the linear regression method. According to the data obtained from the HadGEM2-ES and MPI-ESM-ER models, downward trends were detected both under the RCP4.5 and RCP8.5 scenarios. GFDL-ESM2M model estimated a slightly positive trend under the RCP4.5 scenario but downward trend under the RCP8.5 scenario. The trends detected for the RCP8.5 scenario with GFDL-ESM2M and MPI-ESM-ER models were statistically significant at the 0.01 level.

Potential	RCP4.5		RCP8.5	
Recharge	Trend (m³/year)	P Value	Trend (m³/year)	P Value
HadGEM2-ES	-4063	0.572	-14767	0.087
MPI-ESM-ER	-13901	0.092	-25580	0.002
GFDL-ESM2M	2999	0.784	-26828	0.002

Table 3: Trends in annual potential groundwater recharge series and their statistical significance

# 4. CONCLUSIONS

In this study, we used precipitation projections from three different global circulation models – GFDL-ESM2M, HadGEM2-ES and MPI-ESM-ER, to understand how potential groundwater recharge can change in a semi-arid agricultural basin from 2021 to 2098. The analyses were based on two RCP scenarios; RCP4.5 and RCP8.5. RCP4.5 scenario can be defined as a scenario where the factors triggering global warming are more under control. Two models HadGEM2-ES and MPI-ESM-ER projected a downward trend in potential groundwater recharge values from 2021 to 2098 under the RCP4.5 scenario. Only GFDL-ESM2M model projected a slight upward trend under the RCP4.5 scenario. RCP8.5 scenario assumes a situation where the factors triggering global warming are more intense. Under the RCP8.5 scenario, the annual potential groundwater recharge values went down from 2021 to 2098 and the downward trends were much stronger than the ones detected with the RCP4.5 scenario.

As a result, potential groundwater recharge is expected to decrease in the Palas Basin. A reduction in potential groundwater recharge means that groundwater to be used for agricultural purposes will become more limited. This situation can have social and economic consequences for the region. Groundwater is also important for the Tuzla Lake ecosystem. A decrease in precipitation and groundwater recharge can have adverse effects on the hydrological and ecological characteristics of Tuzla Lake ecosystem.

In order to maintain the hydrological balance in the region under changing climatic conditions, measures should be taken to reduce water use in irrigation. This can be achieved by changing irrigation technologies and crop types or using different irrigation scheduling and water saving technologies. The results obtained in this study can be helpful for more comprehensive studies such as net recharge calculation, surface water modeling, socioeconomic modeling.

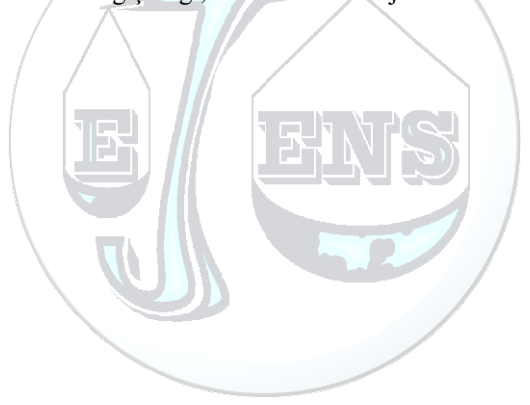
# ACKNOWLEDGMENT

This study was supported by the Scientific and Technological Research Council of Turkey (Project No: 118Y178) and Erciyes University Research Fund (FYL-2019-9562).

# REFERENCES

- [1]. M. Napoli, L. Massetti, S. Orlandini, "Hydrological response to land use and climate changes in a rural hilly basin in Italy," *Catena*, vol. 157, pp. 1-11, 2017.
- [2]. P. G. Whitehead, R. L. Wilby, R. W. Battarbee, M. Kernan, A. J. Wade, "A review of the potential impacts of climate change on surface water quality," *Hydrological Sciences Journal*, vol. 54, pp. 101-123, 2009.
- [3]. R. G. Taylor, B. Scanlon, P. Döll, M. Rodell, R. Van Beek, Y. Wada, L. Longuevergne, M. Leblanc, S. J. Famiglietti, Edmunds, M. "Groundwater and climate change," *Nature Climate Change*, vol. 3, pp. 322-329, 2013.
- [4]. M. Hamdi, K. Goïta, H. Jerbi, M. F. Zagrarni, "Modeling of the natural groundwater recharge under climate change: Sisseb El Alem Nadhour Saouaf basin (Central Tunisia) case study," *Environmental Earth Sciences*, vol. 79, pp. 1-25, 2020.
- [5]. M. Herrera-Pantoja, K. Hiscock, "The effects of climate change on potential groundwater recharge in Great Britain," *Hydrological Processe*, vol. 22, pp. 73-86, 2008.
- [6]. A. J. C. Neto, L. N. Rodrigues, D. D. da Silva, D. Althoff, "Impact of climate change on groundwater recharge in a Brazilian Savannah watershed," *Theoretical Applied Climatology*, vol. 143, pp. 1425-1436, 2021.

- [7]. E. Rodríguez-Huerta, M. Rosas-Casals, L. M. Hernández-Terrones, "A water balance model to estimate climate change impact on groundwater recharge in Yucatan Peninsula, Mexico," *Hydrological Sciences Journal*, vol. 65, pp. 470-486, 2020.
- [8]. M. Almazroui, Z. Şen, A. M. Mohorji, M. N. Islam, "Impacts of climate change on water engineering structures in arid regions: case studies in Turkey and Saudi Arabia," *Earth Systems Environment*, vol. 3, pp. 43-57, 2019.
- [9]. M. Özdoğan, "Modeling the impacts of climate change on wheat yields in Northwestern Turkey," Agriculture, *Ecosystems Environment*, vol. 141, pp. 1-12, 2011.
- [10]. Ö. Tatar, "Climate change impacts on crop production in Turkey," Agronomy Series of Scientific Research/Lucrari Stiintifice Seria Agronomie, vol. 59, pp. 135-140, 2016.
- [11]. M. Turkes, M. T. Turp, N. An, T. Ozturk and M. L. Kurnaz, Impacts of climate change on precipitation climatology and variability in Turkey, *In Water resources of Turkey, Springer, Cham*, 2020.
- [12]. I. Yucel, A. Güventürk, O. L. Sen, "Climate change impacts on snowmelt runoff for mountainous transboundary basins in eastern Turkey," *International Journal of Climatology*, vol. 35, pp. 215-228, 2015.
- [13]. A. Mehr Danandeh, A. U. Sorman, E. Kahya, M. Hesami Afshar, "Climate change impacts on meteorological drought using SPI and SPEI: case study of Ankara, Turkey," *Hydrological Sciences Journal*, vol. 65(2), pp. 254-268, 2020.
- [14]. O. Yagbasan, "Impacts of climate change on groundwater recharge in Küçük Menderes River Basin in Western Turkey," *Geodinamica Acta*, vol. 28, pp. 209-222, 2016.
- [15]. F. Dadaser-Celik, M. Celik, "Modelling surface water-groundwater interactions at the Palas Basin (Turkey) using FREEWAT," Acque Sotterranee *Italian Journal of Groundwater*, vol. 6, pp. 53-60, 2017.
- [16]. Anonymous, "Kızılırmak Havzası Master Planı Hazırlanması İşi-Hidrojeoloji Etüt Raporu," T.C. Devlet Su İşleri Genel Müdürlüğü, Ankara, 2017.
- [17]. A. Akçakaya, U. M. Sümer, M. Demircan, Ö. Demir, H. Atay, O. Eskioğlu, H. Gürkan, B. Yazıcı, A. Kocatürk, S. Şensoy, E. Bölük, H. Arabacı, Y. Açar, M. Ekici, S. Yağan, F. Çukurçayir, "Yeni Senaryolar İle Türkiye İklim Projeksiyonlari ve İklim Değişikliği," T.C. Meteoroloji Genel Müdürlüğü, Ankara, 2015.



# Analysis of Temperature and Relative Humidity Variations in the Large-Caliber Ammunition Containers of NATO and Eastern Concept Depending on the Change of Seasons

Berko Zecevic<sup>1</sup>, Nurin Zecevic<sup>1\*</sup>, Jasmin Terzic<sup>1</sup>, Miroslav Sain<sup>1</sup>

<sup>1</sup> University of Sarajevo, Mechanical Engineering Faculty, Department of Defense Technologies, 71000, Sarajevo,

Bosnia and Herzegovina

\*Corresponding Author email: zecevicn@mef.unsa.ba

#### Abstract

The design and materials used for large-caliber ammunition containers significantly effect on its shelf-life, safety and functional reliability during the handling and storage process. All ammunition containers should protect the ammunition in the required operating environment during extreme weather conditions, in terms of water resistance and protection from corrosion and fungi, and ammunition inside of the container needs to withstand all shocks caused during handling and transport. There are significant differences in the design, construction and materials used for the containers of NATO concept and ammunition containers of Eastern concept. The basic differences between these two concepts are reflected in the degree of protection of ammunition during extreme changes in temperature and relative humidity in ammunition storage and inside of containers. The NATO concept of ammunition container is consisted of outer and inner lining, where outer lining is usually made of wood or steel sheet. The inner lining protects the contents from the influence of environmental parameters (temperature, relative humidity). The Eastern concept of a large-caliber ammunition containers usually does not have an inner lining. The aim of the experimental research carried out in four different containers, was to identify and analyze the degree of variations in temperature and relative humidity in ammunition containers of NATO and Eastern concept during the storage, depending on the change of seasons. Using a Tiny tag Plus TGIS-1580 data logger, the changes in temperature and relative humidity were measured, inside and outside of ammunition magazine, inside the ammo box and inside of fiber container. Experimental research showed large influence of the design of outer and inner lining of ammunition containers on the variation of environmental parameters. Since the ammunition is expensive and tends to have a longer shelf life, it is necessary to implement NATO concept of ammunition containers on ammunition packaging of the Eastern concept

# **Key words**

Ammunition, Shelf-life, Storage, Measurement, Packaging, Fiber container, Environmental parameters

#### 1. INTRODUCTION

At the end of 20th century, drastic changes were made in political and military relations between the great powers in the World, resulted in the number of a new conflicts, some of which continued to last with varying intensity. These conflicts are characterized by a mass use of large caliber ammunition, where ammunition is transported by all available means of transport (road, air, sea, rail etc.), stored in the open air or earth covered magazines, on different climatic and geographical locations. In such conditions, it is extremely important to know and respect all parameters that can affect the shelf-life of ammunition, and to ensure that ammunition and explosives (AE) are fully ready and safe for potential transport, handling and use of the same.

One of the main and most influential parameters that affect the safety of AE and its storage, are environmental parameters, because temperature and relative humidity of the air in ammunition magazine have significant impact on the condition and overall life of ammunition. Climatic changes, through large oscillations of daily temperatures and relative humidity, whose values deviate from the set of safety standards, directly effect on the process of ammunition performance degradation, performance of propellants in propellant charges, explosives in warheads and pyrotechnic components and igniter systems.

The issue of ammunition maintenance is a very important and every effort should be made to ensure safe conditions prevail in the process of storage and transportation, because factors as higher temperature, rain, dampness and humidity can cause enormous damage to AE in a very short time [1]. If the manufacturers' environmental conditions are not met, the performance of explosives will be unpredictable and the safety will be reduced [2]. From financial side, aspect of ammunition storage is significant, since about 50 % of the total costs for the process through which the ammunition goes (design, production, storage and demilitarization), is necessary for AE storage. But more often the importance of adequate storage is being neglected. Unfavorable condition for AE storage, with significant temperature fluctuations and high relative humidity for a longer period of time, can also cause a drastic shortening of ammo life and the need to use it as quickly as possible. The service life of such ammunition in the new real storage conditions is no longer as prescribed by the manufacturer. The issue of maintaining such ammunition has become essential. The need for periodic inspection and inspection of ammunition has become one of the vital activities of modern Armies focused not only on safety, reliability and performance functionality, but also on issues of operational status of ammunition in low-intensity wars.

# 1.1. The effects of air temperature and relative humidity on ammunition

Ambient air temperature does not necessarily mean that is also the temperature of ammunition, temperature of explosive substances in warheads, rocket motors or propulsion charges in cartridge. This is particularly the case when the ammunition is stored and used in dessert areas, where solar radiation significantly increases local temperature on some parts of ammunition [3]. Storage of AE on air temperature of 60 or 70°C in dessert has totally different effect than storage in the magazine at 15 °C temperature in Central Europe [4]. Experience from the use of ammunition in the combat conditions showed that if ammunition prepared for combat use, stored outdoors for a longer time, under the strong influence of solar radiation, it can in some cases reach temperature on lancer up to 100°C or ammunition inside of tanks and armored fighting vehicles without air conditioning can reach 90°C [3].

Recommended temperature in the storage should be in the range 5 do 25°C. In the situation of storing AE for a longer period, it is necessary to take into account the temperature values are not the same during summer and winter period, and there are differences in daily values. Temperature values, lower and higher than standard, can have a very negative effect on the structure and performance of AE in the storage. Very low temperature are not as objectionable as higher ones, but explosive that contain nitroglycerin can become dangerous at very low temperature or it can change physical properties of material of which explosive is composed. Higher air temperature can intensify degradation reaction of certain components inside of explosive matters and reduce ballistic performance or cause chemical degradation of material and appearance of gases causing cracks of propellant [5]. Increasing the temperature for about 10°C above the recommended temperature of 25°C, can generally speed up chemical reactions by 2 to 3 [6].

Impact of the humidity can be very complex and significantly depends on the air temperature. Higher relative humidity can cause ammunition damage and lower humidity causes static electricity for some type of stocks. The penetration of moisture through the hermetic systems in complex projectiles can cause failures of the functions of vital components, causing chemical reactions in ignition systems based on aluminum and magnesium. In ammunition packaging systems or in the case of poor packaging, the free moisture released during the daily temperature cycle can cause long-term corrosion of the metal components of the ammunition and thus reduce the functional capability of the ammunition in combat use. The physical effects of the influence of temperature changes during diurnal temperature cycling and high temperatures in the warehouse can cause the appearance of high stress states and the appearance of cracks in the zones of contact of explosive matter with the ammunition structure [5].

Contemporary research of the impact of environmental parameters on the condition of ammunition have shown that it is no longer enough to read the temperature once a day, but it is necessary to continuously monitor the temperature and humidity inside the ammunition packages. In this way, the precise data, necessary for estimating the remaining life of ammunition, are obtained [5]. This is based on significant deviations in the measurement of real air temperature during the daily cycle in comparance to the measurement of a long-term mean temperature over time for a given storage location. In addition, a very important factor is the monitoring of temperature and humidity within the ammunition packages themselves, as this provides more accurate data necessary to estimate the remaining life of the ammunition.

62 Zecevic et al.

Since ammunition may deteriorate or become damaged unless it is correctly stored, handled and transported, with the result that it may fail to function as designed and become dangerous for storage, transport and use [5, 7], therefore it is important to know environmental conditions where the ammunition is stored, considering important parameters as actual atmospheric parameters outside the magazine over a longer period of time, parameters inside the magazine, efficiency of natural ventilation in the magazine and variation of temperature and relative humidity inside the package of ammunition. The design and used materials of the packages can significantly influence on the ability to reduce the impact of external influences of environmental factors.

# 1.2. The importance of ammunition package

Ammunition packaging is a crucial factor in maintaining the integrity of ammunition. It represents a key safety measure in the process of handling, storing and transporting ammunition until the moment of the use on the battlefield. The design and materials of the ammunition container significantly effects on its service life, safety and functional reliability during the handling and storage process [2]. NATO and Eastern (China, Russia) ammunition container concept is the mostly used in the world. But there are significant differences in design approach, construction and used materials between these two concepts.

The basic differences between these two concepts are reflected in the degree of protection in extreme changes of temperature and relative humidity in magazines (during the change of seasons) and the ability to absorb shocks during handling and transport. The NATO concept of a large-caliber ammunition container implies that the container contains an outer coating that protects the contents during the transport, handling and storage process. The outer cladding is usually made of wooden materials or sheet steel, and more recently of reinforced plastic. Internal linings protect the contents from the effects of the environment (temperature, relative humidity) and have additives that prevent displacement and absorb the effects of shock and vibration. The inner linings are in the form of fiber containers or made of composite plastic materials. The Eastern concept of a large-caliber ammunition containers usually did not have an inner lining, larger ammunition was placed in wooden crates with very primitive accessories to prevent the movement of ammunition. There were packaging designs where the ammunition was loaded into special metal containers and then together with the projectiles into wooden crates (125 mm tank ammunition). In a recent years, the situation has changed and the packaging of the Eastern concept ammunition has been improved. Theoretically, all ammunition containers should protect the ammunition in an extreme weather conditions in demanding operational environments, it should be waterproof and resistant to corrosion and fungi, and allow the ammunition inside the container to withstand all shocks caused by handling and transport.

# 2. AIM AND METHODOLOGY OF RESEARCH

The aim of the experimental research which was performed in four different ammo containers, is to identify and analyze the degree of variations in temperature and relative humidity values, measured in NATO and Eastern concept ammunition containers during changes of seasons [7].

Ammo containers were stored in the Earth Covered Magazine (ECM), located on geographical area surrounded by forest and mountains, and it was not under direct influence of the Sun. Due to it, it was characterized with periodical intense changes in temperature and relative humidity. Containers were located next to the wall of magazine, 5 m from the entrance door. Magazine does not have HVAC system for an indoor climate control and the ventilation is natural. It has two front openings for air entry and one air outlet. Within the ammunition magazine, four types of ammunition packaging were placed, which differ in the design of the outer and inner packaging and the used materials for the packaging structure. Measurements performed during all four seasons made it possible to monitor changes in temperature and relative humidity in the storage area of ECM, inside the outer packaging and inside the inner containers.

Measurement of temperature and relative humidity was performed with Tiny tag Plus Intrinsically Safe Dual Channel Temperature / Relative Humidity (-40 to  $+85^{\circ}$ C / 0 to 100% RH) by Gemini Data Loggers (UK) Ltd, which provide continuous monitoring of temperature and relative humidity within hazardous storage areas and during transport of hazardous substances. Data loggers are powered by batteries and can continuously measure changes in atmospheric parameters 24 hours a day, seven days a week, 12 months a year.

Data logger TGP-4500 Tiny tag with dual channel for measuring temperature and humidity (-25 to +  $85^{\circ}$ C / 0 to 100% RH) has a high resolution and accuracy of data reading, waterproof (IP 68) and designed for outdoor use and industrial applications. The TGP-4500 sensor was placed in the entrance area of the ECM. Data logger TGIS-1580 Tiny tag with special safety with double channel for measuring temperature and humidity (-40 to +  $85^{\circ}$ C / 0 to 100% RH) is an ATEX certified data logger for use in hazardous areas, as which are ammunition depots. TGIS-1580 data loggers were placed inside ammunition magazines, inside crates, fibers and metal cylindrical containers to measure changes in temperature and humidity.

Measurements of air parameters with data loggers were performed every 20 min. The obtained results of daily maximum and minimum parameters values, differences between daily maximum and minimum air parameters and mean parameter values for each measurement day were identified and processed. Parameters of temperature and relative humidity in ECM represent the basis for comparison with the data inside the ammunition packaging.

#### 3. RESULTS OF EXPERIMENTAL RESEARCH

Throughout the research period, environmental parameters in front of and inside the magazine were measured. Measurement results were processed in the way that the average daily values of temperature and relative humidity were determined for a clearer comparative analysis.

Over a period of one year of research, the difference between the maximum and minimum values of daily temperature changes in front of the ammunition magazine ranged from a few degrees Celsius to 27°C. In the winter, the lowest temperatures were down to -19°C and the highest in summer up to 34 °C (Figure 1a). During the research period, the relative humidity was higher most of the time, often up to 100 % (Figure 1b).

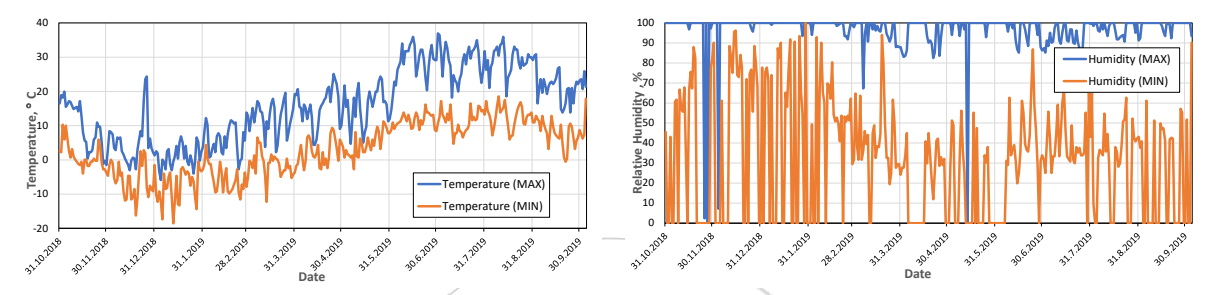


Figure 1. (a) Measured temperature values on the site of analyzed ECM

(b) Measured relative humidity values on the site of analyzed ECM

Characteristics of the magazine, as earth covered concrete structure, and the existing concept of natural ventilation system, had influence on measurement results. Average temperature in the magazine for considered measurement period, in the winter ranged up to 5°C, while in summer period it reached maximum 18°C. The deviations of daily maximum and minimum temperatures in the magazine did not exceed a few Celsius degrees (Figure 2a).

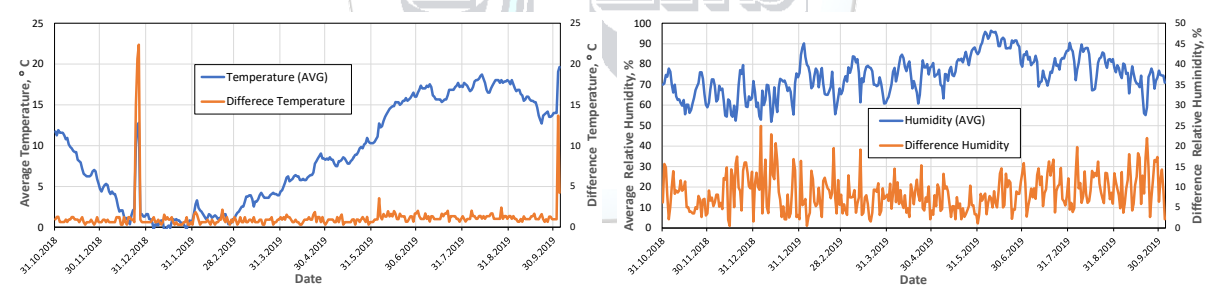


Figure 2. (a) Average temperature in ECM

(b) Average relative humidity in ECM

Average daily relative humidity for a measurement period was in the range 55-95 %, while in some parts of the day, relative humidity value reached up to 100 % (Figure 2b).

First measurement packaging, cartridge propelling 105 mm L35, was consisted of metal box, where inside were placed two cylindrical plastic containers (Figure 3, left). Plastic container was consisted of brass cartridge case, electric igniter and five incremental charges (Figure 3, right).

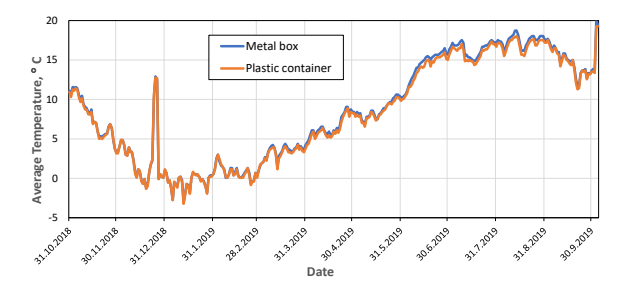




Figure 3. Cartridge propelling 105 mm, L35, packaging

64 Zecevic et al.

Measurement results of air parameters inside of metal box and plastic container for Cartridge propelling 105 mm L35 are shown on the Figure 4. Character of temperature changes in a metal box and in plastic container is similar to temperature changes inside of ECM. Variations of daily temperature values inside of both packages were up to do 4°C, in comparance to the temperature in ECM.



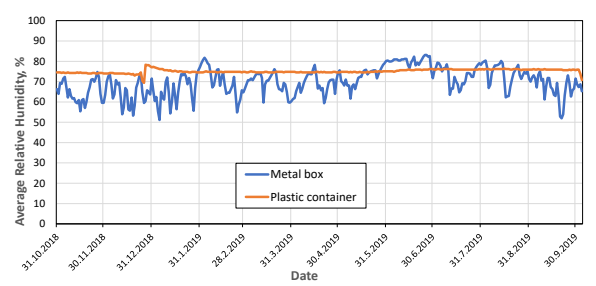


Figure 4. (a) Measured temperature values in Cartridge Propelling Packaging 105 mm, L35

(b) Measured relative humidity values in Cartridge Propelling Packaging 105 mm, L35

Relative humidity inside of the metal box was lower by 15 % in comparance with relative humidity inside of ECM. Character of relative humidity variations inside the metal box during measurement period was similar to variation of relative humidity inside of magazine because metal box of this package has several openings on its structure and there was air circulation through openings. In the case of a plastic container, there is a sealing system that prevents air penetration from the metal box to the inside of plastic container and there were no significant changes in the relative humidity in comparance to the parameters, at the time of closing the container. The variations of relative humidity was up to 3% (Figure 4b). More precisely, the relative humidity at the time of closing the plastic container remained "frozen" in comparance to the initial state.

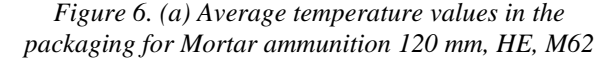
Second measurement packaging for mortar ammunition 20 mm, HE, M62, was consisted of wooden box, were two fiber containers with ammunition were placed (Figure 5). Fiber container is made of craft paper and from the outside, it is impregnated with a layer of asphalt varnish in order to protect it from moisture penetration.



Figure 5. Mortar ammunition 120 mm, M62, packing

Temperature and relative humidity variations of Mortar ammunition 120 mm, M62 are shown on the Figure 6. Intensities of temperature changes inside of wooden box and fiber container were similar to the character of temperature changes in the ECM during measurement period. Daily variations of relative humidity in the wooden box in comparance with relative humidity in the magazine had lower intensity by about 10 %, with a certain delay in reaction due to the process of heat transfer through the structure of packaging.







(b) Average relative humidity in the packaging for Mortar ammunition 120 mm, HE, M62

Relative humidity changes in fiber container had minor variations over the time in relation to changes in wooden box, due to the outside waterproof layer of asphalt varnish on the fiber container surface (Figure 6b). Initial parameters of relative humidity in the moment of installation of ammunition in the fiber container, and after closing the lid with a hermetic coating, retained same in the container. Resulting small variations of relative humidity inside of fiber container are the result of temperature changes and ability of material inside of fiber container to absorb and release moisture.

Third measurement packaging for tank ammunition 125 mm, APFSDS-T, M88, was consisted of wooden box, in which were two metal containers placed (Figure 7). One container contained a projectile 125 mm, APFSDS-T, M88 with additional propelling charge, and in second container, main propelling charge was placed.





Figure 7. Tank ammunition 125 mm, APFSDS-T, M88, packaging

Variations of temperature and relative humidity inside of ammunition 125 mm, APFSDS-T, M88 are shown on the Figure 8. Intensity of temperature changes inside of wooden box and metal container during daily cycles was similar to temperature changes in the ECM. There are significant differences in the character of daily variations of relative humidity inside of wooden box, in comparance to relative humidity variations inside of ECM, characterized with more intensive variations. Relative humidity averagely ranged between 70% and 80%.

Measurement results of relative humidity in the metal container had slightly variations during entire research period in comparance to the changes in wooden box. Variations of relative humidity were for about 25 % lower compared to the relative humidity of wooden box. Metal container practically "freezes" the state of air from the aspect of relative humidity in the moment of installation of ammunition and closing the container.



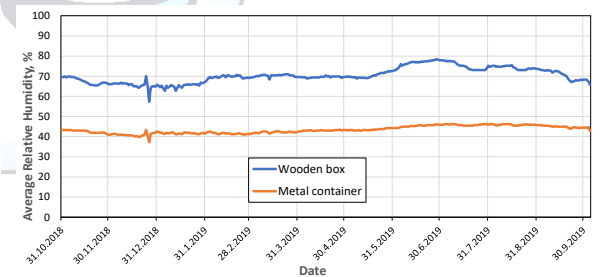


Figure 8. (a) Average temperature values in packing for ammunition 125 mm, APSDFS-T, M88

(b) Average relative humidity values in packing for ammunition 125 mm, APSDFS-T, M88

Fourth measurement container is for propelling charge, intended for HE ammunition 155 mm. It was consisted of cylindrical metal body and a lid with a sealing system (Figure 9).





Figure 9. Propelling charge for ammunition 155mm, Metal container

66 Zecevic et al.

Variations of temperature and relative humidity inside of packaging for propelling charge for ammunition 155mm are shown on Figure 10.

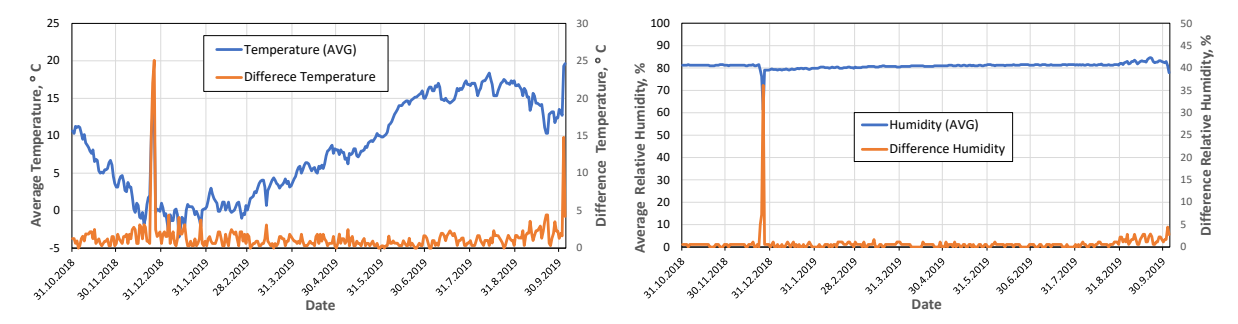


Figure 10. (a) Average temperature values in Metal Container for Propellant charge of 155 mm Ammunition

(b) Average relative humidity values in Metal Container for Propellant charge of 155 mm Ammunition

Character of the temperature changes in a metal container was similar to the changes inside of a magazine, as it was previously described for three ammo packages cases. Relative humidity in a metal container also had slightly variations as it was a case for the metal container of a third package for a tank ammunition 125 mm, APFSDS-T, M88

By comparing the measurement results of air parameters changes for all four ammo packages, several important facts can be observed. The character of temperature changes inside all three ammo packages and metal container for propellant charge of 155 mm ammunition, during daily cycles was similar to the changes of temperature inside of magazine, during entire research period. Temperature inside of packages was for a few degrees of Celsius lower than the temperature inside ECM (Figure 11).

With metal propelling container for ammunition 155, changes of relative humidity is insignificant, because there are system for hermatization of the container, where the current condition of the air from the aspect of relative humidity is maintained until the next opening of the container (Figure 11, right).

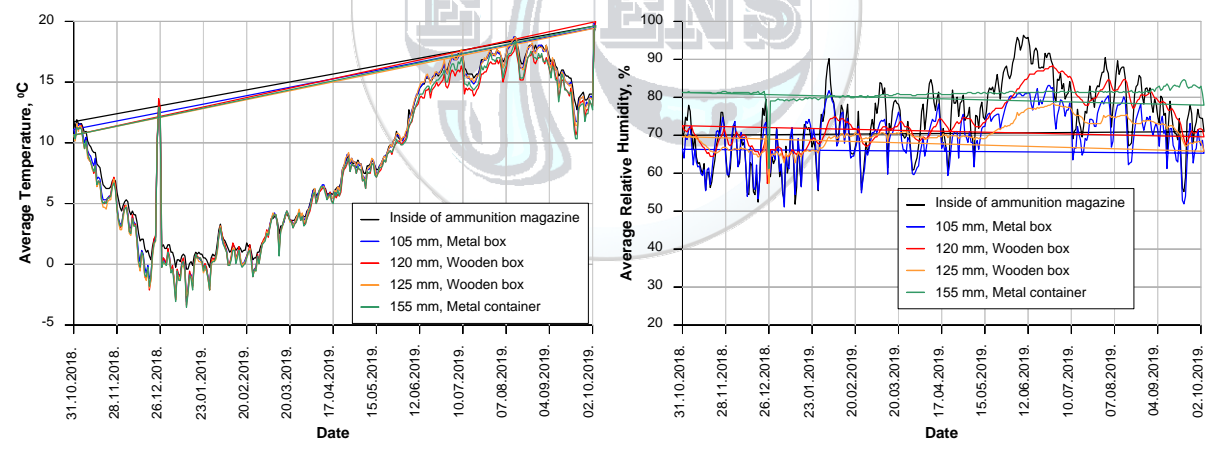


Figure 11. Comparative temperature and relative humidity air measurement data for external packaging of ammunition

Changes of relative humidity inside of plastic, fiber and metal container were less intensive in comparance with the case of ECM (Figure 12). Slightly greater variations are observed in fiber container 120 mm, M62, whose inner layer is made of craft paper which is not watertight, and then in metal container for ammunition 125 mm, APFSDS-T, which also has inner layer made of craft paper, but with a better sealing system for a metal container.

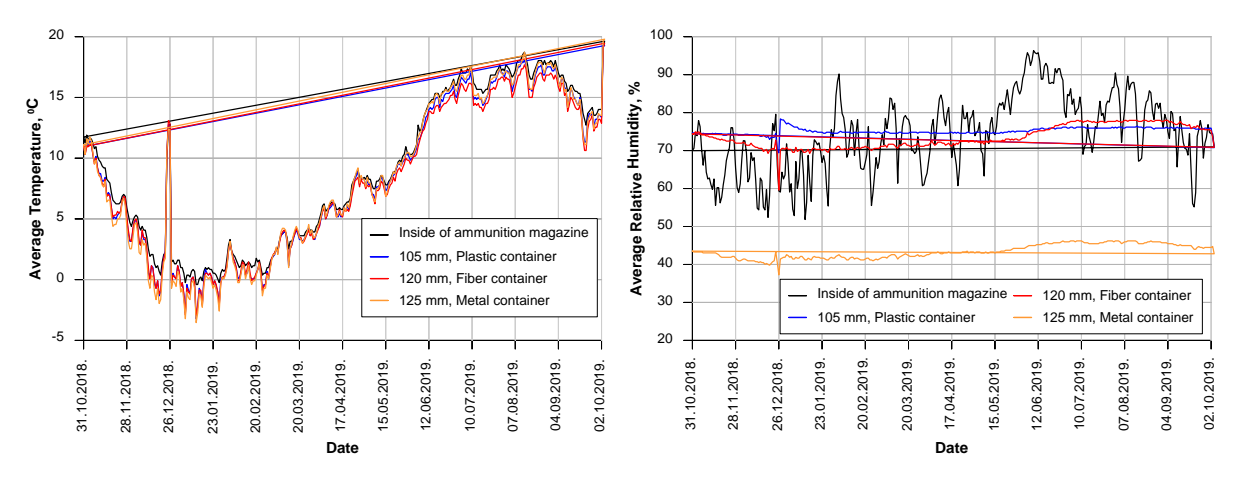


Figure 12. Comparative temperature and relative humidity air measurement data for internal packaging of ammunition

#### 4. CONCLUSION

Based on results of measurement period of one year, it can be concluded that variations of temperature inside of outer and inner lining of ammunition packaging followed variations of temperature inside of ECM.

Changes in relative humidity inside of outer packaging that were not hermetic followed the relative humidity changes within ECM, with a certain delays in reactions. Variations of relative humidity changes were slower and with lower intensity. This is especially pronounced with the outer wooden packaging, while in the case of metal container with openings on its structure, variations of changes are more intense due to the direct contact with the air in the magazine.

Changes of relative humidity at inner packages are insensitive on changes of relative humidity inside ECM, but strongly depends on initial values of air parameters, temperature and relative humidity, at the moment of closing container, amount of component inside of container that have ability to absorb moisture and method used for container sealing.

ECMs as one of the mainly used types of magazines, very often in some cases can have moisture-intrusion problem due to its characteristic covered layers and poorly performed hydro isolation. If ventilation system is not adequate, higher values of air parameters can seriously affect safety of magazine and ammunition inside of it.

Maintenance of ammunition is crucial and every effort should be made to ensure safe conditions for storage, transport, handling and use of ammunition. Some of the most significant and influential factors to achieve that are well performed and maintained ECM with efficient ventilation system to provide adequate ventilation, well designed ammunition packaging, periodical inspection and continuous monitoring and maintenance of temperature and relative humidity at a reasonable level.

# REFERENCES

- [1]. SEESAC, "Ammunition and Explosive Storage and Safety", RMDS/G 05.40, 4th Edition, UNDP Belgrade, Serbia, 2006.
- [2]. GICHD, "A Guide to Ammunition Storage", First Edition, Geneva, ISBN 940369-15-1, 2008.
- [3]. Storage of Ordnance, Munitions and Explosives (OME) In Support of Operations, Chapter 11, Ministry of Defence explosives regulations for the safe storage and processing of ordnance, munitions and explosives (OME), MOD explosives regulations (JSP 482, Edition 4) and Joint Service Publication, UK, 2013.
- [4]. Wim Deklerk, Gerhard Reelingbrouwer and Huub Keizers: "The delicate matter of lifetime", TNO Defence, Security and Safety, Munitions and missile surveillance, [Online]. Available: https://www.tno.nl/media/2756/def\_lucht\_levensduur\_em4200716173.pdf
- [5]. B. Zecevic, N. Zecevic, J. Terzic and M. Sain, "Researching influence of climatic environmental parameters on performance of large caliber ammunition during storage", 1st International Conference on Environmental Science and Technology, pp. 63-73, 2015.
- [6]. Wim Deklerk: "Lifetime prediction of ammunition", TNO Defence, Security and Safety, Ammunition Safety, [Online]. Available: https://www.tno.nl/media/8944/lifetime\_prediction\_of\_ammunition\_dv2\_05d006.pdf.
- [7]. B. Zecevic, N. Zecevic, J. Terzic and M. Sain, "Monitoring changes of temperature and humidity in ammunition storages under the Armed Forces of Bosnia and Herzegovina", UNDP, Bosnia and Herzegovina, Sarajevo, February 2015.

# Approach for a Simplified Meshing Network as Monitoring Solution in Farming Applications

# Dennis Bakir<sup>1</sup>\*, Florian Engels<sup>1</sup>, Robin Bakir<sup>1</sup>

<sup>1</sup>INNOVATOR\_INSTITUT gGmbH, Nachbarsweg 25, 45481 Muelheim an der Ruhr, Germany. \*Corresponding Author email: db@innovator-institut.de

#### **Abstract**

In this paper an approach for transferring complex and demanding ICT from industrial production to agricultural infrastructure requirements will be presented. This will enable SME farming businesses to tap the full growing potential of their arable land. The overall goal is to increase yields, crop-quality, efficiency of fertilizer and resource deployment with real-time growing-related data

Core aspect will be a meshed network of single sensing nodes, that monitor growth-relevant parameters on arable fields. The underlying technique has been approved in manufacturing SME that already utilize production data for controlling and optimizing their production processes, flow of material and machining steps via a thorough ICT-system. Therefore, a qualitative and explorative research design was conducted under 70 German SMEs.

Hereof, a frugalization inspired process led to a microcontroller-operated sensor network that is based on a long-range communication and low-power set up. The system uses specific data rates and is able to permanently cover broad monitoring areas. The respective prototype was empirically examined and provides a reasonable solution space that needs to be further elaborated in long-term field studies.

Besides potent companies that can afford to develop, test and run respective systems, as for instance smart- or precision farming, there is a huge gap to small and medium sized enterprises (SME) that are not able to deploy such technology but count for the majority of companies. That provides the impetus for further research on how to utilize the data for a decision support model

# **Key words**

condition-based-monitoring, cultivating, decision, measuring, smart-farming

## 1. INTRODUCTION

Persistent transformation processes in the industry and economy drive technological progress and affect value creation in most businesses and branches. Technological progress acts as an accelerating catalyst in manyfold ways and offers, in result, new procedures of solution [1]. An intelligent and smart control of processes positively affects resource deployment and its efficiency and is pertinent to quality. Thus, data itself and the velocity of information processing advanced to crucial competitive factors for most businesses. Besides potent companies with highly elaborated production facilities that can afford to develop, test and run respective technologies, there is a huge gap

to especially SME, that are not able to deploy such complex systems yet. Whereas, speaking of numbers of scale this kind of enterprises has the potential to disseminate such key technologies for a broader range of users.

The pervasion of powerful technologies from prototypal demonstration to a broad and resilient application is already examined in literature and depicted in product life cycle models. It states that new technologies are primarily available to a closed circle of early adopters at typically higher costs [2]. Thus, most enterprises and especially SME cannot afford such high-tech applications besides the fact, that there is no sophisticated machine park available, that would allow digitized operations and enhancing efficiency anyway.

In fact, there is already an increasingly dissemination of data driven production solutions in manufacturing companies to be recognized and includes condition-based monitoring solutions for many applications. So, in terms of technical progress, there is both the need to develop new solutions in the first place and facilitate such concepts later for a broader application and market penetration.

Data technology concepts have been adapted to farming needs and brought up so called smart farming technology (SF), that utilizes modern information and communication solutions. After plant breeding and genetic modelling this technique is referred to the third green revolution and considered as the next milestone in bio-economy and agricultural research [4]. It combines information and communication technologies (ICT), the internet of things, sensors and actuators, geo-positioning, big data, drones, robotic etc. to level up resource efficiency in the field of food production. The technology is said to contribute to a secured food supply, too [3].

The concept of SF is, until now, only common in industrialized countries and enables for cultivating vast landscapes. From a farmer's point of view, the technology provides sufficient data to support decision making and optimize processes that even allow growing on difficult terrain.

In numbers this means there are in total 266.000 farming companies in Germany that produce goods with a value of 58 bil. EUR on total arable land space of about 17 mil. ha [3]. Indeed, more than 90 % of the farmers already make use of assisting technological solutions, whereas this refers to rather low-tec applications and the extend of automatization of mechanical devices.

Regarding this, it requires at the same time further development of the technology itself and carefully selected simplifications in order to ensure applicability along the value chain and price sensitive users. By this, the research contributes to overcome food supply shortage and resource scarcity.

# 2. MATERIALS AND METHODS

This paper is based on an explorative research design in the first place, focusing on understanding dependencies and market demands of operators in the farming business regarding monitoring technologies for growth relevant tasks. In addition, a literature study complements the observation with current publications and general market trends on solutions for precision and smart farming technology set-ups, that can be applied even with low technological infrastructure and consider the current technology-related challenges in for small farming businesses.

In order to narrow down these results on a specific research field, a complementary qualitative research design was planned. After the explorative phase with several generic talks with companies and customers who supply agriculture farming tools, in total eight guideline-based expert interviews were conducted. The data were evaluated and benchmarked with literature findings, using pairwise comparison on the identified key parameters. This prioritization enabled for a definitive solution space. Besides interview result from German companies, that represent rather developed market players, an additional research journey to Cuba was conducted as part of the explorative phase.

Hence, the work aims to provide a simplified solution space for further design of a sensing and communication technology for agricultural businesses, a suitable starting point needed to be selected. This approach is considered frugalization and was be applied on a surveillance system for growing-related operations. The underlying technique has already been approved in small and medium-sized manufacturing companies, that use relevant production data via a comprehensive and practical ICT-system in order to control and optimize their production processes.

However, a quantitative study to underline the importance of current processes in the farming business is already being planned to test assumptions derived from the solution path. Considering the total population size, i.e. 266.000 farming enterprises, a sound confidence level of 95 %, which equals 5 % error margin, this leads to a sample size of 384 enterprises to be surveyed from now on. Hence, the goal is to analyze cause and effect relationships within this first instance and secondly establish a comprehensive proposal of the described solution, based on actual customer needs.

70 Bakir et al.

#### 3. RESULTS AND DISCUSSION

#### 3.1. Results

The field study revealed the very basic requirements of farmers on the infrastructure. Besides proper tools and machinery (both considered as most important) another 70 % states that ICT support is inevitable to deal with increasing calculation tasks.

Generally, the vast majority (93 %) strives for technological assistance but is not capable to operate such complex solutions. The reasons are missing infrastructure (42 %), high investment and running costs (41 %), time (9 %; for implementation and learning) and minor other factors. Especially the tight supply of reasonable systems seems to be the most important impediment. This is true for both, developed (Germany) and less developed (Cuba) countries.

# 3.2. State of the art

Latest manufacturing technologies apply cyber physical systems that use data as additional resource for process design, steering and decision-making in production facilities. Characteristic feature of such systems are small areas that are monitored by high frequency communication devices with high data-rates. In addition, steady power supply and ambient conditions isolate this certain use case from farming applications, where wide-area production grounds with versatile surrounding conditions are typic.

There are multiple solutions to transfer data between a data link which comes with different characteristics to handle. First, there are different restrictions about the usable frequency on most continents. That means, a multilayer hardware-layout, which is able to exchange different radiofrequency modules without modifying the software, is a prerequisite for international usecases. Common frequencies for European and north-/south American application are 433, 868, 915 MHz and 2,4 or 5 GHz. Due to the limit of physics, a higher frequency is linked to a higher rate of transmission but induces lower coverage. There already exist various concepts to transmit specific data, even via huge distances, i. e. 25 km, and aggregate them in a networked system [5].

Generally speaking, there is a strong correlation between a stable connection over wide areas and the sampling rate (samples per seconds). For instance, agriculture use cases typically require relatively low sampling rates (1/15 min.). Due to a higher path of transmission to a Server/Datahub lower frequencies with a lower bandwidth are deployed.

Typically, it is based on Long Range (LoRa) or a similar narrowband application (see given frequencies before) in different meshed clusters.

Furthermore, there is an additional technology deployed which uses the 4G-IoT-Narrowband. The advantage of this technology is that multiple measurement-tasks can be run at the same time, only requiring 4G-connection. Afterwards, the data will be transmitted to a web-based API, which processes the Data to useful information. Indeed, even with this technology the described dependency between a high reach and small sampling rate of the data still exists.

Along with the second mayor trend in the agricultural business, precision farming (PF), there arises a huge economic potential [6]. Focusing on a precise cultivation, this approach includes especially digital process technology, that will be examined in this paper. The term itself refers to a farming management concept, based on observing, measuring and responding to inter and intra-field variability in crops. It aims at the targeted deployment of growth relevant factors and separates the fields accordingly into identifiable units. In contrast to common manners, the identified areas are not based on property lines or on the expected average yearly crop yield but on their true potential of bringing up plants in an ecological way. Thus, this approach enables farmers to manage their fields based on the spatial variability, such as the availability of nutrients and expected crop yield [7].

To a much greater extent than ever before, plant protection is guided by the pressurized expectation to avoid damage and economic efficiency. The precision farming method involves measures of small-scale soil cultivation, sowing, fertilization, application of pesticides and other operations.

Prerequisite for this technology is an elaborated and mostly expensive IT infrastructure, that can cope with the amount of data and offer the required computing power. Subsequently, certain barriers to entry arise that leave less developed economies and/or farmers behind and moreover interfere the pervasion of a future technology.

# 3.3. Approach

#### 3.3.1. System design

In the following the systematic approach, on how to establish resilient, reasonable ICT-systems to professionalize farming tasks with low infrastructure requirements will be introduced. The solution is inspired by SF technology and offers a straight potential for resource efficient and sustainable farming with a centralized and condition-based cultivation.

It uses the combination of empirical and experience-based knowledge with data-driven process information to support decision making processes about growth-relevant parameters. The aim is to raise agricultural yields in terms of harvest and returns along the value chain by using mostly given resources by taking advantage of sustainable movements.

The solution is thought to be a platform, enabling a linked sensor network over agriculture surfaces. This platform-architecture includes sensor-nodes that enables a continuous monitoring of growth relevant parameters (see Figure 1).

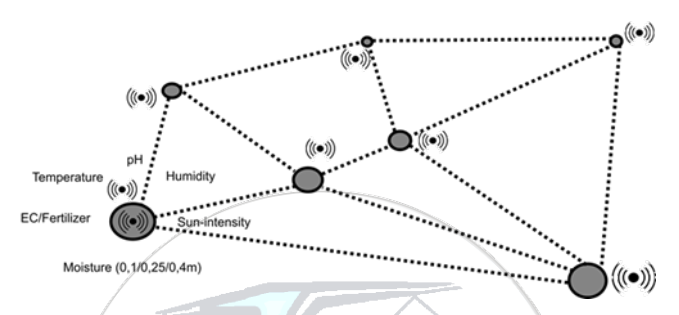


Figure 1: Network with nodes and master hub (left)

#### 3.3.2. Resource monitoring

The solution provides a high-performance low-power measuring set-up for arable land. It is based on a scalable amount of meshed sensing nodes. These can easily be modified and adapted to variable scenarios in order to be implemented for different agricultural applications and are operated with a variable set of input parameters.

Instead of intense capital expenditure for enhancing the technological base and time-consuming efforts for the initial operating as well as maintenance, a smart work-around based on Long Range meshing communication technology is used.

By this, farmers will be provided with a reasonable solution that can be scaled easily. As data will take on a core resource in the set-up, a profound and especially interdisciplinary know-ledge base will be established that will provide an impetus for fostering agricultural business concepts.

By this, practical knowledge and empirical data, as they are already considered as crucial input in manufacturing applications, are transferred to a new application. For different measuring tasks the central hub will be enriched by a scalable CAN-BUS API. This will allow for modification of the used measuring set-up and installed sensors, even in the working environment. As solution, the active transmission of signals of a single entity can be realized via microcontrollers, e.g., type AP2921 by Siemens. Although this type is primarily designed for high-data rates, it provides further advantage regarding scalability (see Figure 2).

This layout can be run with a raspberry-pi infrastructure that enables for an inexpensive and performing approach. Besides, the gathered data of a masterhub can easily be interpreted on the Pi and be forwarded to a WebSocket API. Especially a WebSocket application promotes the intended usability because it enables for a direct transfer of data to a browser. By means of design, the API can even be directly integrated on the hub. Via a separate control panel, that interface can be used to control external further application, for example data retrieval form a browser.

Regarding the actual sensing tasks, precision will be favoured over resolution. This seems to be appropriate because of the rather raw case of application and a generally lower meaning of resolution on the field. This alignment supports a possibly low cost solution. Nonetheless, both are required for metering tasks, which are not part of the paper.

72 Bakir et al.

A distinctive control routine will ensure the long-term applicability of every respective entity in the field. That means, a dynamic battery management will be employed to control sensing intensity depending of the actual power level (i. e. electric potential). With lower power level, the device will prolong its measuring and sending intervals.

According to this, further research will be conducted to determine power limits and respectively timed intervals. In order to even expand on ultra-low-power operation an extension with photovoltaic powering could be realized, indeed causing additional costs and maintenance efforts.

# 3.3.3. Resource monitoring

The generated data-streams get linked via a 433MHz/868MHz/LoRA to a masterhub, which collects all data und send them online to a custom endpoint, like an API, web-dashboard or a cloud-based data storage. The API/dashboard is run by various analysis/graphs, so the user can evaluate the detailed condition of the monitored area. There are various technology of communications existing. If the use case is to create a local network, which even can work offline, a LoRa- or other ISM-Band (free to use) is recommend. If there is need to send the data immediately to a remote web-based server, the IoT-Narrowband on 4G/LTE-base can be used. For a migration of the data by a remote masterhub, LoRa is a data protocol dedicated for low-latency transmission of single data packages.

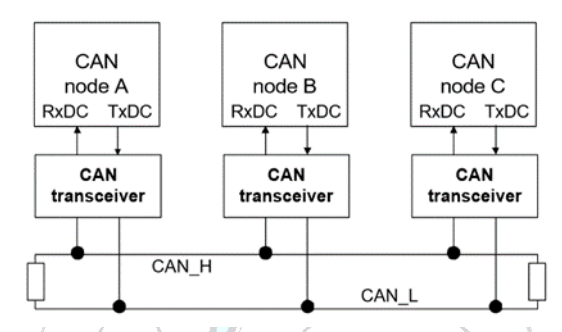


Figure 2. API-layout on the hub to integrate sensors

In contrast to high-frequency production solutions it covers up to 35 km distance between transmitter and receiver. By this it qualifies especially for the application in agriculture with vast landscapes and partly low internet coverage, such as the 3G standard or even lower.

Typical for measuring tasks in agricultural surrounding lower sampling rates are sufficient. A continuous sampling rate of e.g. 0,02 Hz can easily be operated via LoRa-protocol and prepare the technology to inform even about unexpected conditions and changes with less latency – which by means increasingly happens as a matter of short-term climate changes.

So, the distinctive advantage is its independency from network coverage. In case there is no local internet-connection, the 4G-IoT-Narrowband shall be used to send the data to an online-endpoint, even on outlying geographical areas. This would create a reliable entry point for smart farming even in developing countries with low infrastructure and limited resources to make use of high-end precision farming technologies.

With respect to interoperability and security matters, it seems adequate to use the popular MQTT network protocol that transports massages between devices – in this case a masterhub and several APIs. This technology as well supports the intended meshing for enlarging the potential measuring area.

# 3.3.4. Security

The security of the collected and processed data gets a high place value. In this concept, all data are heavily secured by a strong AES256 encryption. This kind of encryption seems slightly to be overpowered for agriculture use cases, but due to the frugaliziation of technology, which can be integrated deeply into many industry-processes, it is already developed within the "privacy by design" rule and prepares for potential scale-up operations later on.

Furthermore, the sensor nodes can create a hashvalue considering especially time and potentially geo-information of the collected data, so the receiver (masterhub) can compare the incoming data streams with the hashvalue as a kind of verification.

To prevent a processing of false/corrupted sensor signals, especially in pH, fertilizer or soil moisture measurements, all input-signals have to pass a galvanic isolation. Even though this isolation would result in slightly

higher manufacturing costs, it increases the reliability of the system. Furthermore, the galvanic isolation protects the electronic on-chip-circuit against electric discharges.

To detect an incorrect wiring or a damage of the electric circuit between a sensor and the sensor-node, all inputs got a open circuit detection. This means, if a e. g. Negative Temperature Coefficient Thermistor shows an implausible value for the expected temperature-ranges, there must be an incorrect wiring or damage within the sensor itself. The sensor-node detects this error and extends the existing telegram structure with unique errorcodes, so the Graphical User Interface can display a warning sign and push-notifications to the user.

Another security-related task is the prevention of data-loss, which leads to white gaps in the measurement stream. The current approach to prevent this loss is a local, timestamp-based storage on each sensor node. After transmitting data to the masterhub, a checksum is transmitted, so the node and masterhub can identify incorrect transmissions of data. After a transmission is successfully completed, the masterhub saves the data on a timeseries database, like InfluxDB or Prometheus, which is hosted on the desired endpoint like API or cloud. Within the dashboard environment, which is connected to the encrypted timeseries database, the user can create different backup-tasks, like backup to a cloud, local storage or other servers.

For a continuous monitoring of all nodes, each telegram gets added relevant status-information about all connected sensors, battery-level, connection strength and the ratio of successfully vs. unsuccessful transmitted data-packages. So, the user can easily see, which node may need to be checked to prevent more failures.

# 4. CONCLUSION

High-end SF and PF technologies have the potential for enhancing efficiency. They use digitized arable landmarks that can digitally be managed in order to increase yields and lower resource deployment continuously. For executing such tasks, drones, autonomous harvesters. Accordingly, these can be found most of all are on vast farming areas with already digitized processes and well financed operators. Another prerequisite is an highly elaborated infrastructure with 5G-Networks for a bidirectional data-transmission.

As an effect, this kind of technology requires an already digitized staring point with ICT infrastructure. The full potential of such systems lays in a centralized control entity with high processing power, that can analyze and process the amount of data via artificial intelligence in order to control the machinery on the field. Any bettering and enhancement of such a set up regarding digitization, efficiency and yields require disproportional efforts and especially additional expenditures. Considering this, the technology is rather suitable for already digitized environments and inappropriate for small-scale farms and low-infrastructure landscapes.

In consequence, especially smaller farming-businesses cannot participate in this development and underachieve the growing potential of their arable land. Thus, there is the need for a low-tec application as enabling technology towards fully digitized manufacturing of farming goods.

So, it is evident, that transferring individual sub-technologies, like high performance sensor-meshing, into a more applicable context for regular farmers that could promote the pervasion of the respective technology. In the first place, farmers should gain insight into the actual conditions of their fields by monitoring key performance indicators, such as pH, density, humidity, atmospheric pressure, sun intensity, amount of irrigation water, temperature, fertilizer. This can be realized effectively by implementing meshed sensors across the measuring field. Moreover, large-scale benefits are expected as a result of scale effects.

The presented approach shall provide a basic and thus applicable method for science- and evidence-based farming, complementing to experience based decision. In concrete terms there will be given a solution for monitoring arable space regarding growth-related parameters and derive data-based actions to be taken. With specific data transmission set-ups it will be possible, to easily integrate specific sensor nodes in an agricultural environment to regularly gather at least data on soil, environment and plant conditions. These will be transformed into specific information for machinery and assisting technological entities. The added value will be an enhanced knowledge-base, regarding condition-based cultivating of arable land. By the use of such data, even re-cultivation will be possible, as irrigation water, fertilizer etc. can pointedly be deployed, relating to the actual nutrient concentration in the soil and/or water.

Further advantages, that come along is the predictability of some kinds of pest, which depend on the humidity, sun-intension or amount of fertilizer. The specific advantage will be the maximal scalability of the system by at the same time very low cost of approximately about 200 EUR per node. As a matter of fact, this leads to economic and ecological savings for the farmer resulting from lower expenditures for supplies and working hours.

Ultimately this has positive effects on the economy, too, regarding sustainable and efficient growing of agricultural products by using modern data-driven technologies.

74 Bakir et al.

For promoting this approach, further research in terms of empirical assessments will be conducted. This is intended to improve transparency on the actual demand-side, especially about the current state of digitalization, available machines and ICT facilities. In addition, there will be further technical research necessary on the node design and its power supply.

#### REFERENCES

- [1] Koester U, von Cramon-Taubadel S. Technischer Fortschritt in der Landwirtschaft und Agrarpreise. In: Discussion Paper, No. 191, Leibniz Institute of Agricultural Development in Transition Economies. Halle an der Saale; 2019
- [2] Moore G. Crossing the Chasm. 3rd ed. New York: Harper Business; 2014
- [3] Modern und verantwortungsbewusst: Landwirtschaft in Deutschland, retrieved from https://www.iva.de/verband/landwirtschaft-deutschland, 01.29.2021
- [4] von Witzke H. Die dritte Gruene Revolution: Landwirtschaft als Schluesselindustrie des 21. Jahrhunderts. In: Humboldt Forum for Food and Agriculture. Augsburg: Oelbaum; 2010
- [5] Smart Farming-Die Landwirtschaft von morgen. Retrieved from https://www.wirtschaft-digital-bw.de/aktuelles/thema-des-monats/smartfarming, 11.29.2021
- [6] Auernhammer H. Precision farming the environmental challenge. In: Computers and Electronics in Agriculture. Volume 30, Issues 1–3, February 2001, Pages 31-43. Freising-Weihenstephan: Institit für Landtechnik
- [7] Definition precision farming. Retrieved from https://ihingerhof.uni-hohenheim.de/en/precision-farming-en, 11.29.2021

## CONFLICT OF INTEREST STATEMENT

The authors declare that there is no conflict of interest

